UNIVERSITY OF THE
WITWATERSRAND,
JOHANNESBURG

Exploration Geology of Structurally Controlled Sediment-Hosted Gold Mineralization at Kasenseli, Northwestern Zambia

By Kapalakasha Mulenga - 1522958

Supervisors: Prof. Paul Nex & Prof. Judith Kinnaird

University of the Witwatersrand

School of Geoscience

A research report submitted to the Faculty of Science, University of the Witwatersrand, Johannesburg, in partial fulfilment of the award of the Master of Science degree.

DECLARATION

To the best of my knowledge this research report does not contain any material that has been used and accepted in the award of any academic qualification in any University or College. Due recognition and acknowledgement has been given for materials used for reference purposes.

Signed: 

Kapalakasha Mulenga

This thesis has been submitted to the University of the Witwatersrand's Faculty of Science, School of Geoscience as partial fulfilment for the award of a Master of Science in Economic Geology.

ABSTRACT

Occurrences of economic quantities of gold within the Roan and Nguba groups of the Katanga sedimentary units are not a common phenomenon. This is a new area of exploration for gold, and very little exploration work has been done to act as a guide in such a geological environment. More common are post-Nguba unit or Kundelungu group related gold occurrences which respectively occur around the Kasempa and Mumbwa areas and these are related to the Hook granite as well as the major shear zones that traverse these areas.

The study area lies within the Lufilian Arc Fold and Thrust Belt and is located on the western end of the external fold and thrust zone which is part of the western extension of the Zambian Copperbelt. The area covering Mwinilunga is subdivided into four terranes based on regional structural features and metamorphism. The four terranes are; the Kasai Shield, the Kabompo Dome, the Western Foreland and the Lufilian Arc.

Four main units that are present within the study area include the Roan member shale unit, the arkosic sandstone and its related sub-units which occur as lenses within this main unit, the Grand Conglomerat marker unit (diamitite), and the Nguba member shale which is interbedded with siltstone in some zones. Based on the contact relationship of the units to Grand Conglomerat marker unit, the oldest unit within the study area is the Roan shale unit (which could be of Mwashya age or older), followed by the arkosic sandstone, the diamictite unit which is the Grand Conglomérat marker unit and finally the Nguba shale. Polished thin section and mineral liberation analysis was undertaken on most of these units.

Among the notable features of the stratigraphy in the area is the presence of a redox boundary between the pinkish-grey coarser arkosic sandstone unit (oxidising facies) and the greenish-grey clast-poor diamictite (reducing facies) where richer pockets of gold mineralisation have been observed. Gold mineralisation has been mainly observed to be hosted in the clast-poor diamictite mostly in the alteration halo which forms around the arkosic sandstone-quartz vein-diamictite contact. Further away from this contact and away from other related structures such as faults, veins and folds, mineralisation gradually diminishes. Gold mineralisation in this area shows a strong correlation to copper with the high-grade zones having elevated copper mineralisation both in the mineralised zone and in the residual soils.

On a district scale, the study area and its surroundings are extensively folded and faulted, and the area has undergone episodic deformation resulting in the development of various structures. Among the notable structures within the study which are relatable to the Lufilian Arc Fold and Thrust Belt (LAFTB) on district to regional scale include folding, shear faulting, normal faulting, and the development of joints.

The structural aspect plays a critical role with regards to the location of mineralisation. Observed structural features which were critical as pathways and deposition site of auriferous/mineralised fluids include first order folding with a NNE – SW oriented axial trace as well as first order NE – SW oriented shear faults and shear zone, the second order NW –

SE oriented faults and veins which are the structures that host the mineralisation, and the NW – SE oriented (axial trace) folding where saddle-reef hosted mineralisation has been observed within the study. The physiochemical redox boundary between the Nguba member diamictite (reducing facies) and pre-Nguba arkosic sandstone (oxidised facies) played a critical role in the location of the mineralisation in the area.

One thousand six-hundred and fifty (1650) soil samples were collected from the entire study area which covers a surface area of about 13 square km. Analysis and interpretation of soil assays showed that only copper may reliably be used as pathfinder in the exploration for gold mineralisation and/or deposits particularly in Nguba group member units. In addition, based on stratigraphic correlation, the possibility of Kamoa-style copper mineralisation has been suggested.

ACKNOWLEDGEMENTS

Firstly, I would like to thank all the team members from the Geology Section at the Kasenseli Gold Project who were quite handy during the field data collection and many of the field excursions undertaken on numerous occasions. I would also like to extend my gratitude to the ZCCM-IH Technical Department, which has been very supportive during the entire period of my studies.

Many thanks to the Mopani Copper Mines Plc Analytical and Mineralogy Laboratory team for the assistance in analysing mineralogy samples, which was quite critical in understanding the mineralogy of most of my very fine-grained rock samples.

Many thanks to Prof. Paul Nex and Prof. Judith Kinnard for their insightful guidance and constant support that made the completion of this report possible.

Most importantly, I would like to thank my family for their unconditional support during the entire period of my studies. Despite numerous challenges along the way, they kept encouraging me to soldier on.

TABLE OF CONTENTS

LIST OF FIGURES

LIST OF TABLES

CHAPTER ONE

INTRODUCTION AND REGIONAL GEOLOGY

1.1 INTRODUCTION

For the past nine decades or so Zambia's mining sector has traditionally been known for copper mining, however despite the major focus being on the copper production, mining of other commodities such as gold has also been taking place. Further details on gold mining and occurrences in Zambia are highlighted in section 1.7 of this report. Occurrences of economic quantities of gold within the Roan and Nguba groups of the Katanga sedimentary units are not a common phenomenon. More common are post-Nguba unit or Kundelungu group related gold occurrences which occur in the Kasempa and Mumbwa areas and these are related to the Hook granite as well as the major dislocation zones that traverse these areas (Fig 1).

Following the discovery of gold around the Kasenseli area (study area) of Mwinilunga by artisanal miners, this area has attracted a lot of exploration interest. Primarily the Mwinilunga area which geologically is overlain by the Nguba and Roan member units has traditionally been targeted for copper and cobalt exploration, with multinational corporations like Anglo America undertaking exploration in the area between 1990 and 1998 and most recently between 2015 and 2018. Other multinational companies that have previously explored the area include Cyprus Amax, Rio Tinto, Phelps Dodge and First Quantum Minerals Zambia, with most of them focusing on the Luamata Copper-Cobalt prospect which is located 30 km east of the study area. However around 4050 ounces of hard-rock hosted gold, grading 90% purity have thus far been produced from gravity processing of ore from this area. This was mined on a small-scale with a production rate of around 1 kg per day.

Some of the major operating mines located in proximity to the study area include the Trident Mining Project (Sentinel and Enterprise) which are located approximately 150 km east of the project area, the Kamoa copper deposit which is located approximately 150 km northeast of the study area (in the Democratic Republic of Congo – DRC) and the Kansanshi copper-gold mine located 250 km east of the study area (Fig. 1).

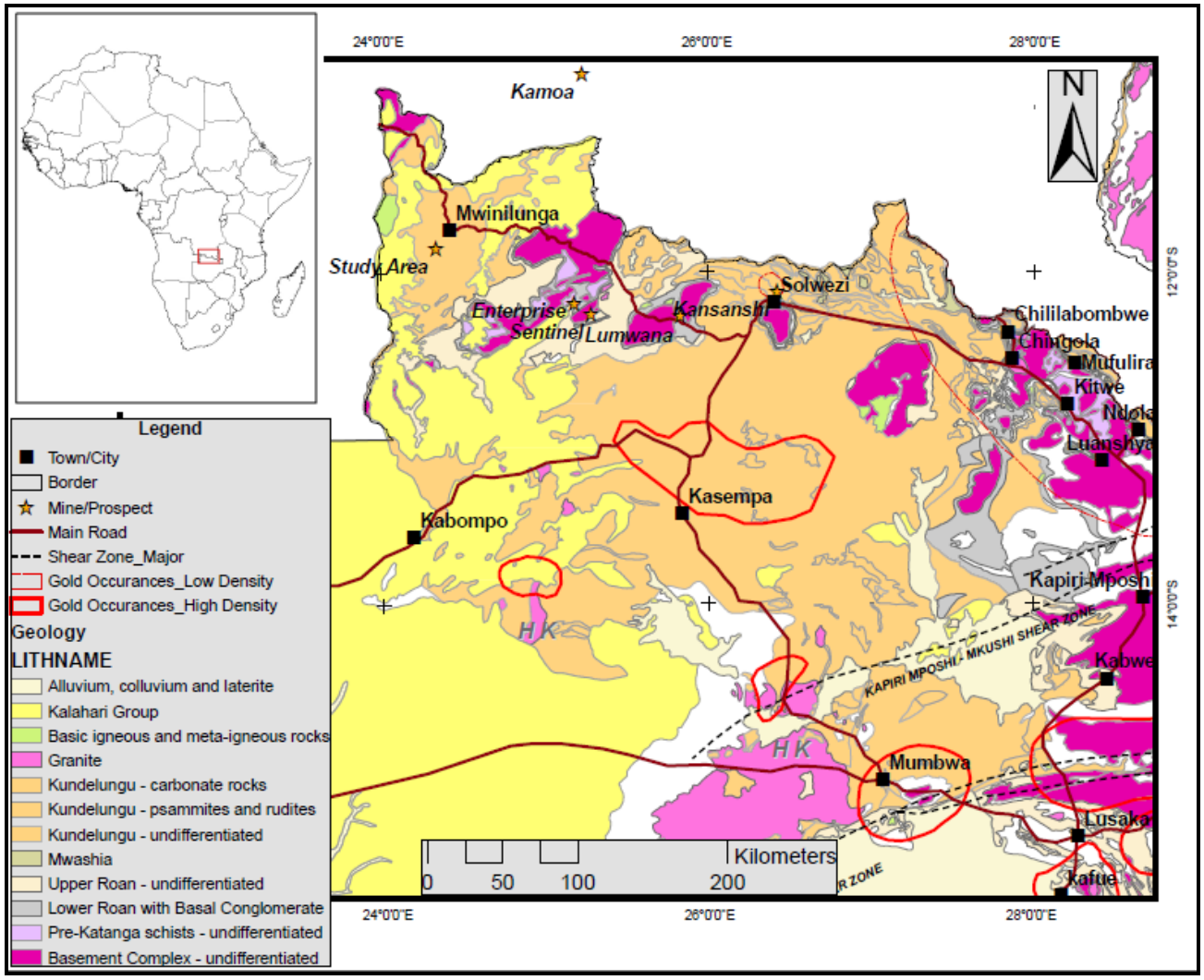

Figure 1. *Regional geology map showing units that underlie the Northwestern (NW), Copperbelt (CB) and parts of Central Province. Also shown are the locations of Mumbwa and Kasempa towns. HK = Hook granite.*

Exploration in the study area for the current project includes soil sampling, analysis and interpretation, review and interpretation of historical aeromagnetic and ground magnetic processed images, and diamond drilling.

As of June 2021, over 50 shallow diamond drill holes at varying depths of between 50 and 200 metres have been drilled, with the aim of evaluating the area for the possible occurrence of gold mineralisation in economic quantities. From these works a total of 7800 metres of borehole core were drilled. Geological core logging and structural interpretations were among some of field activities executed during the study.

1.2 LOCATION

The study area (Kasenseli Gold Prospect) lies within the Northwestern province of Zambia and is located some 20 km southwest of the Central Business District of Mwinilunga (Fig 2). It is located approximately 285 km from the provincial capital Solwezi and 900 km away from the capital city of Zambia, Lusaka. It is close to the Zambia-Angola and Zambia-Congo borders which are respectively located 50 km east and 90 km north. The area is characterised by elevations of between 1300 m and 1400 m above sea level. The overall size of the study area is approximately 1300 hectares.

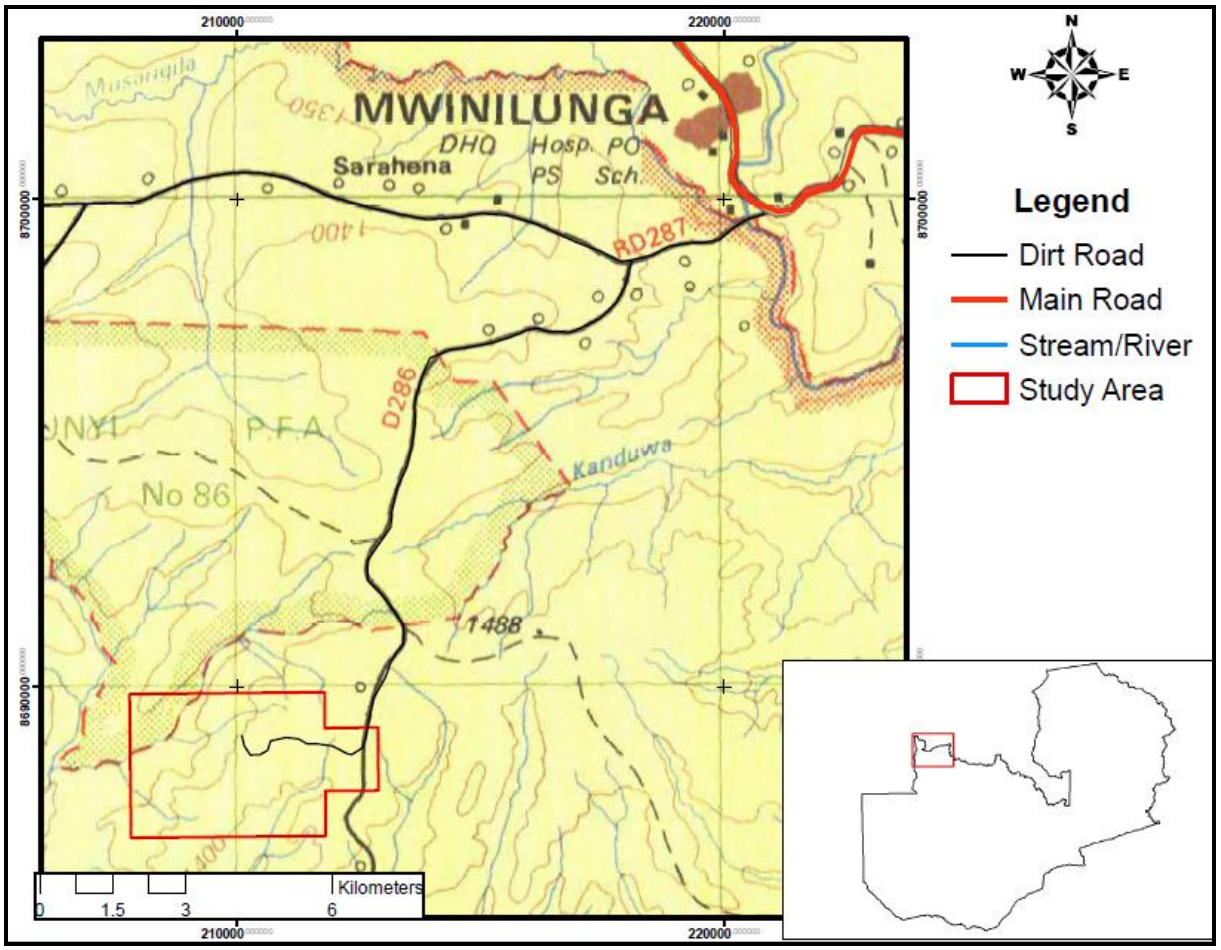

***Figure 2**. Locality Map of the study area (red box) relative to Mwinilunga Town. Coordinates in UTM Arc 1950, zone 35 south.*

1.3 ACCESSIBILITY

Access to Mwinilunga town is via the Solwezi-Mwinilunga T5 tarred road. Access to the study area is to the south via the D286 all-weather gravel road and at about 20 km from Mwinilunga, branching off at Kasenseli village heading due west using a poorly maintained gravel road (Figs 1 and 2). The D286 gravel road links Mwinilunga to Manyinga and is periodically maintained by the Government of the Republic of Zambia (GRZ). No alternative access routes exist.

1.4 PRINCIPAL OBJECTIVES OF THE STUDY

The occurrence/enrichment of gold in the Katanga sedimentary units is not a common phenomenon, therefore the presence of gold particularly in the Mwinilunga area required the establishment of the possible mineralisation controls through geological and structural interpretation, understanding the petrography with a focus on alteration and mineralisation, and interpretation of soil geochemical data with a focus on the geochemical response of the respective formations. The overall objective is to provide a geological model

for gold mineralisation in the Mwinilunga area that can be useful for future exploration work.

The principal objectives of the study are therefore;

- Review and interpret all existing historical data relating to the study area;
- Analyse and interpret soil geochemical data for the area obtained from the soil sampling campaign conducted between 2019 and 2021 with aim of establishing its implications on the current exploration model;
- Undertake petrographic studies with a focus on alteration and mineralisation on both outcrop and selected drill core samples and relate the observations to the general geology and the observed structures in the study area;
- Undertake stratigraphic correlation of the study area to some of the mines that stratigraphically sit on the same geology as the study area; and
- Do structural interpretations based on all the gathered structural and geological information, with focus on understanding the possible zones of ore deposition.
- Produce a geological model for gold mineralisation in the area.

This research report is sub-divided into six chapters which are;

Chapter 1: Is mainly the literature review and covers the introduction, regional geology and history of gold mining in Zambia;

Chapter 2: Covers the petrographic studies on the rock samples collected from the study area with emphasis on alteration and mineralisation.

Chapter 3: Covers the structural geology data and interpretation

Chapter 4: Covers the soil geochemistry acquisition, data and interpretation

Chapter 5: Provides a novel version of the geological model for gold mineralisation in the Mwinilunga area

Chapter 6, Presents the discussion and conclusion on the observations and synthesises all the collected data

1.5 METHODOLOGY

The study involved a review and analysis of recently acquired soil sampling data, detailed geological mapping, mineralogical and petrographic studies, as well as a review of historically acquired and processed aero-magnetic data, which was obtained from the Geological Survey Department of Zambia. Other tasks included the downloading and processing of satellite images for remote sensing as well as a review of geological literature for the Mwinilunga area and the greater Central African Copperbelt. Geological core logging, surface geological mapping and structural mapping were among the field activities which were undertaken as part of the data collection.

The literature review involved an examination of historical regional geological and structural information of the Zambian Copperbelt and that of the study area on a district scale. The reviewed information will be used to establish how it relates and conforms to the geology in the study area.

The mineralisation in the study area and the surrounding areas is suggested to be structurally controlled with the mineralisation associated with faults, shear zones, foliation and fold hinges. Therefore, there is a requirement to analyse satellite images, drill core samples and polished thin sections from the study area to further understand the mineralogy and structures that may have controls or may directly be related to the mineralisation in the area.

Petrographic studies have been conducted in order to establish the major lithologies that underlie the study. From the lithologies, the local lithostratigraphy of the study area is deduced and correlated to the general stratigraphy of the Zambian Copperbelt and the Central African Copperbelt in general. Some of the challenges encountered during the execution of the research include; mineralogical sample analysis as most of the collected samples from the study area were fine grained with the exception of the conglomerate subunit, this therefore required the use of QEMSCAN mineralogical analysis, however due to the cost of this analysing technique which was beyond reach, a Tescan Integrated Mineral Analyser (TIMA) was used as an alternative.

A few selected samples have been collected and analysed using a Tescan Integrated Mineral Analyser (TIMA). Analysis of samples also involved sample preparation by crushing the samples with the aim of liberating the various sizes of mineral grains contained in each sample. The crushed sample was placed in a beaker with distilled water then be allowed to settle for 24 hours, which will result in coarser material of the sample settling at the bottom and finer particle at the top. The collected graded sample will then be vacuum dried and fused into a bead, which was analysed using TIMA. TIMA analysis is able to give the full mineral composition, the only shortfall in this case is that it involved a destructive approach of sample preparation which entails that grain relationship cannot be fully ascertained. Mopani mineralogy laboratory was only able to offer destructive preparation of mineralogy samples based on the current set-up of the TIMA analyser, which has been set-up to analyse a fused bead. The destructive sample approach also ensured full liberation of all the minerals contained in the sample

Soil geochemistry involved a statistical review of the assay data with the aim of identifying potentially mineralised zones for gold and copper whilst also trying to establish if copper, cobalt, molybdenum, and zinc can be used as pathfinder elements to gold mineralisation in this area. Statistical methods were employed in distinguishing the normal background assays from the potentially mineralised zones, which are potential drilling targets for future exploration work. Use of pXRF for the identification of cobalt at low levels was difficult due to spectral interference from the iron and nickel, hence the only reliable analytical approach is via wet chemistry analysis, which proved reliable.

1.6 REGIONAL GEOLOGICAL SETTING

Zambia is generally made up of diverse geological environments which range from Neoarchean to Paleoproterozoic cratons to structurally complex mobile terranes to recent Kalahari or Quaternary cover (Fig.3). Based on the age relations, the rock units that underlie different parts of Zambia can be subdivided into four major lithostratigraphic groups with their related structural terranes. The oldest rock units are the basement complex which comprises deformed igneous and metamorphic rocks and these are mostly exposed in eastern and southern Zambia as well as in the dome areas in the Northwestern province. Overlying the Basement rocks are the Muva Supergroup units comprising a sedimentary and metasedimentary sequence mainly exposed in Eastern, Northern and Southern Zambia with their deposition occurring between post Ubendian (2050 -1800 Ma) and pre-Irumide (1300 – 1100 Ma) events (Daly and Unrug, 1982). Overlying the Muva Supergroup are a Precambrian to Cambrian aged, thick sequence of sedimentary units known as the Katanga Supergroup, which have been affected by the Pan-African Orogenic events. The older geological units are overlain by relatively undeformed Karoo units which cover much of western Zambia and rift valley areas in Southern and Eastern Zambia. Kalahari and Quaternary sediments conformably and unconformably overlie various geological units, and these are more pronounced in the western and north-western parts of Zambia.

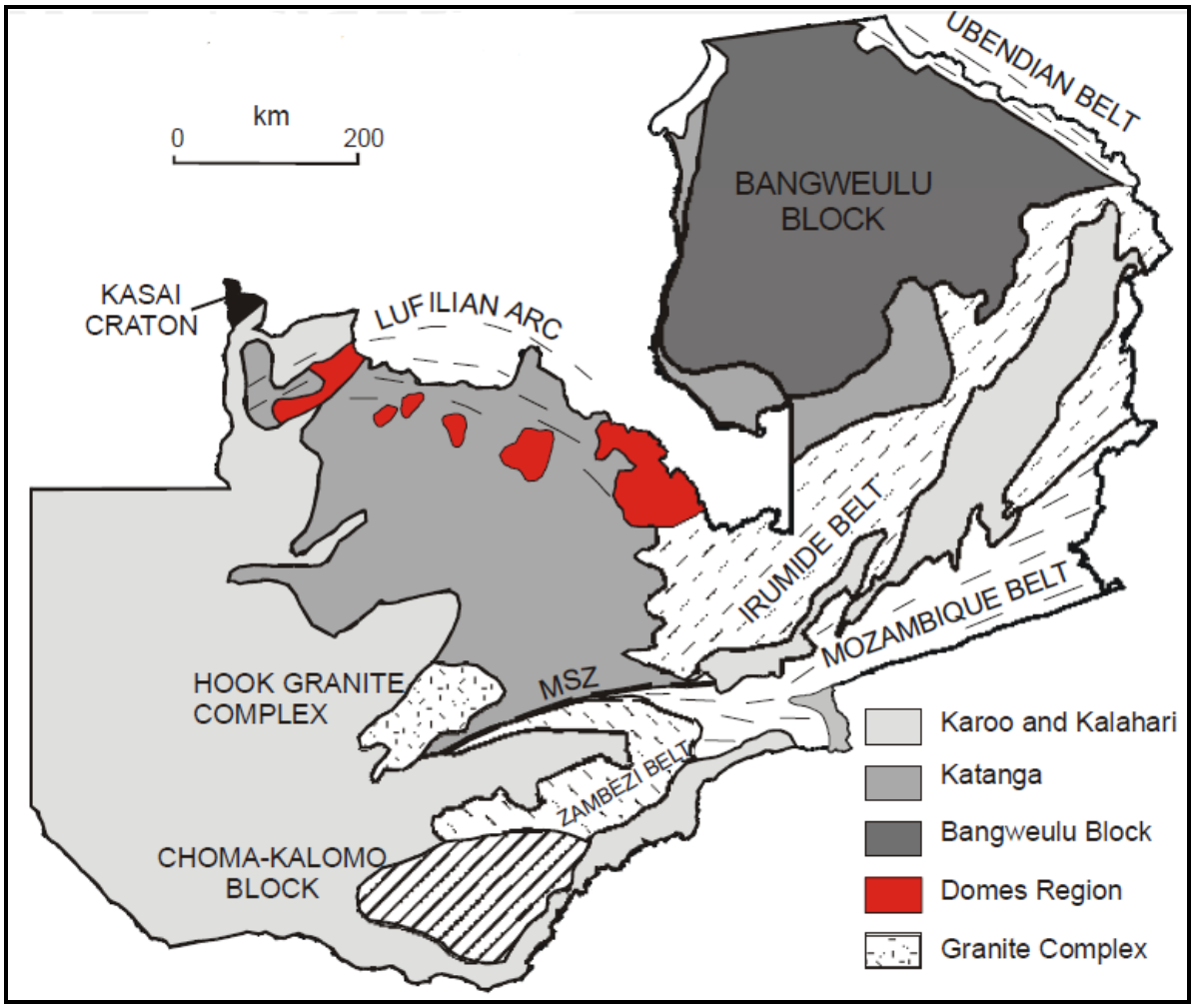

Figure 3. *Simplified Geology Map of Zambia with major structural terranes. After, Coats et al., (2001).*

Of major exploration interest, are the Katanga Supergroup rocks of the Central African Copperbelt (CAC), particularly those that underlie the areas that geographically cover the Copperbelt Province, Northwestern Province and Central Province in Zambia and Southern parts of the Democratic Republic of Congo (DRC) (Mendelson, 1961; Fleischer, 1976; Cailteux et al., 2005b). The Katanga strata are the traditional host to the world class copper and /or cobalt mineralisation. Apart from hosting the copper and cobalt, the CAC is also a host to other important commodities including U, Pb-Zn, Au and Ag.

The CAC hosts one of the largest concentrations of copper and cobalt in the world, accounting for more than 50% of the mineable cobalt globally. Among the major world-class deposits with ≥ 10 Mt Copper include Nchanga, Mufulira, Nkana in Zambia and Tenke Fugurume, Kamoa and Kolwezi in the DRC (Hitzman et al., 2005; Kampunzu and Cailteux, 1999; Selley et. al., 2005; Schmandt et al., 2013). With the inclusion of previously sub-economic orebodies (Cu content greater than 1% weight), the total amount of copper contained in the Katanga basin of CAC is close to ~140 Mt and 6 Mt cobalt, Cailteux et al., (2005) for DRC and Freeman, (1988) for Zambia.

Copper and cobalt deposits on the Zambian Copperbelt are sediment-hosted and stratiform in nature with most of them occurring along stratigraphic and / or structural redox boundaries. This implies that for the copper deposits to form, an oxidised metal source in form of red beds, is leached by saline fluids, the metals are transported in the brines, and precipitated in metal traps such as in reducing carbonate and shale units (Hitzman et al., 2005; Hitzman et. al., 2009;). Orebodies in the CAC mainly comprise disseminated sulphides hosted in fine-grained carbonate or siliciclastic Katanga sedimentary units.

The CAC occurs within an arcuate shaped structural feature known as the Lufilian Arc Fold and Thrust Belt (LAFTB) which geographically stretches from Lonshi in the southeast through to Luanshya (Roan basin) to Kolwezi in the north through to Mwinilunga in the west, covering the Copperbelt and Northwestern Provinces of Zambia, parts of the southern DRC and Eastern parts of Angola (Fig. 4). It has an approximate length of 600 km with an estimated width of 150 km (Porada and Berhost, 1998). Relative to the major cratons in the region, the LAFTB is bounded by the Bangweulu Block to the northeast, the Congo Craton to the north and the Kalahari Craton to the south. The LAFTB is Neoproterozoic to lower Paleozoic in age 900 – 450 Ma, (Porada and Berhost, 2000), with deformation occurring during the Pan-African Damara-Lufilian orogeny which lasted between ~590 to 450 Ma (Daly et al., 1984; Master et al., 2005; Selley et al., 2005).

With regards to deformation mechanisms of the LAFTB, local kinematics indicate a northly directed thrust trend with the metamorphic facies also decreasing in the northly direction (Cailteux et al., 2007). The Zambian side is characterised by greenschist to amphibolite facies with the Congolese side having lower greenschist to unmetamorphosed facies.

1.6.1 STRATIGRAPHY AND MINERALIZATION

The underlying geology in the Zambia Copperbelt (ZCB) and some adjacent areas in the southern parts of DRC, are the Katanga rock units with Pre-Katanga Palaeoproterozoic basement inliers such as the Kafue anticline and the Domes Region of Northwestern Provinces of Zambia (Unrug, 1983; Daly et al., 1984; Cosi et al., 1992). The core of these basement rocks is thought to be a representation of deeper occurring thrust ramps in the Kafue Anticline (Porada and Berhorst, 2000).

The Katanga sedimentary sequence is estimated to be between 5 and 10 km in thickness and comprises three major lithostratigraphic subdivisions namely the Roan Group, the Nguba Group and the Kundelungu Group (Mendelson; 1961; Francois, 1974, 1995; Cailteux et al., 2005, Bull et al., 2011) (Table 1).

Table 1. *Stratigraphy correlation chart between the greater Central African Copperbelt and the Western Copperbelt which covers the Mwinilunga area in Northwestern Zambia. (After, Key and Banda, 2000; Liyungu et Al.,2000; Cailteux et al., 2007; Torremans et al., 2013).*

Supergroup	Group	Subgroup	Formation	Age (Ma)	Thickness	Lithologies (Copperbelt -Nchanga, Nkana, Konkolab)	Lithologies (Western Copperbelt - Mwinilunga area)	Events (Western Copperbelt - Mwinilunga area)
Katanga	Kundelungu	Not well defined in ZCB		±500	Unknown but considered to be relatively substantial	Arkoses, conglomerates, sandstones, shales	N/A	
							N/A	Part of the Pan-African orogeny that produced the fold and thrust pile in LAFTB
				±620		Petit Conglomerate (Glacial diamictite)	N/A	
	Nguba	Not well defined in ZCB		±735	Unknown	Dolomites & dolomitic shales	Dolomitic siltstones, shales & calcareous siltstones. (underlying Andestic basalts dated 735 Ma)	Volcanism within nguba strata
			Kakontwe			Carbonates	?? Massive dolomitic limestones	
				±750		Grand conglomerate (Glacial Diamictite)	Diamictites (of shale & siltsones with extraclast disseminations)	Deposition of sediments in Glacial-marine environment (Sturtian Glaciation)
	Roan	Mwashia	Mwashia Shale	±765	~600	Dark/ black Carbonaceous shales, dolomitic shales, arenites & arkoses	?? Siltsones, shales, shale with mudstone, volcaniclastic sediments (WF) (underlying Andesites dated 765 ± 5 Ma),	Creation of large volcanic edifice along westerm margins of Katanga member units (Mwashia Group). Possible emplacement of the north trending dykes
		Kirilabombwe			~800	Dolomites & dolomitic siltstones, gritty shales		
		Kitwe	Chingola (Pelito Arkosic)		~1000	Dolomites, sandstones, argillites beds		
			Oreshale			thinly bedded siltstones & Carb sandstones		
		Mindolo Clastics	Mutondo			Conglomerates, coarse arkoses, arkosic sandstones	?? Arkoses & conglomerates	
			Kafufya			Arkosic quartzites & Sandstones	?? Arkosic quartzites, siltstones, Flaggy siltstones & basal quartzite	
			Chimfunshi	< 900 Ma		Pebble & Cobble conglomerate		Beginning of Roan sedimentation on crystalline rocks of the Kasai Shield (not dated)
Pre-Katanga				±2050 - 1870 Ma, 2560 Ma		Gneissic, granitic and schistose basement rocks	Migmatites & granitic rocks, associated with felsic magmatism (2560 Ma)	Major intrusion of granites and minor leucogranitic dykes (members of Kasai Shield).

In the ZCB, the Roan Group is subdivided into three lithostratigraphic groups; the Lower Roan which consists of clastic rich sedimentary lithologies; overlain by the Upper Roan and Mwashya, with the Upper Roan dominated by carbonate, -evaporite and breccia lithologies; with the Mwashya comprising a succession of siltstone-shale units.

Overlying the Roan Group are the Nguba and Kundelungu Groups in which the lower boundary of each of these successions of units is respectively characterised by a chronostratigraphic basal marker, known as the Grand Conglomerat in the Nguba sequence and the Pétit Conglomerat in the Kundelungu Group (Cailteux et al., 2005; 2007; Wendorff and Key, 2009). These conglomerate markers are interpreted to be of glaciogenic origin (Key et al., 2001; Hitzman et al., 2009).

On the traditional Zambian Copperbelt, which geographically covers the Luanshya, Ndola, Kitwe, Mufulira, Chingola, Chambeshi and Chililabombwe deposits (Fig. 4), mineralisation is mainly hosted in the Roan Group of the Katanga Supergroup. Larger world-class deposits are hosted in the ore-shale unit of the Lower Roan subgroup namely at the Nchanga, Konkola, Roan, Chambeshi and Nkana deposits (Mendelson, 1961; Fleischer, 1976; Freeman, 1988). At Mufulira the orebody is hosted both in the ore-shale formation and the hanging wall arenites. Footwall-hosted deposits relative to the ore-shale include Chibuluma East, Chibuluma West and Chifupu deposits and minor deposits that occur south and southwest of the Nchanga deposit which include the Mimbula, Chingola orebodies and Fitwaola (Annels and Simmonds, 1984; Woodhead, 2013). The Kansanshi copper-gold deposit is hosted higher up in the stratigraphic sequence, within the Nguba group. The Kalumbila deposits (Sentinel and Enterprise) are stratigraphically correlated to the traditional Copperbelt deposits and are hosted in the Roan Group (Halley et al., 2016). Minor vein-type copper mineralisation has been reported within the basement rocks. (Mendelson, 1961; Fleischer, 1976; Freeman, 1988; Halley et al., 2016).

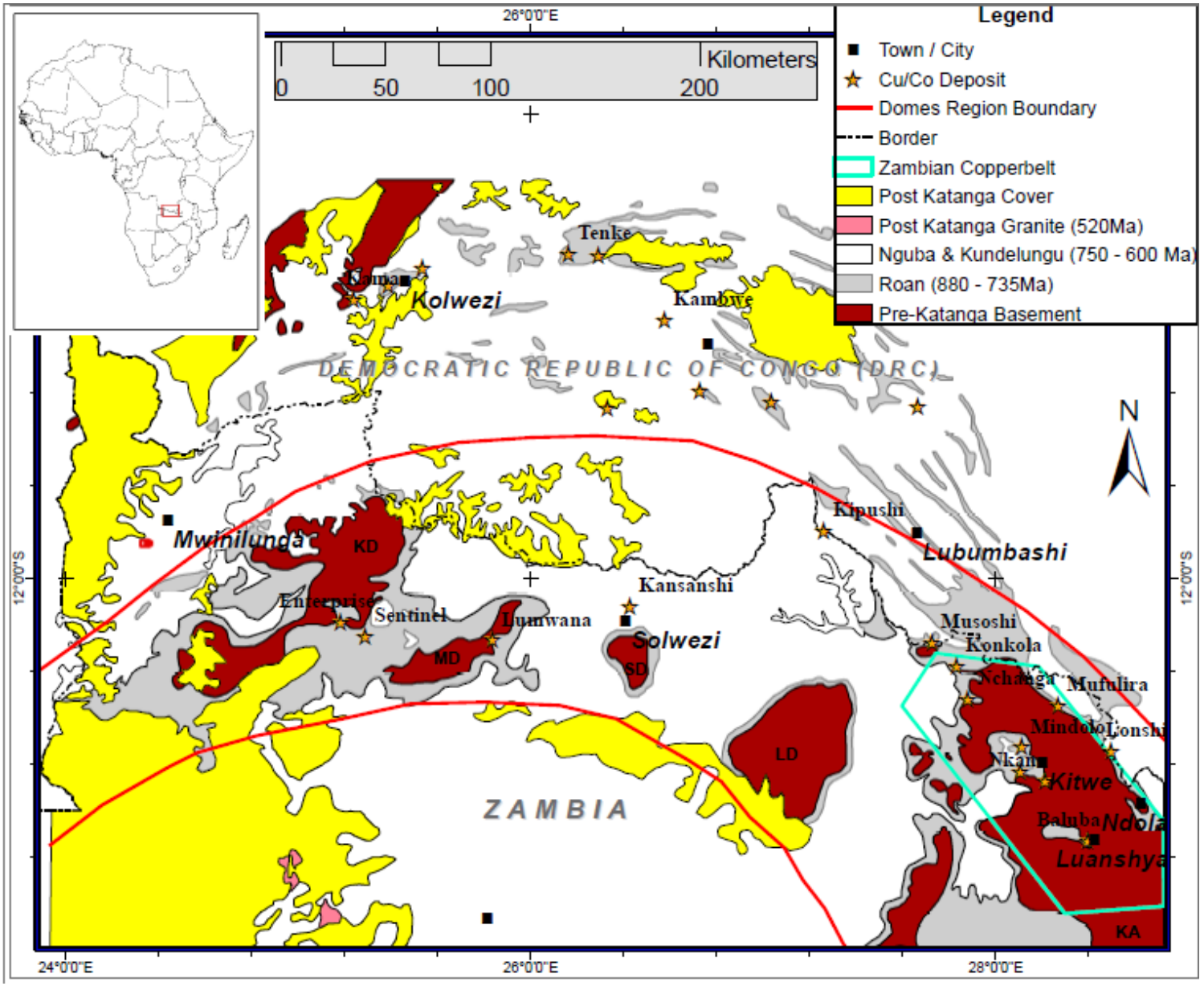

***Figure 4**. Generalised and simplified geological map of the Central African Copperbelt covering Zambia and DRC. (KD= Kabompo Dome, MD=Mombozhi Dome, SD = Solwezi Dome, LD = Luswishi Dome and KA = Kafue Anticline). Modified after Cailteux et al., 2005; Hitzman et al., 2012.*

1.6.2 REGIONAL GEOLOGICAL SETTING – MWINILUNGA AREA

The study area lies within the LAFTB and is located on the western end of the external fold and thrust zone which is part of the western extension of the Zambian Copperbelt (Fig. 5). The greater Mwinilunga sheet /area is bounded by UTM coordinates 340,000 mE to 170,000 mE from east to west and 8,780,000 mN to 8,670,000 mN from north to south.

Based on the location in which the rock units occur and / or are exposed, the oldest known rock units in the Mwinilunga sheet include the gneisses, migmatites and mafic dykes and intrusions which cover the extreme northwest of the Mwinilunga sheet and its surroundings northwest of the Kalene Hill, which is located 80 km northwest of Mwinilunga town. These have been dated as Neoarchean in age (2550 Ma) (Key et al., 2000) and occur within the Kasai shield which is part of the Congo craton (Cahen et. al., 1984; Key and Banda, 2000).

The Eburnean granites which are typically porphyritic and, in some cases, equigranular, leucocratic and variably coarse-grained are also exposed around the Kasai shield area. These are best exposed at the Zambezi rapids in the Kalene Hill area. Doleritic to dioritic stocks and dykes as well as minor leucocratic granites also occur around the pre-Katanga basement. The Kabombo Dome is characterised by pre-Katanga Paleoproterozoic-aged migmatitic, gneissic and granitic rocks with associated schists which form the core of the dome which are rimmed by basal Neoproterozoic Katangan units (Thieme and Johnson, 1981; Halley et. al., 2016). The Kabompo Dome area is host to a number of economic deposits which include Kalumbila-Sentinel (Cu) and Kalumbila-Enterprise (Ni-Cu-Co) (Fig. 4) as well as other smaller prospects like Mujimbeji and Kalaba which are currently being explored for copper and other base metals.

The broader part of Mwinilunga is underlain by Katanga strata though these units are poorly exposed in this area (Fig. 5). To the northwest, the area is covered by Katanga units which occur as platform sediments with a mappable extrusive igneous unit, unconformably overlying the Kasai shield within the tectonic terrane known as the Western Foreland (WFL) to the Lufilian Arc. The contact between the basement and the Katanga is denoted by a basal conglomerate which outcrops in the Kalene Hill escarpment (Key and Banda, 2000). The Katanga units in the WFL are weakly deformed and it is therefore possible to correlate the units within this area within the broader Katanga stratigraphic units elsewhere.

The Katanga units elsewhere in the Mwinilunga area are deformed particularly in the Lufilian Arc. Around the Kabompo Dome, the basal Katanga strata form a rim over the basement rocks and in this area the Roan member of the Katanga units correlates to Katanga units elsewhere in NW Zambia (Mulela and Seifert, 1998). The basal Katanga units are thrust in the northwestwardly direction over extensively deformed units of the outer fold and thrust belt which is also covered by some younger Katanga units including those from Kundelungu. The fold and thrust belt is expressed as the Kakoma – Kamano thrust belt (Fig. 5).

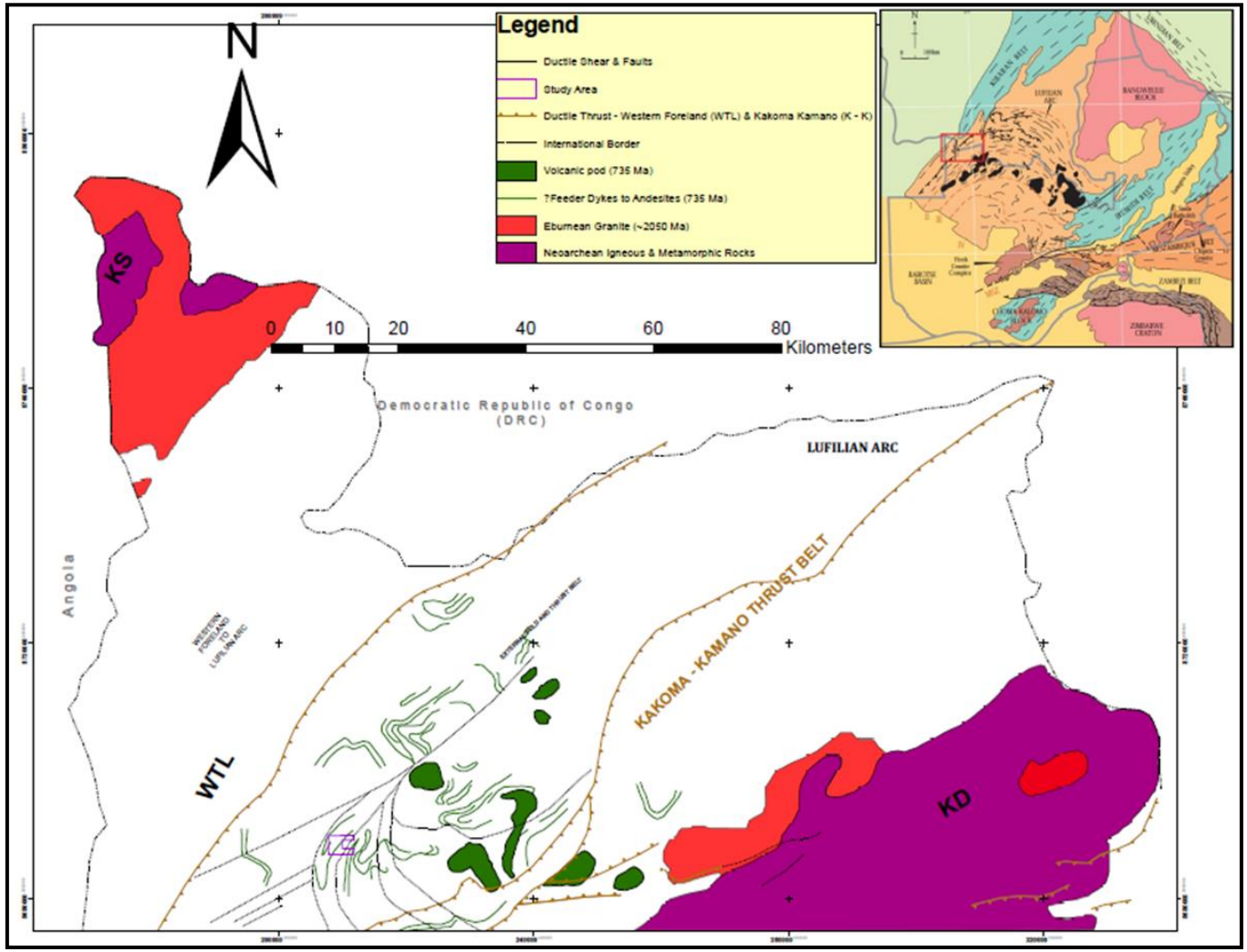

Figure 5. *Map showing the regional geological setting in the Mwinilunga area. KS = Kasai Shield, KD = Kabompo Dome and WTL = Western Foreland. After Key et al.,2001; Key et al., 2004. Insert showing structural terranes in Zambia, (Porada and Berhorst, 1998).*

1.6.2.1 REGIONAL STRUCTURAL SETTING

The area covering the Mwinilunga area is subdivided into four terranes based on the regional structural features and metamorphism. The four terranes are the Kasai Shield, the Kabompo Dome, the Western Foreland and the Lufilian Arc (Fig. 5). Covering the northwestern part of the Mwinilunga area is the Neoarchean to Paleoproterozoic Kasai Shield which is unconformably overlain by the Katanga units of the Western Foreland (Key et al., 2004). The area in the southeastern far end of the Mwinilunga area is underlain by the Kabompo Dome which is comprised of pre-Katanga basement inliers enveloped by basal Katanga strata. The Lufilian Arc is made up of extensively deformed Katanga units and these are represented by pronounced interference folds related to the ductile shearing and thrusting (Liyungu et al., 2000).

1.6.2.1.1 THE KASAI SHIELD (KS)

One of the most significant structural components of the Kasai Craton / Congo Craton is the pronounced curvilinear imbricate thrusts which act as the boundary between leucogranites and migmatites and the NE-trending shears which are considered to be younger (Cahen et. al. 1984; Key et al., 2001). Rocks which are part of the Congo/Kasai Craton outcrop in the northeastern corner of Mwinilunga area/sheet, hence form the Kasai Shield (Fig. 5).

On outcrop scale, the imbricate thrust impressions are represented by an easterly moderately-dipping, strong foliation. However, in one locality particularly on the foot of the Kalene hill escarpment, the exposed foliation is characterised by an E-W trend and steeply dipping in the northerly direction (Key and Banda, 2000). NE – oriented shear structures are poorly exposed but can be picked out using high resolution aeromagnetic mapping. Discontinuities like fractures and faults which have a NE-SW trend are signified by linear streams as well as brecciated silicified zones. Sinistral movement of faults is indicated by markers in some of the major structures like minor offset movements in veins as well as the orientation of the fillings in some of the quartz veins. Both the thrusting and shearing are older than the sediment deposition of the Katanga strata, though the age of both events relating to these respective activities is not clearly understood (Porada and Berhorst, 2000; Liyungu et al., 2001).

1.6.2.1.2 KABOMPO DOME (KD)

The core of the Dome is characterised by discordant amphibolite bodies in migmatites with a steeply dipping gneissosity and foliation. The younger Katanga units form a carapace around these older basement rocks. The early gneiss-forming events for the core of the basement are considered to be of amphibolitic facies (Klink, 1977; Appleton, 1978). On the southern margin of the Dome, the underlying basement includes gneisses as well as biotite-phlogopite-muscovite schists which are overlain by Katanga strata comprising Lower Roan through to Nguba (Kakontwe) units (Mulela and Seifert, 1998). These were all intruded by a gabbro-syenite complex at 735 Ma (Halley et al., 2016).

1.6.2.1.3 WESTERN FORELAND (WFL)

In the Western Foreland, the Kasai Shield is unconformably overlain by Katanga units which either gently dip southeastwards or are sub-horizontal with dip of the bedding increasing in the southeast direction towards the Lufilian Arc (Key and Banda, 2000). Minor deformation of bedding has been observed in larger outcrops particularly those around Kalene Hill summit where a gentle syncline has been observed (Urug, 1983; 1988). Katanga rock units within the Western Foreland are essentially unmetamorphosed (Key and Banda, 2000; Key et al., 2004).

1.6.2.1.4 LUFILIAN ARC (LAFTB)

Katanga units in the Lufilian Arc Terrane have been affected by two major deformation events (D1) and (D2) tectonothermal deformation episodes. These tectonothermal events are not precisely dated but are considered to have occurred between end Neoproterozoic to early Paleozoic (between 645 Ma and 513 Ma) with the main deformation taking place between 560 and 550 Ma (Porada and Berhorst, 2000)

Events pertaining to the first deformation (D1) are linked to the folding which is associated with the thrusting and ductile shearing which gave rise to NE-SW to ENE-WSW structural impressions observed within the terrane (Liyungu, et. al., 2001; Key et al., 2001).

The second deformation (D2) resulted in the formation of open interference folds with related foliation structures, whilst older folding structures which were initially represented by bedding were refolded. Folds with curvilinear fold axes display axial trace trends of ~N to ~NE to ~NW and with varying plunges that are sub-horizontal to moderately dipping in a southward direction.

1.7 GOLD MINING AND ITS OCCURANCES IN ZAMBIA

A number of gold occurrences have been reported in Zambia some of which have been exploited through artisanal or small-scale mining operations. Gold occurrences in Zambia range from alluvial to hydrothermal hard-rock vein-hosted to placer gold (Fig. 6) and these occur in different respective geological terranes (Andrews-Speed, 1984; Watts et al., 1991; Coats et al., 2001).

Historically, one of the earliest known gold discoveries in Zambia was at the Luiri Gold Mine which is part of the Mumbwa gold district (Fig. 6). It is located 30 km southeast of Mumbwa central business district. Luiri (historically referred to as the Dunrobin deposit) was discovered in 1925 by Rhodesia Minerals Concession Limited and between 1928 and 1961 an estimated 37,000 ounces of gold with an average grade of 10g/tonne was mined from this area. The Luiri deposit lies within the Matala Dome, an anticlinal structure with an ENE trend with the Domes surrounded by younger carbonate and siliciclastic Katanga units. Three mineralisation styles have been recognised which respectively include disseminated replacement skarn type ore, pyrite-rich quartz-tourmaline breccias and quartz-pyrite veins with an ENE trend (Naydenov et al., 2015).

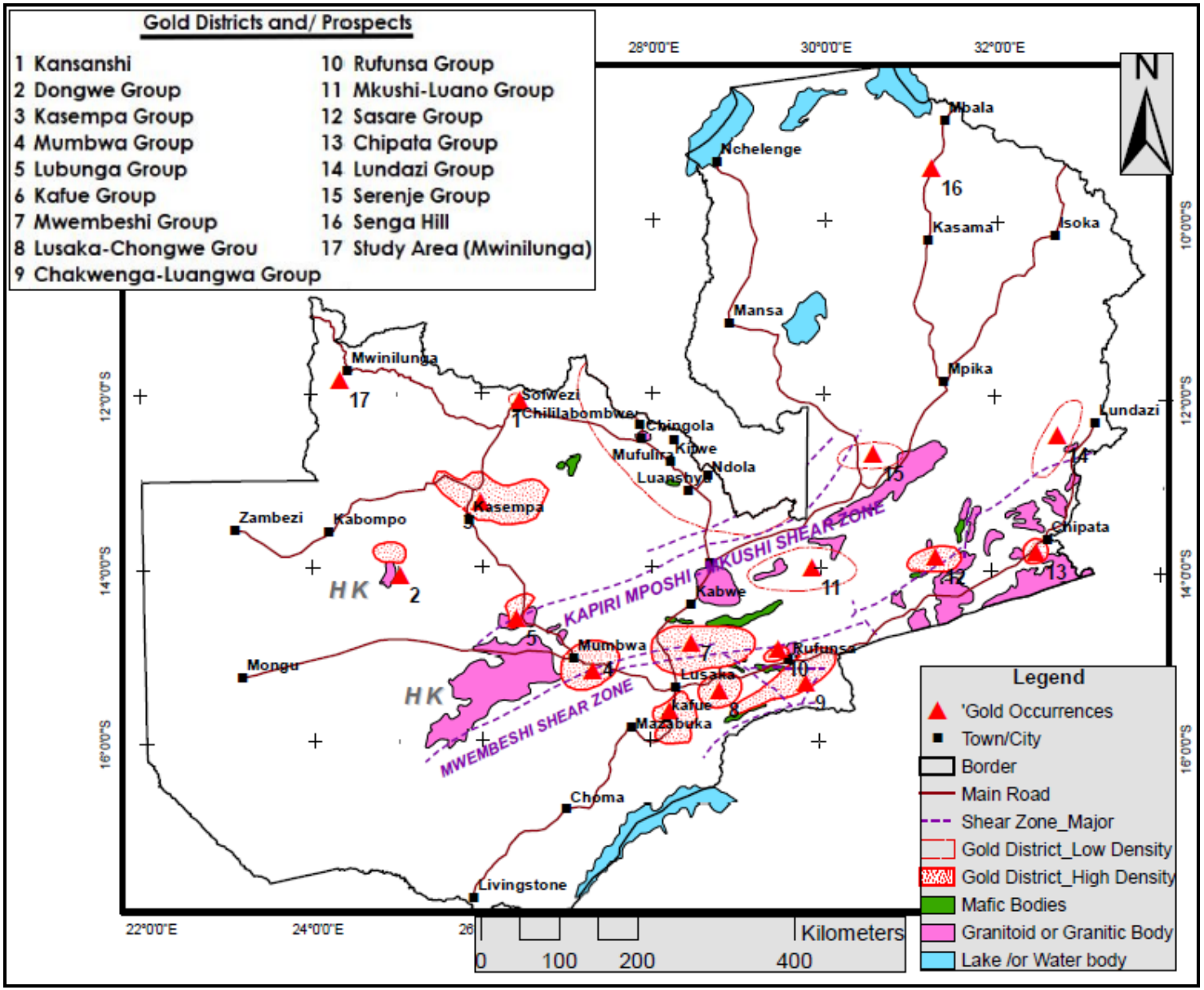

***Figure 6**. Schematic map showing the distribution of hydrothermal and alluvial gold occurrences in Zambia. (Modified after Guernsey, (1941), Reeves, (1963); Andrews-Speed et al., (1984); Andrews-Speed et al., (1986); and Coats et al., (2001)).*

Another mine with notable production is Iron Cap Mine which is part of the Mwembeshi group of gold occurrences (Fig. 6), it is located approximately 65 km southeast of Kabwe town. From this mine, an estimated 38,431 ounces of gold were produced between 1950 and 1961 (Reeves, 1963; Freeman, 1988; Coats et al., 2001).

Under the Ndola Smelter Company owned by the now defunct Zambia Consolidated Copper Mines (ZCCM), gold, silver and selenium were produced from the reprocessing of copper slimes which were collected from copper smelting (Watts, et al., 1991; ZCCM Ltd Annual Production Reports for the period 1984 to 1997). The gold recoveries from the copper production with the grade range of between of 0.3 to 0.5 g/t for every 1 tonne of copper produced revealed an in-situ occurrence of 10 ppb of gold. Based on the official production numbers obtained from ZCCM-IH Mining Archives, around 1250 kg of gold was produced between 1984 and 1997 (Ndola Smelter Company Annual Production Reports for Precious Metals, for the period 1984 to 1997).

Currently the largest producer of gold in Zambia is the Kansanshi Copper-Gold Mine which is located in Solwezi. In 2001, the Kansanshi deposit had an in-situ resource of around 267 million tonnes with average grades of around 1.28% Cu and 0.16 g/t Au which equates to 3.4 million tonnes contained copper and 1.4 million ounces contained gold (First Quantum website http://www.first-quantum.com/, May 2001). A significant part of this resource has since been mined out. The gold occurs with the copper mineralisation and is both vein and sediment hosted within the Nguba Group units of the Katanga Supergroup. It is mined as a co-product of the copper and their estimated production numbers are around 350 kg per month with an estimated annual production of around 4.0 tonnes of gold bullion (SEDAR, Annual Information Form for First Quantum Minerals, for 2019 and 2020 respectively).

Other small-scale to artisanal sized mines have existed and still exist within Zambia, however no historical or current production records are available. Location-based gold districts in Zambia include: the Mumbwa group which has over ten gold occurrences (Fig. 6) and prospects and is of significant importance with regards to gold mining in Zambia (Reeves, 1963; Freeman, 1988; Coats et al., 2001); the Lusaka-Zambezi group which covers the areas such as Chainama, Chongwe, Chinyunyu and Rufunsa and has over fifteen gold occurrences and prospects some of which include historically producing small-scale mines such as Jessie Mine, Chumbwe Mine and Chakwenga Mine; the Kabwe group with over five gold occurrences and prospects and includes historical small-scale gold mining operations such as Iron Cap Mine; the Mkushi-Serenje-Mbala group with over ten gold occurrences and prospects and includes previously producing small-scale mines such as Velocity Mine and Chetina Mine; the Petauke-Chipata-Lundazi group with over ten gold occurrences and prospects and includes previously producing small-scale mines such as Sasare Mine; the Mumbwa-Kasempa group with over eight gold occurrences and prospects (Freeman, 1988; Watts, et al., 1991; Coats et al., 2001) and includes recently discovered prospects such as Katoka-Mema and the Mwinilunga area which encompasses the study area. Some of the stated historical mines and prospects are currently being worked or reworked.

Some of the gold occurrences in Zambia occur in proximity to either granitoids or granitic bodies, or around basic igneous bodies with the presence of regional and district scale dislocation zones as a major controlling structural feature on the location of these gold occurrences (Fig. 6). Gold mineralisation has been observed around the Mwembeshi inter-cratonic shear zone, with most deposits and occurrences spread around this northeast-southwest striking shear zone. Also, north of the Mwembeshi Shear Zone is the Kapiri Mposhi – Mkushi shear zone which is parallel to the MSZ, with a number of gold occurrences hosted within this zone, which include the Hippo deposit in the Mumbwa area (southwest end of the shear zone) and Chetina Mine in the Mkushi area (northeast of the shear zone). In the Mbala area, placer gold mineralisation hosted in the conglomerate formation within the Mporokoso basin has been likened to the Wits basin type of placer mineralisation in South Africa (Unrug, 1984; Andrews-Speed, 1986; Andrews-Speed, 1989). The comparison is based on the depositional set-up and observed mineralisation like conglomerate hosted gold and uranium enrichment, typical in Witwatersrand basin, though the sediments in this basin are much younger (1800-1100 Ma) than those of the Wits basin (3000-2600 Ma).

Between the mid and late 1990's Anglo America Corporation Central Africa Limited undertook exploration works in Mwinilunga area, around Luamata copper-cobalt prospect which lies in proximity to the study area and has similar geological set-up. Around 58 samples were collected from the Luamata prospect and analysed for gold. Of these, only four showed indications of gold. A further 41 samples were collected and analysed using fire assay, and only one gossan sample returned grades of around 0.85 g/t (Steven, 1995; Anglo America, 1997).

CHAPTER TWO

LOCAL GEOLOGY

Detailed surface geological mapping was among the techniques which were executed prior to commencement of soil sampling and test drilling work. It involved synthesis and refining of existing regional geological mapping information as well as use of remote sensing images to identify possible lithological boundaries and geological structures prior to field mapping.

2.1 GEOLOGY OF THE STUDY AREA

Three main lithological units are present within the study area; the Roan member shale unit (RS); the arkosic sandstone (AS) and its related sub-units which occur as lenses within this main unit; a diamictite unit, the Grand Conglomerat (GC); and the Nguba member shale (NS) which is interbedded with siltstone. The general strike of the rock units in the area ranges between 110^0 and 180^0 i.e., strike orientation of NE – SW (Fig. 7) and are characterised with gentle to steep dips (20^0 - 85^0) (see Appendix-3 for structural measurements). A simplified geological model for the area is shown in appendix-5.

The stratigraphic identification of these units is based on their relationship to the Grand Conglomerat, which is the accepted reference stratigraphic marker unit between the Roan and the Nguba Groups. It marks the end of Roan sedimentation and the beginning of Nguba sediment deposition (Cailteux et al., 2005; Sillitoe et al., 2010).

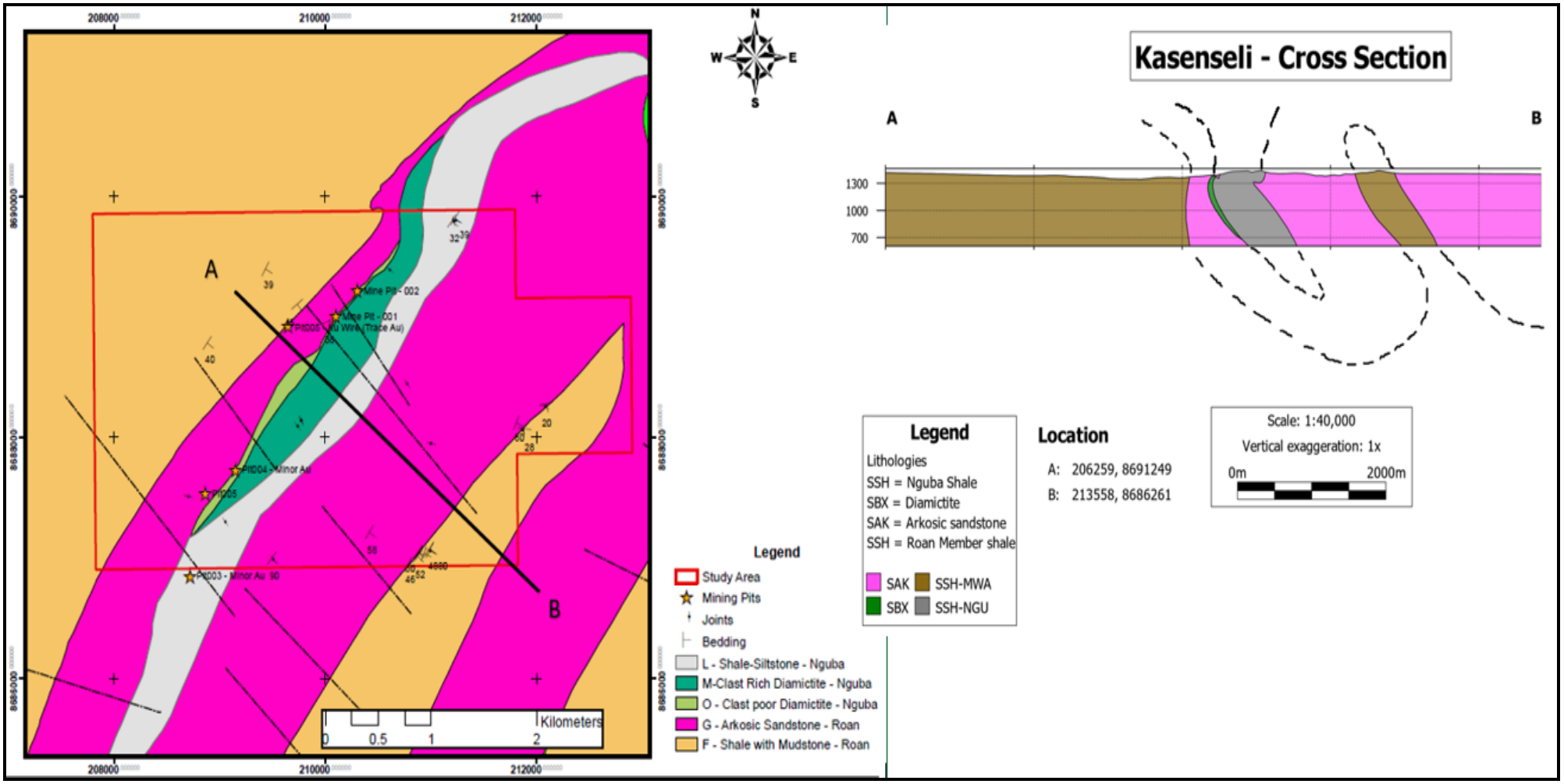

Figure 7. *Geological Map and cross section along A-B, showing the various lithologies and rock units that underlie the study area; brown- Roan shale, pink- Arkosic Sandstone, green – diamicite and grey – Nguba shale. Simplified 3-D geological model for the area is given in Appendix-5a and 5b.*

2.1.1 Roan Member shale unit (RS)

On outcrop scale, the Roan Member shale unit is typically massive, well bedded and/or laminated, pale green to grey in colour, and weathers to a yellowish-green saprolitic soil (Fig. 8a and 8b). It covers the extreme northwestern and southeastern of the study area. In hand samples the discernible mineralogy is mainly clays and quartz with the rock-forming clay minerals altering to chlorite plus limonitic alteration which gives it a characteristic pale green to yellowish-green colour when weathered (Fig. 8a). Minor muscovite flakes are also diagnostic in weathered outcrops of this unit. No sample was collected for mineralogical studies as most of the outcrop samples were strongly weathered. No exploration drill holes have been drilled in this area either as most of the exploration drilling works were concentrated around the Nguba units, on the contact areas between the Nguba and Roan units.

Figure 8. *Exposure of the Roan shale in an exploration trench showing (a) weathered saprolitic shale with FeOx alteration (b) weathered saprolitic shale in historical exploration pit at location UTM Arc 1950 Zone 35 South 208912mE/8688760mN with relics of bedding.*

2.1.2 Arkosic Sandstone (AS)

The arkosic sandstone unit (AS) is pinkish-brown to grey and commonly weathers to purplish-brown loose saprolitic soils, it is fine to medium grained (gritty as well as silty in some zones) and is characterised by lenses or discrete zones of ferruginous mudstone and shale which have varying thicknesses around 0.5 m to 5.0 m. The arkosic sandstone varies in sorting, ranging from poorly sorted to well sorted, with the unit observed to be coarsening upwards shown by the presence of gritty arkose and conglomerate in the upper zone with finer grained and well laminated arkosic sandstone and ferruginous mudstone lenses in the lower zones. The major mineralogy in hand specimens of the arkosic sandstone is quartz, orthoclase and calcite as the cementing material (Fig. 9a).

On a microscopic scale, sample L04032 of arkosic sandstone and quartz vein was found to comprise quartz, albite, biotite, orthoclase and calcite with minor specular hematite (Fig. 9b

and 9c). Sample L04032 was also analysed using destructive preparation of the sample and mineralogical analysis using a Tescan Intergrated Mineral Analyser (TIMA) at Mopani Copper Mine Mineralogy laboratory in Kitwe, Zambia. This analysis was able to give both a quantitative and qualitative composition of the rock samples collected from the study area.

Sample L04032 contains 43% quartz, 47% feldspars and 10% lithics which clearly confirms the unit as an arkosic sandstone based on the feldspar content, though the presence of the quartz vein and alteration minerals like albite altered the overall mineralogy of the unit (Figures 9a to 9e). Minor minerals present include calcite (3%), hematite plus magnetite (1 %), muscovite (1%) while other trace minerals each with less than 1% of the total content included ilmenite, apatite and rutile (Fig. 9e).

Part of the quartz in the sample represents a late-stage silicification, with albite representing a sodic alteration phase and low-magnesium biotite, orthoclase and muscovite representing the potassic alteration (Fig. 9d). Euhedral albite crystals in the quartz vein are clearly discernible in thin section (Fig. 9b and 9c), which represent the hydrothermal phase. Full TIMA mineralogical results of all the analysed samples are given in Appendix 1a and zoomed-in depiction images of TIMA are given in Appendix 1b.

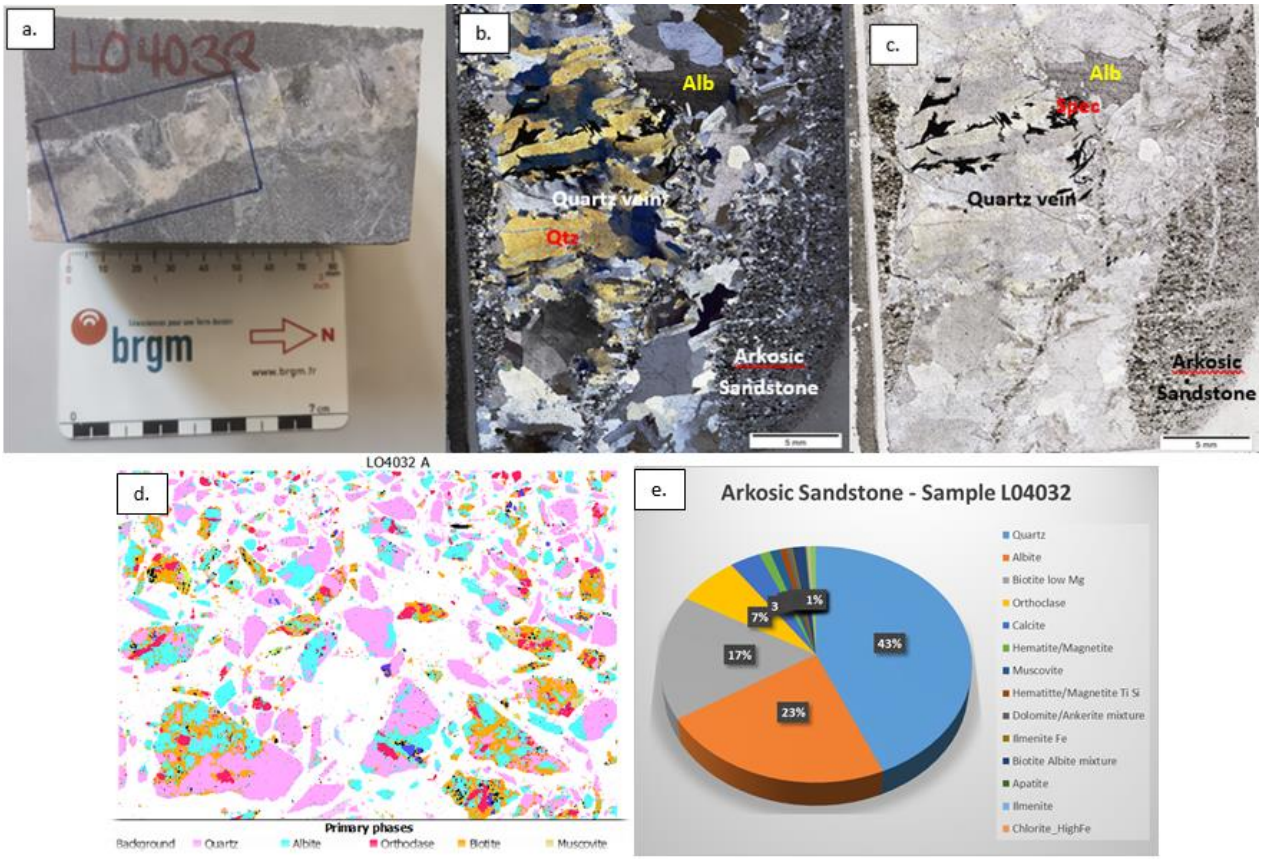

Figure 9. *Photographs of arkosic sandstone sample (L04032). (a.) hand sized sample of arkosic sandstone with fractured milky quartz vein cutting through the unit. (b) cross-polarised photomicrograph of arkosic sandstone with quartz vein, quartz grains cemented by kaolinite, calcite and other intergranular lithics. (c.) Plane-polarised photomicrograph of arkosic sandstone with syntaxial quartz vein, fractures and grain intergrowth within quartz vein are clearly discernable. (d)*

depiction of the mineralogy with pseudo colours of the minerals for the arkosic sandstone sample, image not to scale, generated for presentation purposes. (e.) Pie chart of the mineralogical composition of the composite sample of arkosic sandstone and quartz vein ($Q_{43}F_{47}L_{10}$).

2.1.2.1 Conglomerate

Within the upper horizons of the arkose is a discontinuous conglomerate lithology which has a thickness of between 10 m and 40 m, in some cases this forms consistent interbeds within the arkosic sandstone. The conglomerate comprises rounded gravel to pebble size clasts of quartz/arenite/arkose embedded in pinkish-grey arkosic sandy to clay-rich groundmass (Fig. 10a and 10b). The conglomerate unit comprises (42%) quartz, 28% albite, 16% biotite, 7% orthoclase, and 1% chlorite (Fig. 11b). Other minerals include hematite, magnetite, ilmenite, apatite, rutile, muscovite, calcite, and dolomite which make up 5% of the conglomerate unit (Fig. 11a and 11b). A full list of minerals present in the conglomerate sample L05791 is given in Appendix 1a.

Figure 10. *Borehole core tray of the conglomerate unit. (a) Photograph of conglomerate unit from diamond drill core with HQ core size sampled from hole ID DDH0018. Arrow points in the downhole direction. (b) hand size sample of the analysed drill core collected at depth 75.6 – 75.80 metres.*

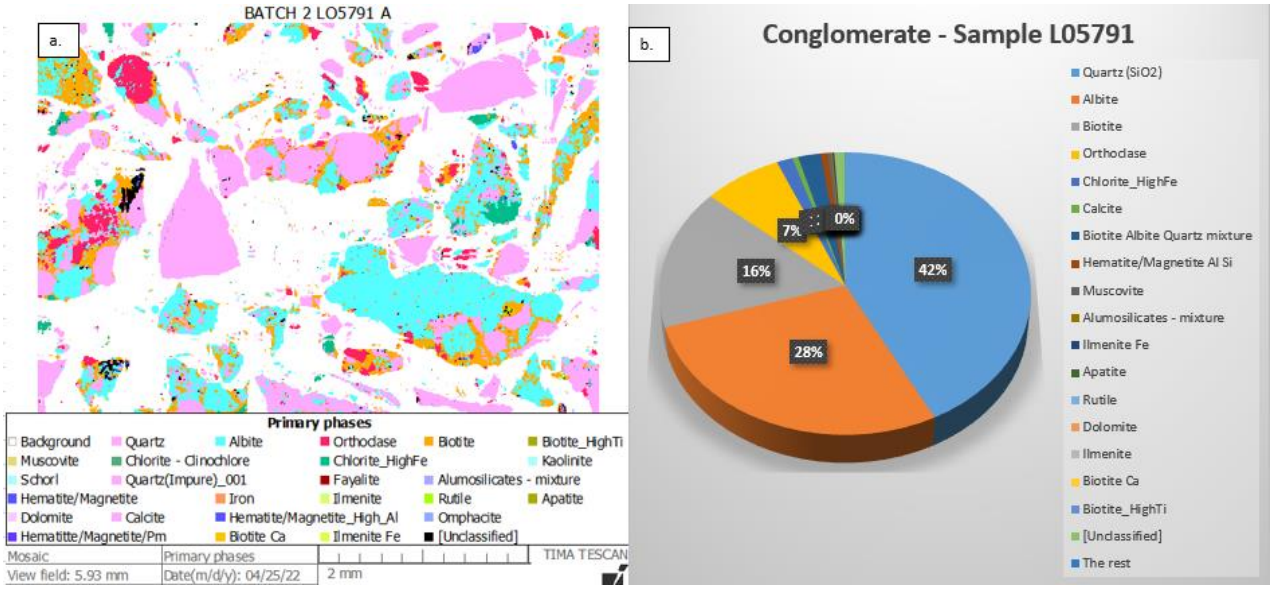

Figure 11. *Data depiction of TIMA results for conglomerate sample LO5791 (a.) depiction of the mineralogy with pseudocolours of the minerals contained in the conglomerate unit, image not to scale, only generated for presentation purposes. (b.) Pie chart on the mineral composition of conglomerate comprising quartz (42%), feldspars (35%), biotite (16%) and others (7%). Based on the mineralogical composition, overall mineralogical composition of the conglomerate unit is similar to the arkosic sandstone.*

2.1.2.2 Ferruginous Mudstone

Also, within the arkosic sandstone, zones of ferruginous mudstone are consistently present and are more common in the lower horizons of the arkosic sandstone. The mudstone varies from massive to laminated with a reddish-purple colour, very fine grained, predominantly made up of clay minerals (Fig. 12a, 12b and 12c) and quartz with younger calcite veinlets cross-cut through it in some cases. The ferruginous mudstone varies in texture and may sometimes occurs as a banded variety in the form of a shale. The reddish colour is indicative of the high presence of iron oxide, signifying deposition of these argillite sediments in an oxidising environment (Fig. 12b).

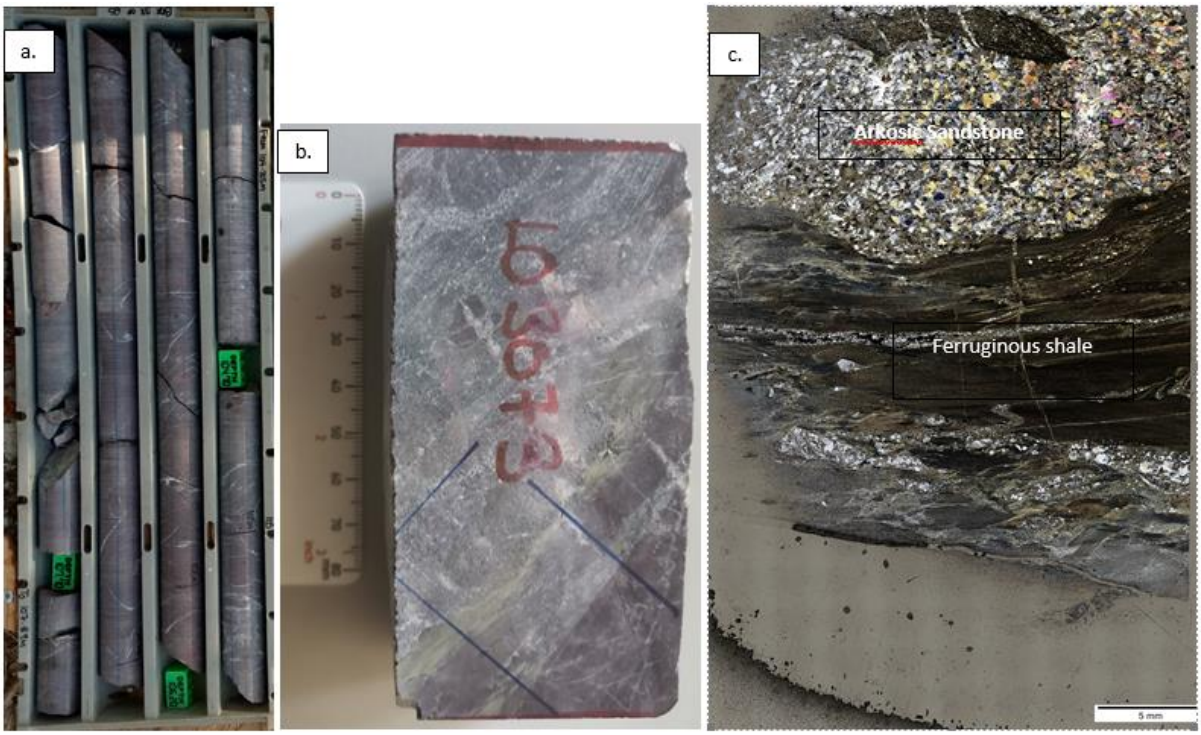

Figure 12. *Sample L03073 of ferruginous shale in arkosic sandstone (a) HQ drill core samples from DDH001 with ferruginous shale between 104 and 107 merers. (b) Photograph of part of sample L03073 which was analysed under the microscope (c) cross-polarised photomicrograph of ferruginous shale sample, mineralogy not clearly discernable in the shale zone with quartz and other lithic minerals in the arkose zone.*

2.1.3 Grand Conglomerat (GC) diamictite

The Grand Conglomerat diamictite overlays the arkosic sandstone unit, although it is suspected that there is a degree of unconformity between these units, with the possibility of the absence of the Mwashya and Upper Roan sequences. Generally, the diamictite unit ranges in thickness from a few metres to 200 m within the study area and has a strike length of around 6 km, although it may extend beyond the study area in the north-east and south-west directions.

GC unit sub-members were classified based on the size and presence of the clasts into clast-poor and clast-rich varieties and distinguished by the appearance of the matrix. The clast-rich variety has clasts ranging from cobble size to sandy size whereas the clast-poor diamictite comprises finer clasts, mainly pebble size to fines. The presence of arkosic sandstone and conglomerate fragments in the diamictite unit is quite common.

The clast-poor diamictite is frequently found near the lower and upper contacts of the underlying and overlaying units i.e., on the lower contact with the arkosic sandstone unit and on the upper side near the Nguba shale unit with the diamictite. Clast-poor diamictite grades into a mudstone-like unit (Fig. 13a) towards the contact with the arkosic sandstone as well as on the upper contact with the Nguba member shale. The clast-poor diamictite is typically massive to brecciated, with the brecciated variety comprising various gravel- to sand-size clasts of shale, arkose, quartz, arenite and mafic igneous rock embedded in a

clayey groundmass (Fig. 13a, 13b and 13c) and in most cases moderate to strongly mafic altered.

From the mineralogical analysis it was observed that the clast poor diamictite sample M1 comprises; biotite plus albite mixture (35%), quartz (28%), albite-biotite mixture (22%), biotite-quartz-albite mixture (11%) and orthoclase (6%) as shown in Figure 14a and 14b. The biotite-albite and albite-biotite mixture are as a result of the TIMA errors which could not distinguish the biotite from albite in the fine-grained parts of the sample during sample analysis (Fig. 14a). Carbonaceous clay minerals of the sample were not identified during the mineral analysis as the TIMA is incapable of detecting any carbon-rich parts of any sample. The diagenetic mineralogical composition of the diamictite is complex to due to the fact that it comprises various rock materials from granitic clasts to arenite to clay materials (Fig. 13b and 13c).

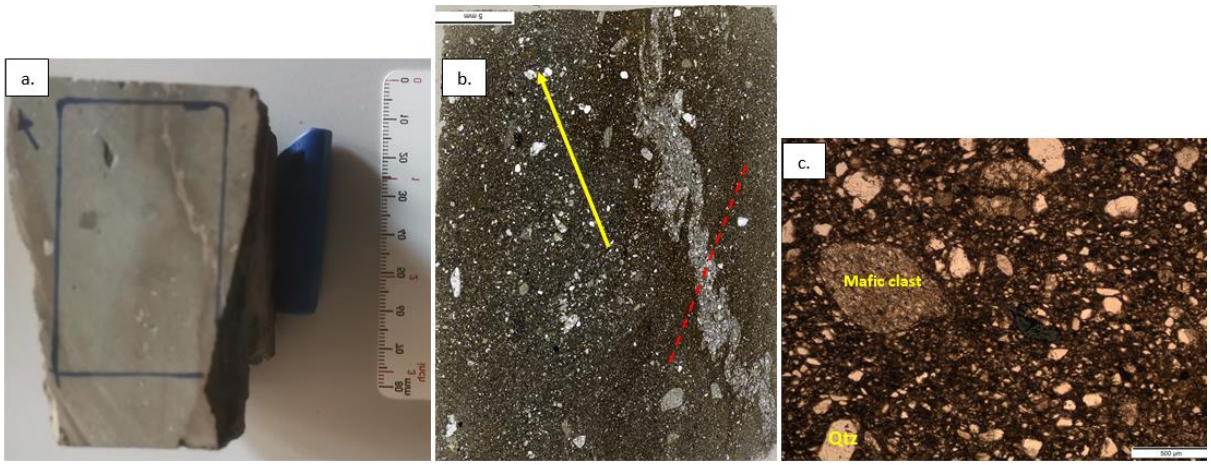

Figure 13. *Nguba member, Sample M1. (a) hand size sample of clast-poor diamictite, with arrow giving the north direction (b) Photomicrograph of clast poor diamictite under cross-polarised light (XPL), parasitic microfolding expressed in calcite-albite-quartz veinlet, relative to fig.a) axial trace of the folding is NNE shown by the red line, with the yellow line highlighting the north direction. Grains are sub-rounded to sub-angular in clayey to sandy groundmass. (c) Photomicrograph of clast poor diamictite at 500 µm scale under cross-polarised light, with sub-rounded quartz and mafic rock clasts.*

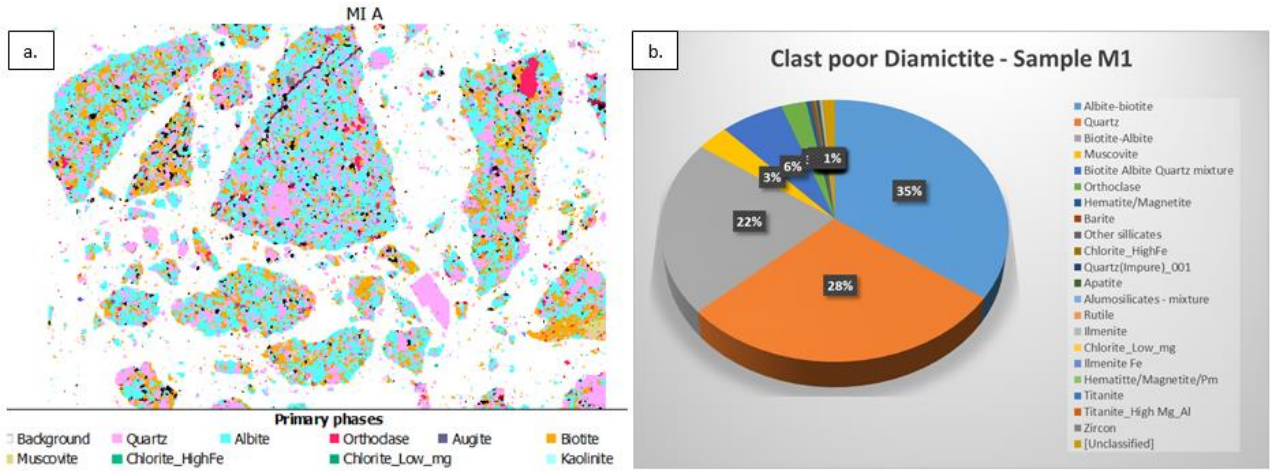

Figure 14. *Liberation analysis of the clast poor diamictite, sample M1 (a) Depiction of the mineralogy with pseudocolours of the mineralogical composition of the clast poor diamictite, prepared via a destructive method and analysed using a TIMA (Image not to scale). Higlights some of the grain relationship in the sample, anhedral fines of quartz and albite evenly distributed throughout the unit. Albite appears to be rimmed by biotite. Image not to scale. (b.) Pie chart showing the mineralogical composition of sample M1.*

Some minor outcrops and float material of clast-rich diamictite have been observed within the central part of the study area. This variety of diamictite is dark-green to grey, and contains rounded to sub-angular clasts of arkose, granite, mafic and arenite rock material (Fig. 15a and 15b). The discernible mineralogy in hand samples includes quartz and plagioclase with alteration mineralogy mainly being of albite, actinolite-tremolite and minor chlorite (Fig. 15b). Accessory minerals include hematite, magnetite, apatite and barite. The outcrops of Grand Conglomerat diamictite and Nguba member shale and near surface units, coincide with the NNE-SW trending magnetic high observed in the aeromagnetic images from the study area.

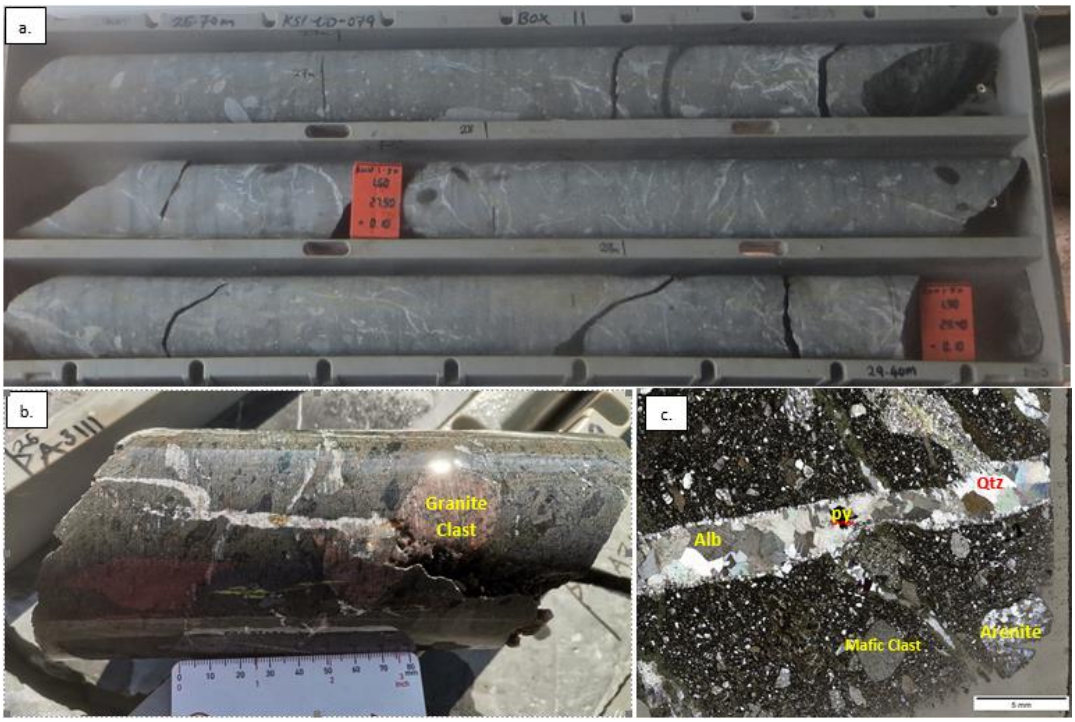

Figure 15. *Clast-rich diamictite unit (a) photograph of PQ core size from drill hole DDH079 of clast rich diamictite unit (b) Photograph of hand size sample of clast rich diamictite with rounded pebble-size clast of granitic rock and sheared clasts of mafic rocks. Sample A3109 was collected from this sample (c) Cross-polarised photomicrograph of clast-rich diamictite of sample A3109, showing mafic and arenite clasts embedded in clayey to sandy groundmass, quartz vein cutting through the unit with interlocking euhedral crystals of quartz and albite.*

Based on the mineralogy analysis from the TIMA, clast-rich diamictite sample A3109 comprises quartz (36%), albite (30%), biotite (21%), iron-rich chlorite (3%), orthoclase (3%), muscovite (2%) and calcite (1%) and minor minerals including hematite, magnetite, apatite, rutile, ilmenite, dolomite, and zircon (4%) (Fig. 16a and 16b). Distinguishing the diagenetic minerals present from the hydrothermal alteration minerals for this unit was challenging in that it comprises rock material derived from different types of rocks coupled with different episodic deformation that have affected the units (Fig. 16a and 16b). However, the albite, part of the quartz, orthoclase and part of the biotite are suspected to be of metamorphic/hydrothermal alteration phases within this unit and the area in general. Sodic alteration is more pronounced in the diamictite units and is represented by albite whereas the potasic alteration phases are represented by the muscovite, orthoclase, and biotite.

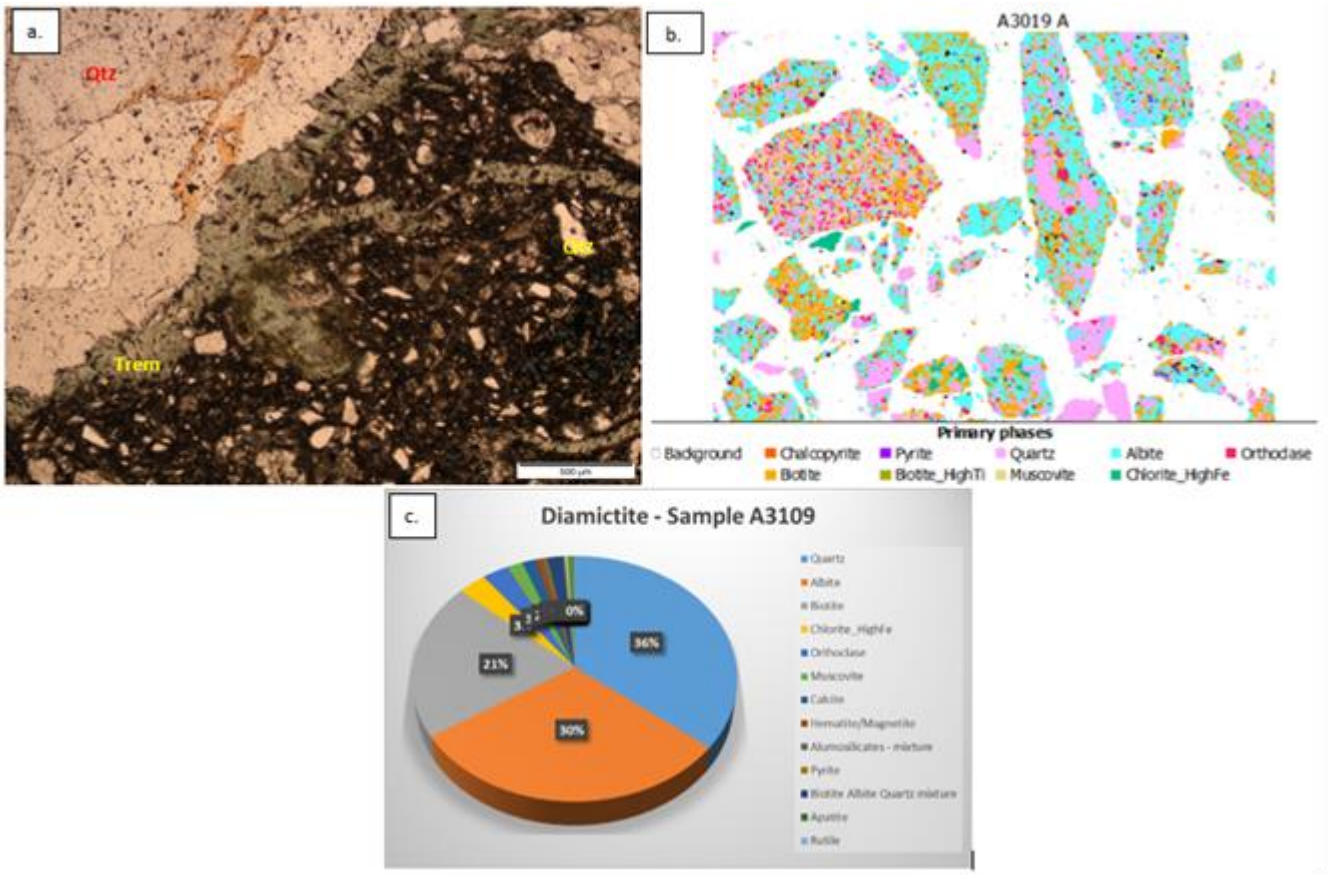

Figure 16. *Clast-rich diamictite, Sample A3109 (a) Photomicrograph in cross-polarised light of diamictite unit at a scale of 500µm. (b) Depiction of the mineralogy with pseudocolours of mineralogical composition of the clast-rich diamictite, prepared via a destructive method and analysed using a Tescan microscope. Image not to scale. (c) Pie chart for the mineralogical composition of diamictite sample A3109.*

2.1.4 Nguba Member shale (NS)

Overlaying the Grand Conglomerat is a banded shale, which is interbedded with siltstone in some zones. In hand-size sample the shale unit is very fine-grained, moderately carbonaceous, with bedding-parallel pyrite growth mostly related to pervasive secondary calcite veining, which is characteristic of this unit (Fig. 17a).

Bedding and laminations show a planar deposition stratification and the observed mineralogy includes clay minerals, and quartz with the silt-rich zones of the unit more enriched in quartz (Fig.17b).

Based on the mineralogical analysis from the TIMA, Nguba Member shale sample L05959 comprises quartz (22%), albite (20%), biotite (10%), orthoclase (6%), iron-rich chlorite (4%), calcite (1%), and muscovite (2%). Minor minerals including hematite, magnetite, apatite, rutile, ilmenite, and zircon (Fig. 17c). Sulphide minerals include pyrite (6%), pyrrhotite (3%), sphalerite (1%) and a trace chalcopyrite at 0.04%.

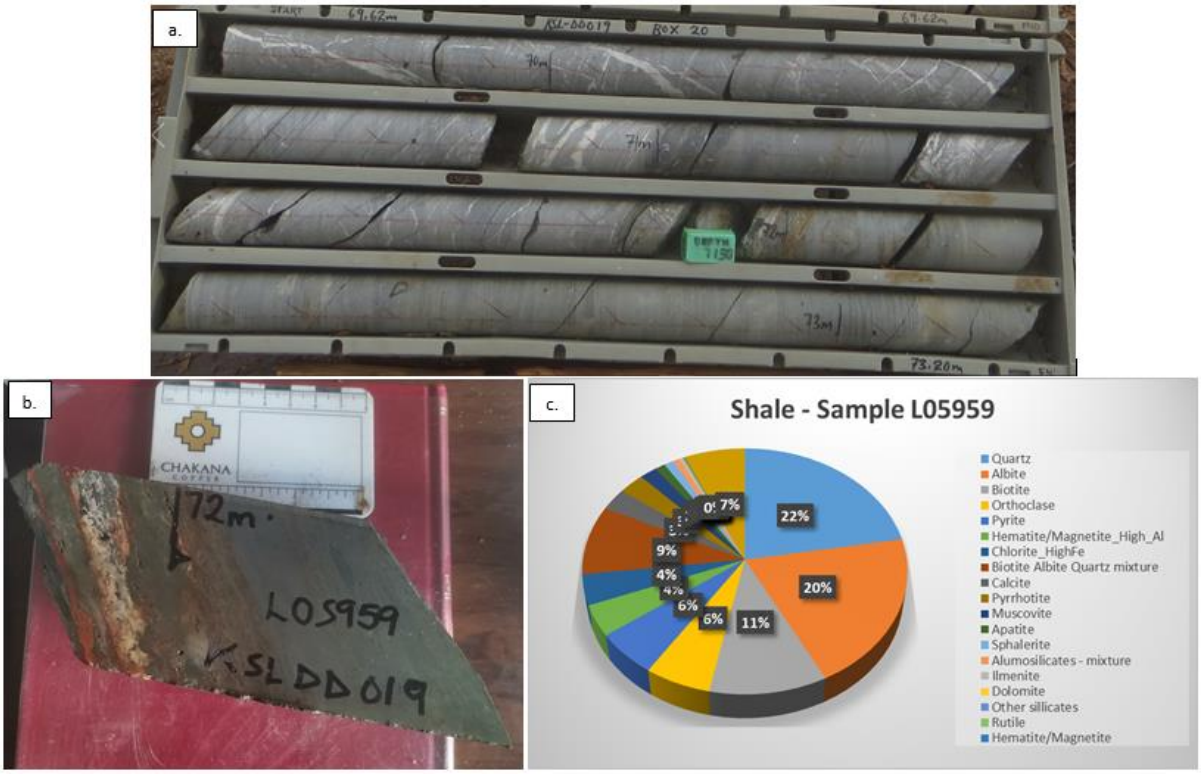

Figure 17. *Nguba Shale unit. (a) Drill core photograph of silty-shale from hole ID DD0019 from 69 – 73m. (b) Photograph of hand size sample from hole ID DDH0019, collected at depth 71.95 – 72.08m. The unit is characterised by a calcite-albite-quartz vein with post-diagenetic pyrite and pyrrhotite altered to FeOx. (c) Pie chart showing the mineralogical composition of sample L05959 analysed using Tescan liberation analysis. Tescan analysis was not able to detect carboneceosus clay minerals in sample L05959 which are a component in the unit.*

2.2 STRATIGRAPHY

The oldest unit within the study area is the Roan Member shale unit (RS) which is of Mwashya age or older, overlain by the arkosic sandstone (AS), then the Grand Conglomerat (GC) diamictite and finally the Nguba Member shale (Liyungu et al, 2000; Key et al., 2000). Volcanic bodies in the greater Mwinilunga area that intruded the Roan (Mwashya) units have been dated at 765 Ma and those that intruded the Nguba units have been dated at 735 Ma (Armstrong, 2000). A stratigraphic column that highlights the sequence of lithologies in the study area and correlates these within the stratigraphy of the copperbelt is shown below (Figure 18).

One of the notable features preserved in the area is the presence of a redox boundary between the pinkish-grey coarser arkosic sandstone unit (oxidised facies) and the greenish-grey clast-poor diamictite (reducing facies). This boundary is indicative of gold mineralisation. In the study area, sandstones and conglomerates correlate well to the lower part of the Lower Roan units in the established copperbelt stratigraphy, therefore there is the possibility of an unconformity or disconformity prior to deposition of the diamictite unit (Fig. 18).

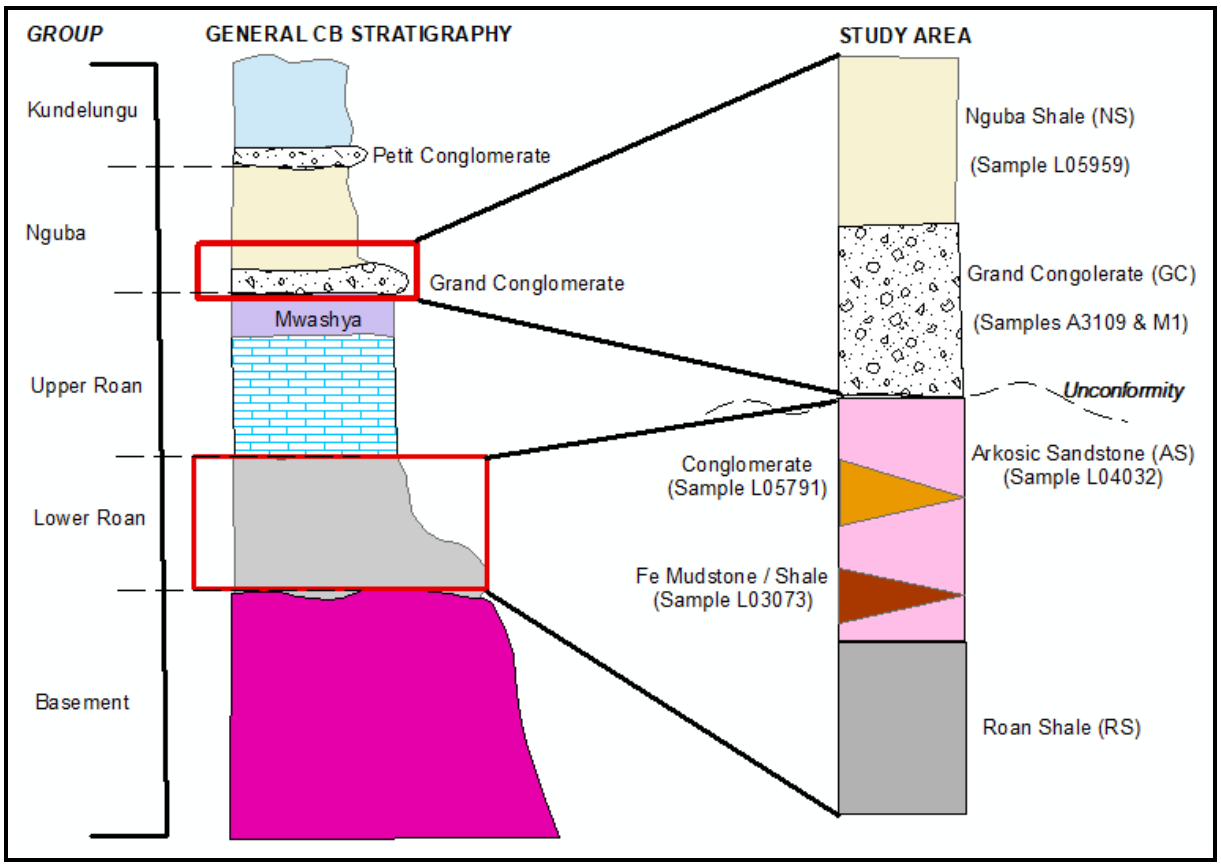

Figure 18. *Simplified diagram showing the stratigraphic correlation between the general Copperbelt stratigraphy and that of the study area (not to scale).*

Stratigraphic correlation of the observed units and formations in the study area with other deposits located in distal proximity was undertaken. This correlation, shows that the study area correlates with the stratigraphy of the Kamoa copper deposit which is located approximately 150 km to the northeast (Table 2). Most of the units correlate well, particularly the diamictite marker unit and Nguba member shale, as well as the footwall unit of arkosic sandstone.

Due to the presence of the gold mineralisation in the area, correlation with the Kansanshi deposit was also undertaken which showed that the study area stratigraphically sits in the same formation relative to Kansanshi, though at Kansanshi the main copper-gold vein related deposit is hosted in the carbonaceous shale unit which is of Mwashya age or older, with the overlaying diamictite unit hosting strata-bound copper mineralisation (Table 2).

***Table 2**. Stratigraphic correlation of the study area with Kamoa copper deposit in DRC, which lies in LAFTB and Kansanshi copper-gold deposit in Zambia, which lies in the Domes Region. Stratigraphic correlation of the units above Mwashya is based on the DRC stratigraphic nomenclature of the Copperbelt. Modified after Liyungu et al., 2000; Key and Banda, 2001; Cailteux et al., 2007; Bull et al., 2011.*

Group	Subgroup	Formation (Kamoa/DRC) - LAFTB	Kansanshi (KML) - Dome Region	Mwinilunga / Study area - LAFTB	Events in Mwinilunga	Thickness (m)	Age (Ma)
Kundelungu	Ngule (former Kuibo)	Sampwe					±500
		Kuimbo			Part of the Pan-African orogeny that produced the fold and thrust pile in LAFTB		
		Mongwe					
	Gombela (former Kalule)	Lubundi					
		Kanianga					
		Lusele					
		Kyandamu ('Petit Conglomerat')					±620
Nguba	Bunkeya (former Monmwezi)	Monmwezi	Momwezi		Volcanism within nguba strata - underlying andesitic basalts dated ±735 Ma		
		Katete (Serie Recurrente)	Katete				±735
	Muombe (former Likasi)	Kakontwe	Kakontwe	Kakontwe - kang'fumbo limestone			
		Kaponda					
		Cu Mwale ('Grand Conglomerate')	Mwale Cu	Mwale - Shale and Diamitites ('Grand Conglomerate') Au - Cu	Deposition of sediments in Glacial-marine environment (Sturtian Glaciation)	30 - 250	±750
Roan	Mwashia		Cu -Au Dolomitic units	Clastics - arkosic sandstone and Roan shale	Creation of large volcanic edifice along westerm margins of Katanga member units (Mwashia Group). Volcanics dated ±765	100 - 1000	±765
	Upper roan	Bancroft					
	Lower Roan	Kitwe	Evaporic sequence				< 900 Ma
		Mindolo Clastics	Basal Clastic units				

CHAPTER THREE

STRUCTURAL GEOLOGY

3.1 STRUCTURAL GEOLOGY OF THE STUDY AREA

Some of the important aspects of gold deposits and mineralisation is the understanding of the crustal architecture that leads to their formation through migration and concentration of mineralised fluids and eventual deposition of elements from these fluids into appropriate sites (Grooves, 2003). These events are a function of structural geometry and evolution of gold prospective areas.

On a district scale, the study area and its surroundings are extensively folded and faulted, and the area has undergone episodic deformation resulting in the development of various structures. Among the notable structures within the study area include bedding, folding shear faulting, normal faulting, and jointing.

3.1.2 BEDDING

Primary structures observed in the lithological units are bedding including fine-scale laminations (Fig. 19). Bedding structures were measured in the Roan shale unit, arkosic sandstone and the Nguba shale unit. Most of the rock units in the study area dip to the southeast with an area average strike of 128^0 and general dip of around 40^0 (Fig. 20). A full table of the collected structural data is given in Appendix 3.

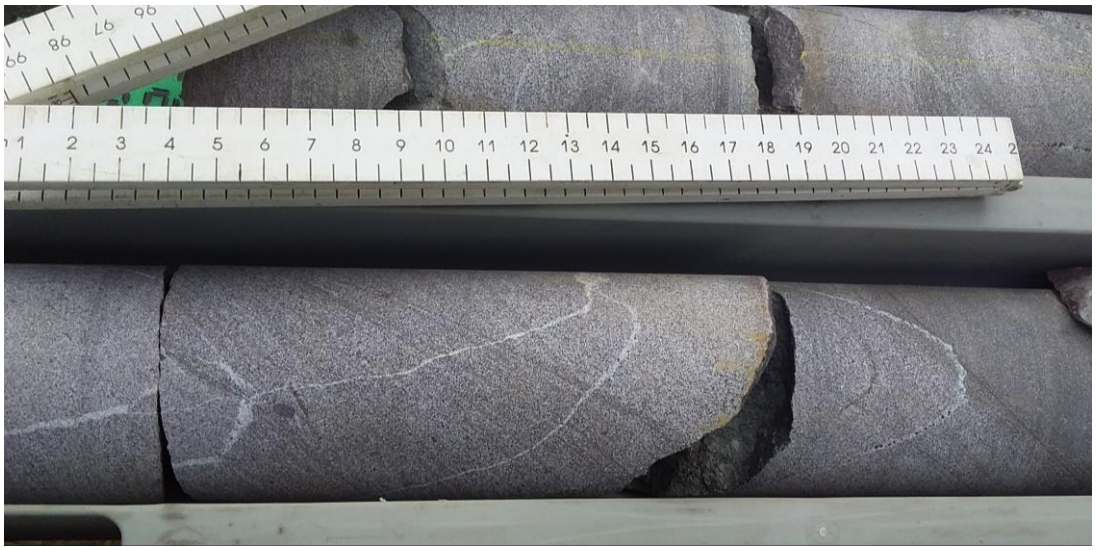

Figure 19. *Photograph of core from DDH0012 with cross lamination in fine grained variety of arkosic sandstone.*

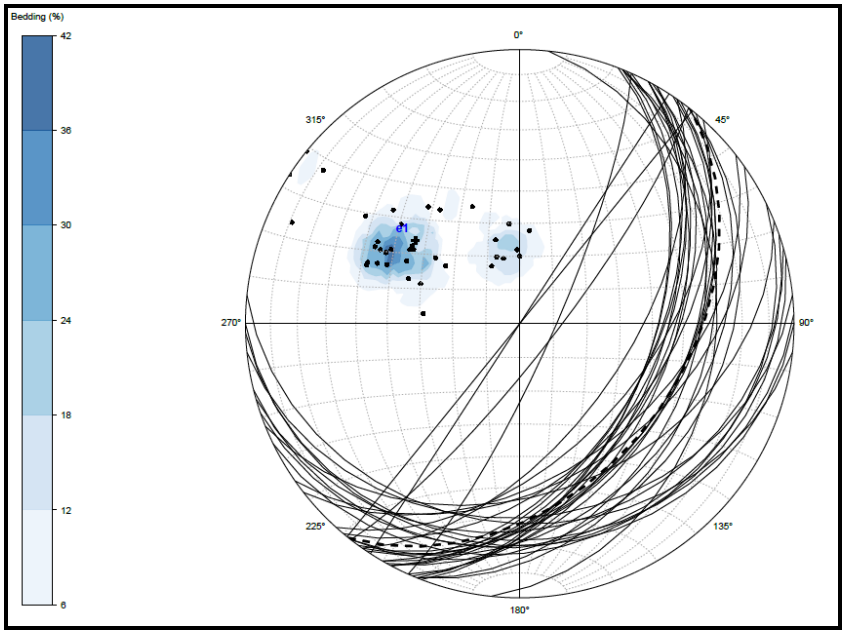

Figure 20. *Stereonet plot of the bedding structures from the study area. Note the more pronounced NNE-SSW to ENE -WSW strike of most of the rock units in the study area, with a general dip to the SE.*

3.1.3 FOLDING

The area has been affected by two phases of folding, based on the field observations and structural correlations. The first phase of folding is interpreted to be open folding which is represented by the observed repeating units of gentle to steeply dipping Roan Shale and arkosic sandstone units within the study area (Fig. 21). A probable NNE – SSW axial trace has been inferred with the lateral hinge of the folding inferred to be located south- southwest of the study area.

Overall, units related to the open folding in the study area mostly dip at angles of between 20^0 and 85^0 to the southeast with a general strike of NNE – SSW (strike trend of between 030^0 and 070^0) which is indicative of both gentle to steeply dipping units.

Large folds of up to 20 km strike length are projected on a broader scale and with a distinctive appearance of 'bunch of bananas like pattern' from the aerial view, which represent large district to deposit-scale folds (Liyungu et al., 2001).

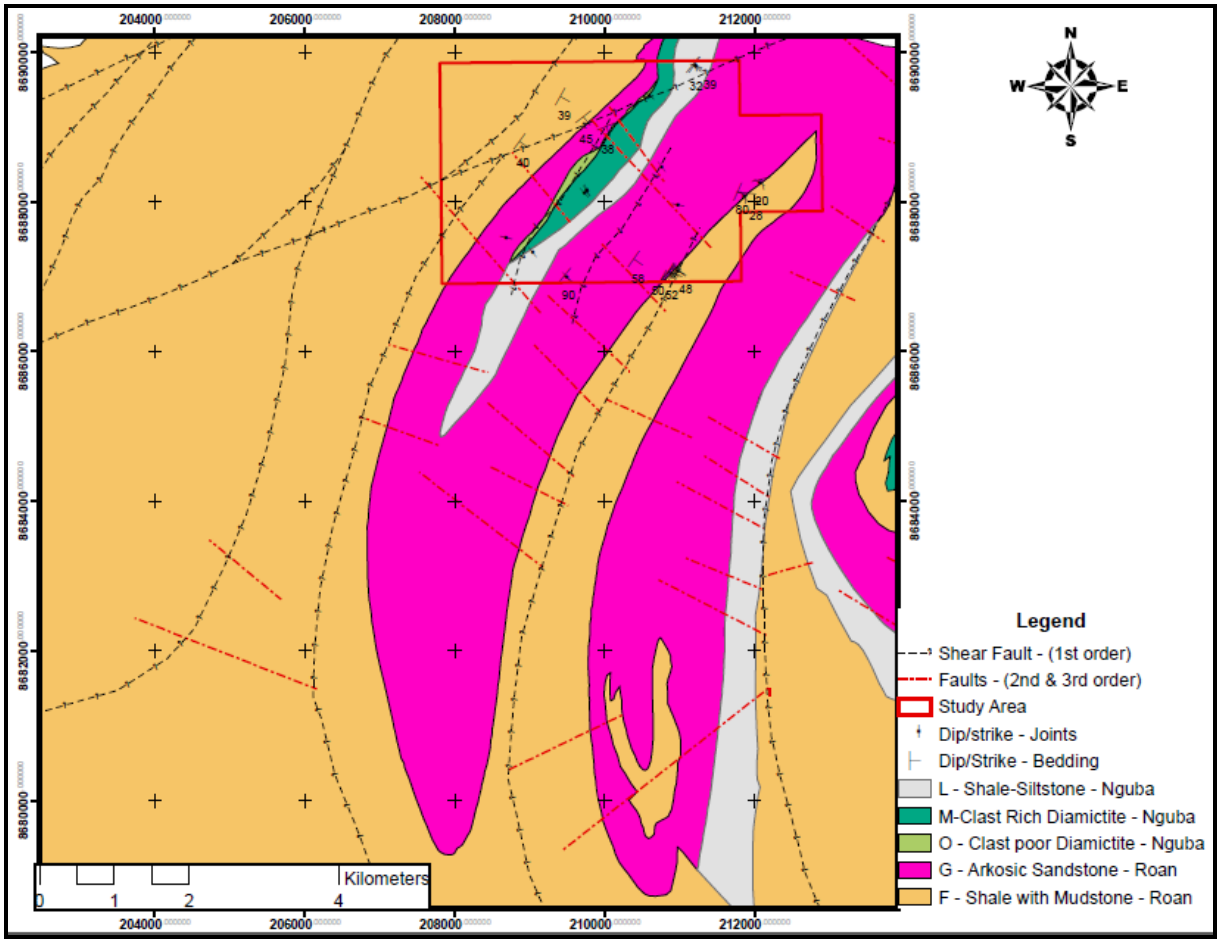

Figure 21. *Geological map showing open folding, shearing and faulting structures interpreted from the compilation of regional geology, processed landsat image, google earth pro images, first vertical derivative aeromagnetic images and collected data from the field mapping. Open folds marked by repeating units of arkosic sandstone and Roan Shale.*

The later-stage folding was observed at metre, centimetre, and millimetre scale within the rock units of the study area. Parasitic folds were observed in the drill core, with the z-folds marked by quartz veins in arkosic sandstone (Fig. 22), these possibly representing the southwestern limb of the larger fold with a NW-SE axial trace. The folding observed in the arkosic sandstone was marked by the quartz veins that cut through this unit. The quartz veins are later-stage fracture filling which post-date both the shearing (from ductile deformation) and the faulting and jointing (from brittle deformation).

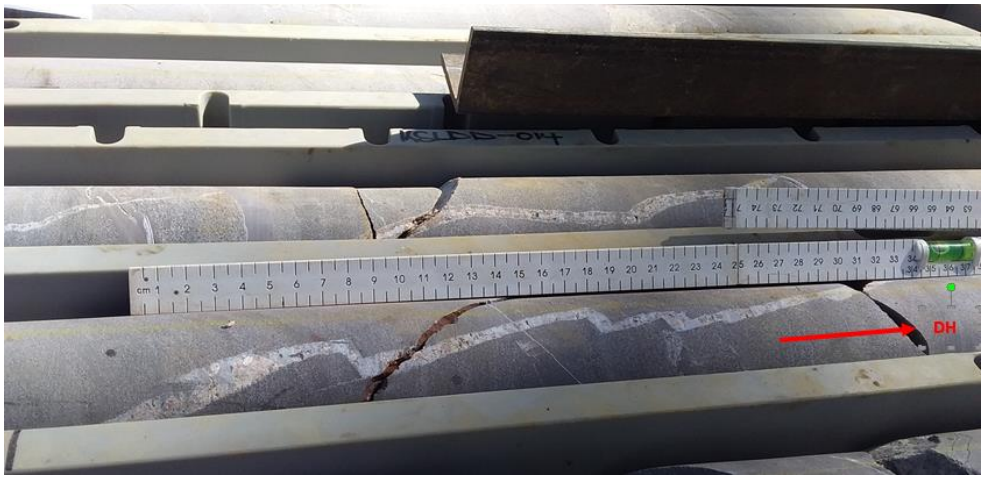

Figure 22. *Z-folding marked by quartz vein in arkosic sandstone unit, from drill hole DDH0014. DDH drilled at location UTM Arc 1950 210,074mE/8,688,900mN. Red arrow pointing in the downhole direction.*

Folding was also observed in the Nguba shale unit from the drill core collected from hole ID DDH 0019, where folding was marked by lamination bedding with pronounced pyrite and pyrrhotite mineralisation enriched in the fold hinge (Fig.23), forming basin and dome-like features on a centimetre scale.

Figure 23*. Centimetre scale folding in Nguba shale marked by lamination bedding, observed in sample L05959. Folding structure observed in drill hole DDH0019 at a depth between 70 – 72m. Note the late-stage silicification in form of quartz veins.*

3.1.3 SHEARING AND FAULTING

Evidence of shearing in the study was mainly observed within the drill cores as well as from the interpretation of processed ground magnetic images.

The faulting and shearing aspect is also evident at metre, centimetre and millimetre scale. Some of the observed structures that signify ductile shearing or shear related folding and normal second (2^{nd}) order faulting and jointing include stretched ellipsoid shaped clasts in the diamictite unit (Fig. 24), sigmoidal veins (Fig. 25), and z and s parasitic folds. Tension fractures or tension gashes are widely spread in the area, and are more pronounced in the folded arkosic sandstone at outcrop scale. En-echelon gashes provide evidence that the study area has been affected by brittle-ductile shear deformation phases, with the sense of movement of the en-echelon gashes interpreted to be dextral (Fig. 24).

Figure 24. *Photograph of diamond drill core from hole ID DDH0069. Clast rich diamictite unit ("Grand Conglomerat" marker bed), with sheared pebble size clast (marked by dashed purple ellipsoid circle) and calcite filled tensional fractures oriented perpendicular to the shear direction. Note the S-type of parasitic folds at 46.00m. Pencil (~15cm) used for scale and red arrow pointing in the downhole direction.*

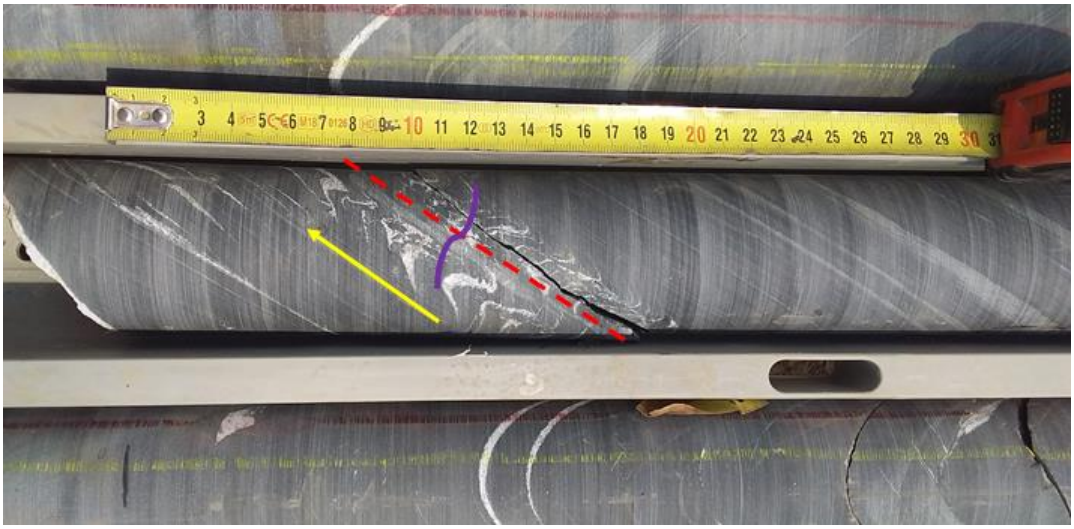

***Figure 25**. Photograph of sigmoidal veins observed in the Nguba Shale unit in drill hole DDH 0031 drilled at location 210458/8688405 (in UTM Zone 35 Arc 1950), observed tension gashes are markers to dextral shearing within this unit and on a broader scale. Red dotted line outlines the orientation of the cleavage plane with the yellow line highlighting the strain direction of the shearing.*

Other indications of shear fracturing in the study area include the slickenlines observed on the slickenside surface which was intersected in drill hole DDH0031 in Nguba shale unit (Fig. 26). Observed slickensides were characterised with an Fe-oxide coating of surfaces and based on the physical appearance of the surfaces, these were formed from mechanical abrasion of the two fault surfaces (and not from fibrous growth as is the case for fibrous lineations). The intersection orientation of these shear related fractures is in a subvertical to vertical manner relative to the ground surface, with drill hole azimuth of 030^0 and dip of 60^0. This therefore implies that the sense of shear of the fault block movement of the two surfaces that formed the slickenside was in an almost horizontal manner (NNE – SSW).

***Figure 26**. Slicklines (marked by white dotted line) on slickenslide surfaces with FeOx coating on surface. Pen for scale (~15cm)*

Inferred first-order shear faults and second-order faults were also interpreted from processed Landsat satellite images and ground magnetic images of the first vertical derivative (1VD) aeromagnetic image which is reduced to pole (RTP) via image filtering and processing.

The shear faults and fault structures have an effect on the course of the streams in the area and this is clearly evident in the google earth satellite images and processed Landsat 8 images (Fig. 27), where NNE – SSW faults are interpreted to be shear faulting and NW – SE faults representing normal faulting. Apart from the observed tension gashes in drill core, dextral shearing is further interpreted on a broader scale via the processed ground magnetic 1VD images where a NW – SE trending magnetic high structure has shown indications of lateral displacement (Fig. 28), with the shear stresses interpreted to be oriented NE - SW. The combination of shear faulting and faulting also suggests the sense of displacement to be dextral.

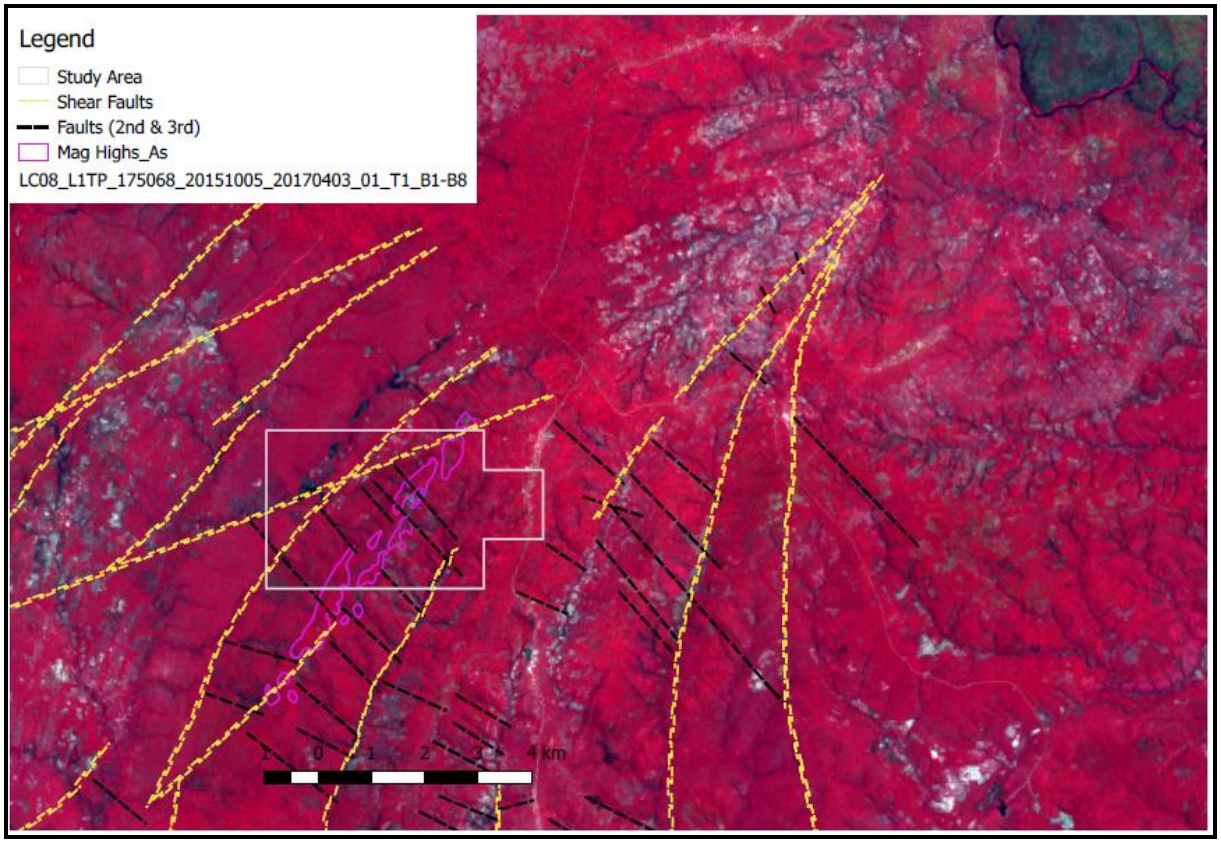

Figure 27. *Processed and enhanced Landsat-8 TM false colour image, captured on Oct 2015. RGB band 5-4-3, inferred 1st order strike-slip faulting marked by NE-SW structural trend (yellow lines) and 2nd order faults (and veins) marked by NW-SE trending faults (black lines).*

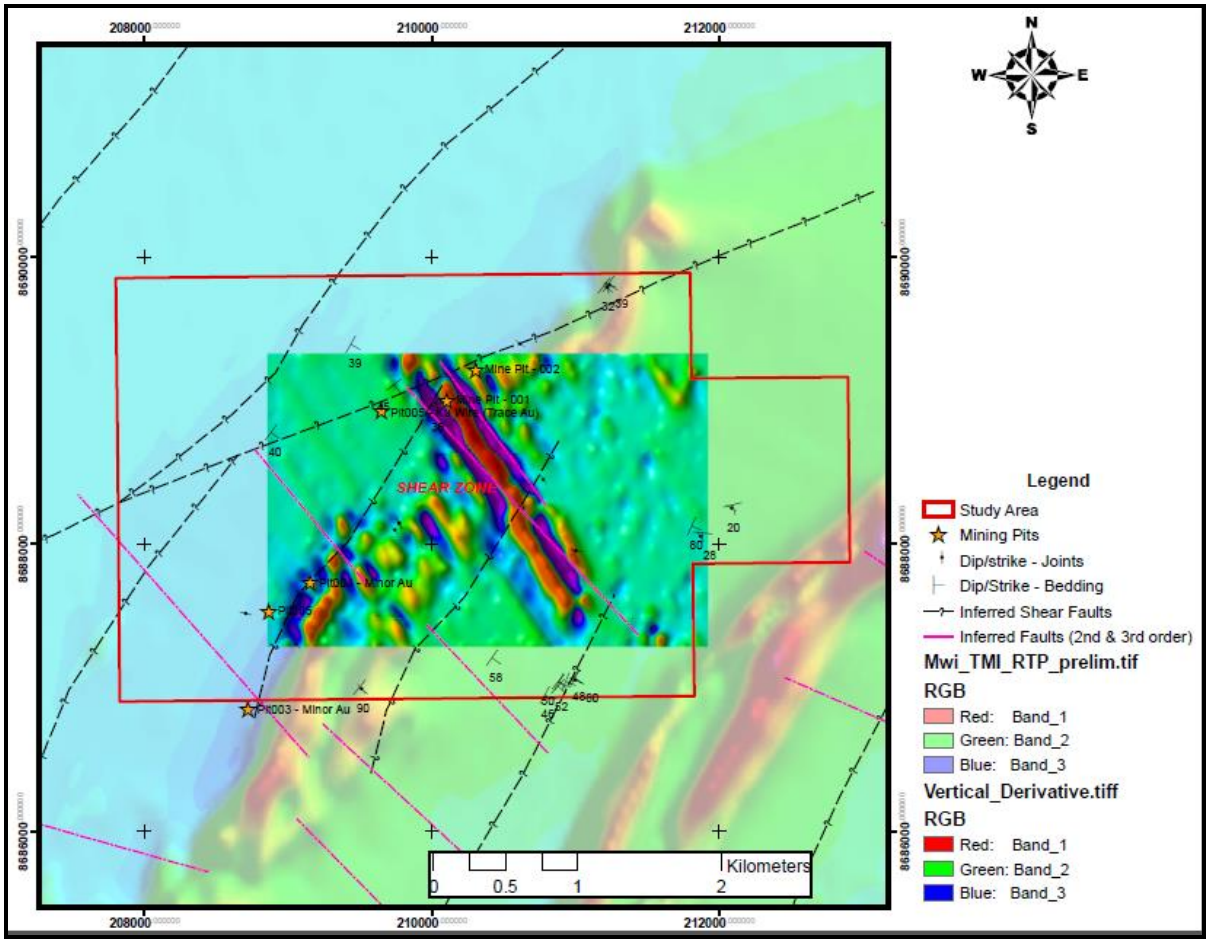

Figure 28. *Ground magnetic image of first vertical derivative (1VD) over airborne magnetic image (reduced to pole or RTP) with inferred 1st order and 2nd/3rd order faulting structures interpreted from both the magnetic image and processed Landsat images. Note the dextral shearing (NNE-SSW) marked by a displaced magnetic high structure with NW-SE orientation. 1VD filtered ground image was able to pick out near surface accommodation structures aligned perpendicular to the strike of the units (RTP).*

Based on the macroscopic and deposit scale observations of the structures in the study area, the NE – SW striking ductile shearing is considered to be the first order structures as the shearing is cut through by brittle structures in the form of faults and joints which are oriented perpendicular to the shearing. These NW – SE trending faults, joints and later-stage quartz veins (with bearing angles ranging between 100^0 and 150^0) are considered to be the 2nd and 3rd accommodation structures, where mineralised fluid deposition occurred (Fig. 28). The relationship between the shear faults and the brittle fracture is further shown by tensional fractures observed at a centimetre scale, where shear strained ellipsoid shaped clasts in the diamictite unit have been cut through by calcite-filled tensional fractures (Fig. 24). Overall, the orientation of the discontinuities and faults related to the shearing and faulting are shown in the stereonet plot (Figure 29).

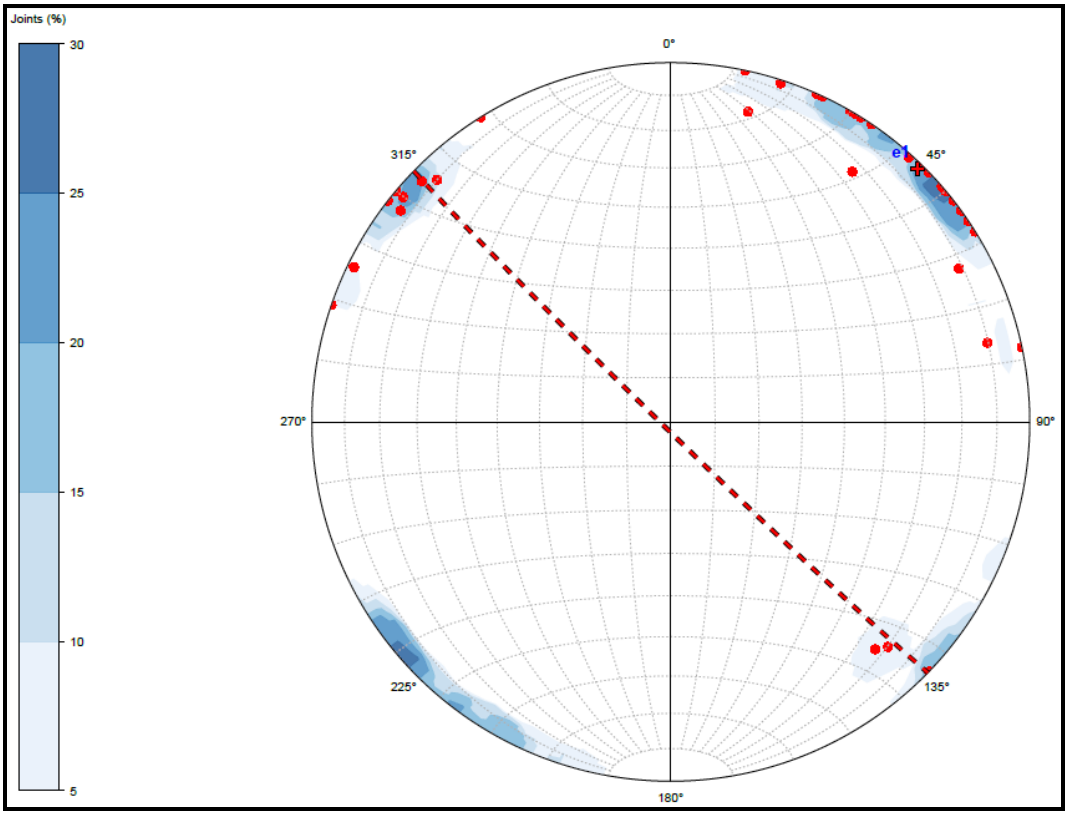

Figure 29. *Stereonet plot of the joint readings collected from the study area, 1st order shear faulting related jointing represented by the NE – SW to ENE – WSW trending structures. 2nd and 3rd order accommodation fault structures represented by NW-SE trend with red dotted line representing the average strike reading of 135^0. Most of 2nd order joints dip vertically to subvertical.*

3.2 MINERALISATION

Noticeable layout of the rock units related to gold mineralisation in the study area is the redox boundary between the pinkish-grey coarser arkosic sandstone unit (oxidised facies) and the greenish-grey clast-poor diamictite (reducing facies) where higher grade (> 10g/tonne) pockets of gold mineralisation have been observed from the sampled areas (Fig. 30 and Appendix 4a). Gold mineralisation has mainly been observed to be hosted in the clast-poor diamictite mostly in the alteration halo which forms around the arkosic sandstone-quartz vein- diamictite contact (Fig. 31). Further away from this contact and other related structures such as faults, veins and folds, mineralisation gradually diminishes. Gold mineralisation in this area has shown a strong correlation with copper as high-grade zones have elevated copper mineralisation both in the mineralised zone and in the residual soils.

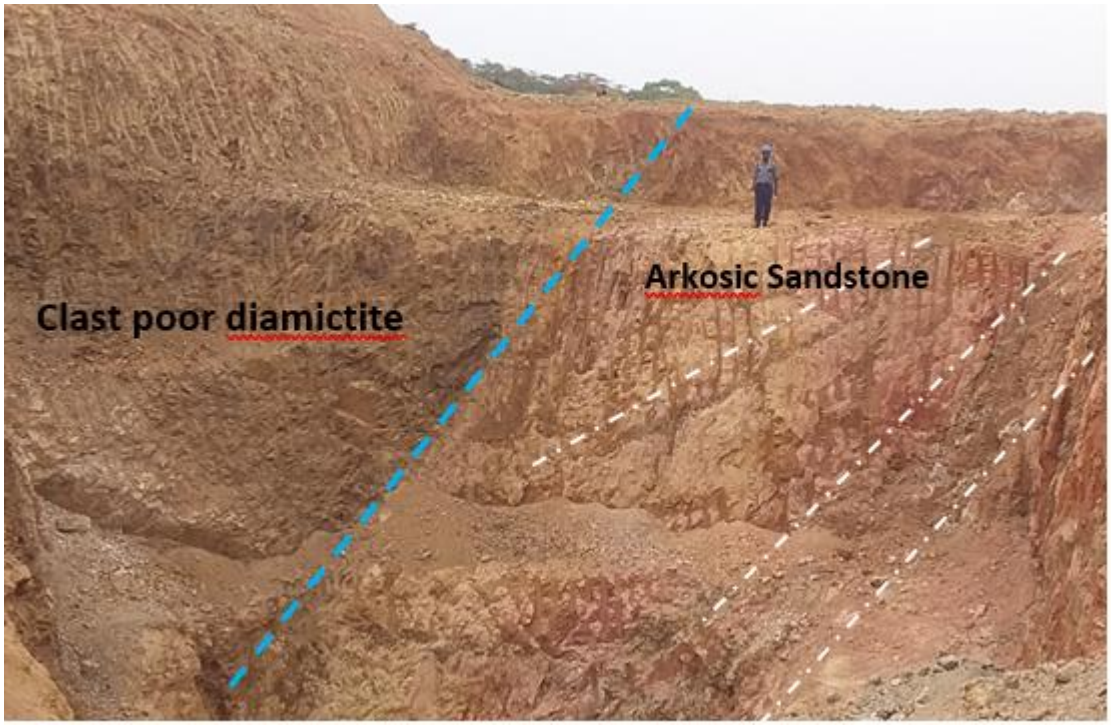

***Figure 30**. Diamictite-arkosic sandstone redox contact zone highlighted by blue dashed line, with poorly mineralised to unminerlised quartz veins in the arkosic sandstone marked by white dashed line. Higher grades of mineralisation have been observed in the clast-poor diamictite of this contact zone.*

***Figure 31**. Hand-size sample showing a gold mineralised quartz vein from the diamictite – arkosic sandstone – quartz vein contact zone, with green chlorite staining from the diamictite unit.*

A sheared clast-poor diamictite sample (L0427) was collected above the diamictite – arkosic sandstone contact. In thin section, it exhibited sheared ellipsoid-shaped clasts rich in quartz, albite and calcite with disseminations of framboidal pyrite in inter-clast spaces. Biotite and minor muscovite were also enriched along inter-clast spaces or in the groundmass. This sample was also analysed using the TIMA, and it was observed that it had minor amounts of copper sulphides present (Appendix 1a). Sulphide minerals in this sample were 0.69% pyrite, 0.09% chalcopyrite and 0.03% pyrrhotite.

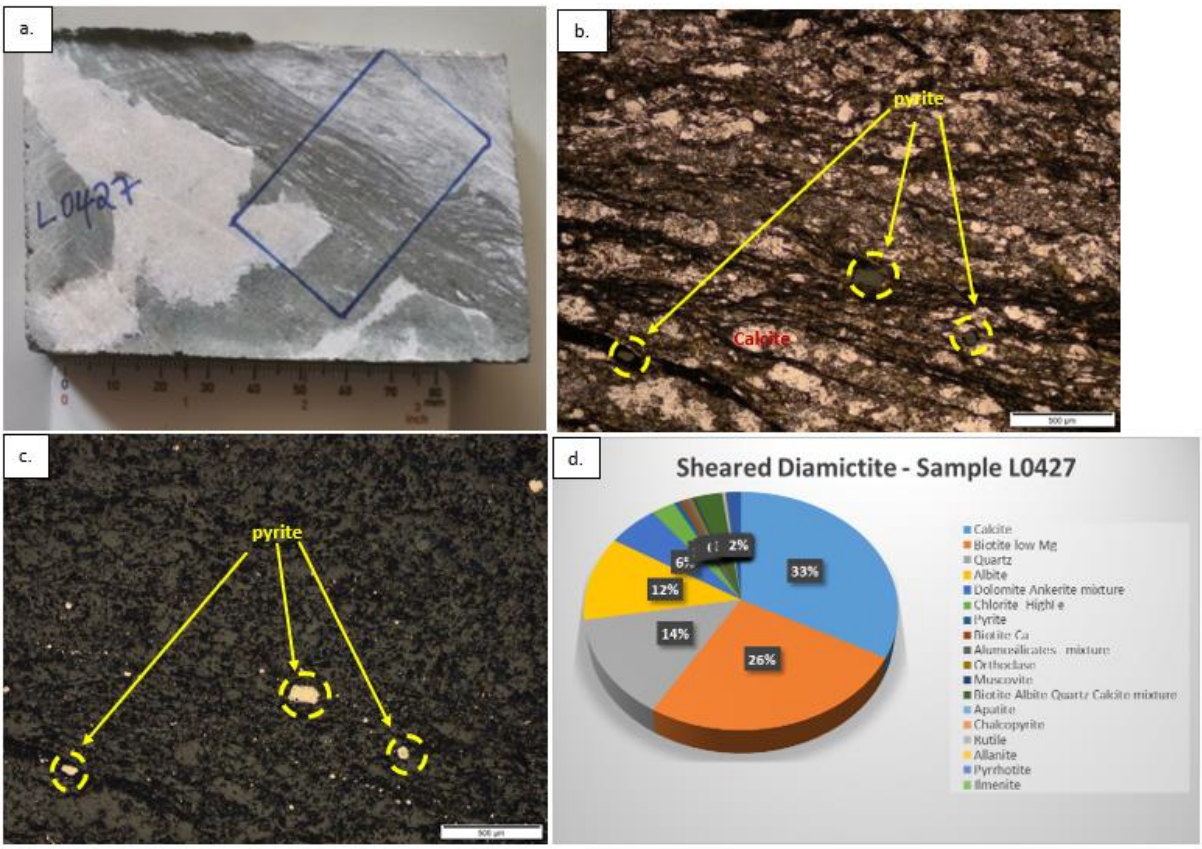

Figure 32. *Sheared diamictite unit, sample L0427 (a.) Photograph of hand-size sample of diamictite with calcite-quartz veins collected along diamitite-arkosic sandstone contact. (b.) Cross-polarised photomicrograph of the gold-related pyrite mineralised sample at 500µm scale. Note the shearing in sample with the pyrite mineralisation hosted in those structures, with potassic alteration represented by muscovite surrounding the calcite grains. (c.) Photomicrograph of pyrite in diamictite in reflected light. (d.) Pie chart on the mineralogical composition of diamictite sample analysed, with pyrite (0.69%), chalcopyrite (0.09%), chalcocite (0.02%) and pyrrhotite (0.03%).*

Overall, observed gold and sulphide minerals in the study area are related to the NW-SE trending structures which are considered as second (2nd) order accommodation structures. The post-diagenetic gold and sulphides were derived and enriched through 1st order NNE ductile shearing; then later-stage events related to the post-ductile shearing which gave rise to the mineralisation mostly enriched and hosted in NW-SE trending structures.

3.3 QUARTZ VEINS

Quartz veins are characteristic of almost all the units found in the study area, with thicker veins of up to one metre thick more pronounced in the arkosic sandstone (Fig. 33). This can be attributed to greater competence which results in thicker brittle fractures when compared to units like shale which deform in a more plastic manner. With regards to the dip/strike, the veins in the area have no specific preferred general dip angle/direction but have random dips with general strike of between 100^0 and 150^0 (NW – SE).

Figure 33. *Unmineralised quartz vein (~30 cm thick) cutting through the arkosic sandstone unit, this is exposed in one of the exploration trenches within the study area.*

The quartz veins in the arkosic sandstone are comprised mainly of quartz (>70%) with minor minerals like albite and calcite and accessory minerals like hematite. The quartz veins are related to the later-stage deformation events and are the youngest rocks in the area relative to the other units. They cut across almost all the stratigraphic units in the licence area. They also represent late-stage silicification related to the late-stage deformation events, and in

some cases form tension gashes and sigmoidal veins of varying sizes. Both syntaxial with elongate crystal growth and antitaxial blocky vein types have been observed in the study area (see Fig. 9a and 9b).

Mineralised quartz vein samples from the NW-SE trending vein structure were also collected and analysed using polished thin section for samples LPV1A and LPV1B and TIMA for sample LPV1A. Laboratory analysis of sample LPV1 using fire assay gave a gold content of 0.2 g/t (Appendix 4). The mineralogical composition mainly comprised 75% quartz, 0.43% albite, 0.6% mixture of aluminosilicate minerals, and 0.42% chlorite. Grain relationship is typically interlocking quartz grain crystals as well as albite.

Mineralisation in LPV1 was observed to occur along grain boundaries and along fractures (Fig. 34b and 34c). The supergene phases in mineralised sample LPV1 were determined to be malachite, and chrysocolla (Fig. 34a and 34c) whereas the hydrothermal phases include chalcopyrite, chalcocite, bornite, pyrrhotite and pyrite (Fig. 34b, 34d and 34e).

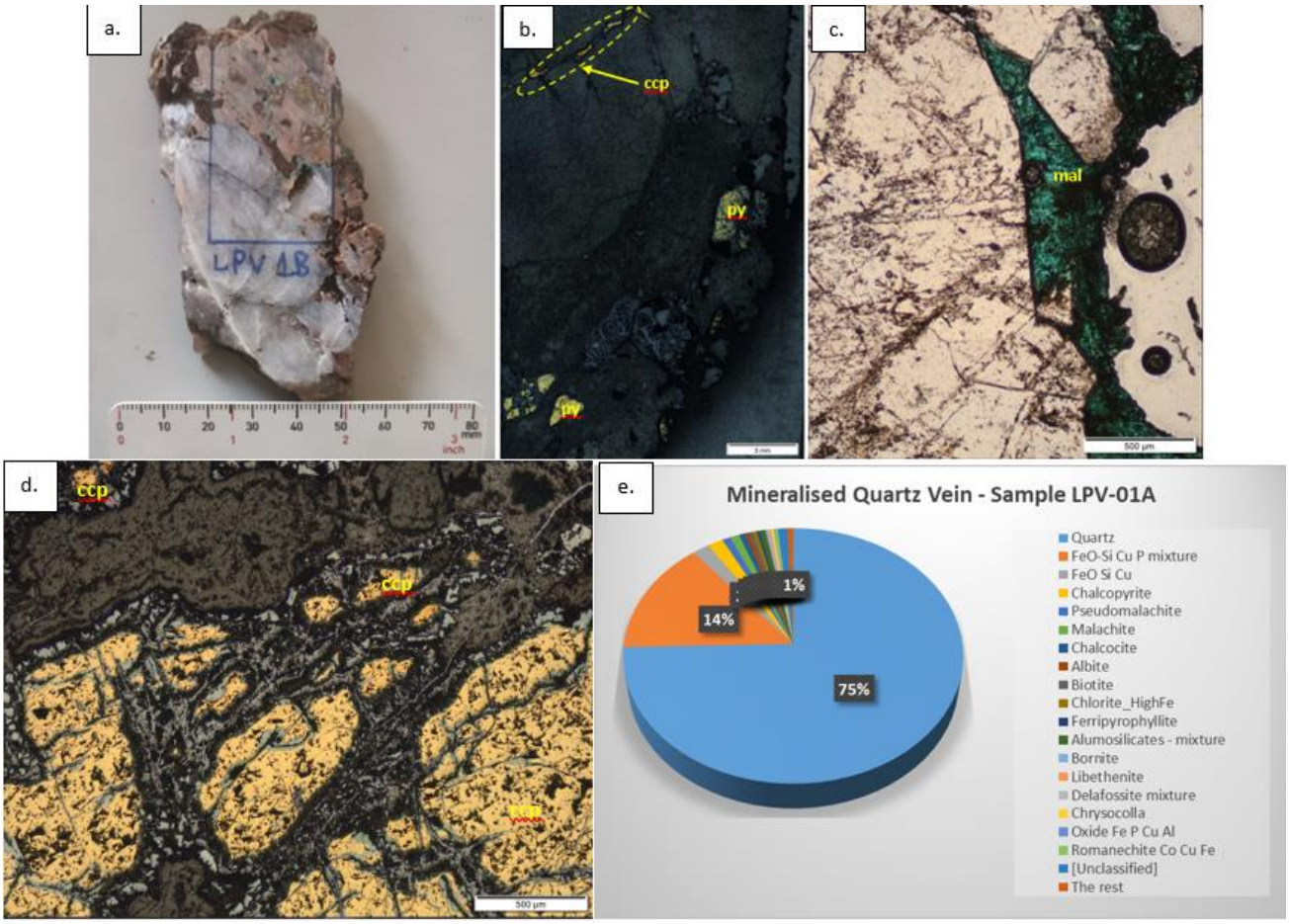

Figure 34. *Quartz vein sample LPV1 (a.) photograph of hand size sample with malachite and pyrite (b.) Photomicrograph of pyrite and chalcopyrite in reflected light, Cu mineralisation was observed to be along grain boundaries and fratures (c.) Photomicrograph at 500µm scale in plane polarised light with malachite (mal) mineralisation along fracture. (d.) Photomicrograph at 500µm scale in reflected light with chalcopyrite (ccp). (e.) Pie chart of the minerlogical composition of sample LPV1, sulphide composition includes chalcopyrite (1.61%), chalcocite (0.62%), bornite (0.22%).*

3.3 STRUCTURAL HISTORY

Based on the structural data, the following is a summary of the events that have affected the study area;

1) Folding and thrusting of units caused by a first deformation D1, which produced NNE -SSW trending folding and thrust structures;
2) A second deformation D2 resulting in NE-SW trending 1st order ductile-shear faults and folds, these were accompanied by post-diagenetic hydrothermal alteration and minor sulphide and gold mineralisation; and
3) The final phase of deformation D2, brittle deformation, which resulted in NW-SE faulting and folding structures which run perpendicular to the shearing. These were mineralisation hosting structures filled with secondary quartz. Some of the mineralisation is mainly hosted in saddle reef set-up (pit-2 of the study area located at UTM Arc 1950 210323mE/8689193mN). The late-stage silicification, sodic, and potassic alteration accompanied the entire D2 stage with more pronounced albitisation in all the units of the area.

CHAPTER FOUR

SOIL GEOCHEMISTRY

4.0 INTRODUCTION

Aim of the soil sampling exercise was to establish the location of a deposit via identification of areas with anomalous values of target elements within a study area. Target elements are usually referred to as "indicator" elements, which are a major or minor component of the orebody or mineralisation that is being sought i.e., when undertaking a soil geochemical survey in search of a Cu deposit, one indicator element that may be used is Cu (Rose et al., 1979).

In the event that the indicator element cannot be used due to its immobility in the surficial environment, an alternative associated element known as a ''pathfinder" can be used to locate the orebody / mineralised area. A clear-cut relationship between the pathfinder and the major components of the orebody being sought should clearly exist, needless to point out that not all elements can be used as pathfinders (Rose et al., 1979; Cohen and Bowel, 2014).

In an area where a deposit or an orebody exists, particular chemical components of the orebody may give anomalously high element readings thereby creating a surface indication which may be picked as an anomaly during a soil geochemical survey. A geochemical anomaly in soil geochemical survey is the enrichment of a particular element (or elements) in the soils which will be above the normal or background occurrence of that element in a particular area (Rose et al., 1979; Cohen and Bowel, 2014).

4.1 SOIL GEOCHEMISTRY OF THE STUDY AREA

In this soil geochemical survey, the initial plan was to use gold as the indicator element, however after the reconnaissance survey and laboratory trial analysis, it was established that the lower detection limit for gold for the two laboratories were relatively high (respectively 0.1 ppm and 0.01 ppm). What was required were detection limits in parts per billion (ppb), as this would give meaningful soil assays for gold which can be analysed and interpreted for target identification. This also meant the use of Inductively Coupled Mass Spectroscopy (ICP MS) analytical techniques, as this technique is able to detect gold in parts per billion but no commercial laboratory currently offers this analytical technique in Zambia. Since gold is relatively immobile in the surficial environment, and it is highly associated with more mobile elements like copper, zinc and cobalt in this area, it was decided to try and test if copper and other elements can be used as pathfinders to gold mineralised zones in the study area. The copper was also be used as the indicator element to check for possible copper mineralisation in the area.

4.1.1 SAMPLING AND SAMPLE ANALYSIS METHODS

Around 1650 soil samples were collected from the entire study area which covers a surface area of about 13.15 km^2. Samples were collected using a sampling grid of 200 m line spacing

by 100 m sample spacing with each sample weighing between 1.5 and 2.0 kg. Samples were collected from the B-horizon of the soil profile which is represented by the first 20 to 30 cm of the profile. All the collected samples were initially analysed using a portable XRF analyser, thereafter 854 of the 1650 samples were submitted to a laboratory for wet-chemistry analysis for copper, cobalt and silver. Sample preparation involved crushing and pulverising bulk samples to -75 microns then undertaking aqua regia acid digest to decompose the sample. Analysis was conducted using Atomic Absorption Spectroscopy (AAS) with the lower detection limit of 0.1 ppm.

4.1.2 REGOLITH PROFILE

A strongly weathered regolith profile occurs around the study area with most parts of the study area covered by in-situ residual soils. The weathering extent varies between a few metres up to 35 m in some parts of the study area. Depending on underlying bedrock, parts of the study area are underlain by clay-rich chloritic altered rock units which are characterised by loamy soil with aluminosilicate-derived minerals in the soil and saprolitic zone of the regolith. The aluminosilicates are weathered to kaolinite and other clay minerals with pronounced iron oxide alteration. Prevailing climatic conditions for the area can be classified as tropical to sub-tropical with consistent rainfall occurring between the months of November and April.

4.1.3 GEOCHEMICAL DISTRIBUTION OF ELEMENTS

Element composition of the gold mineralised zone were established by chemical analysis of mineralised samples collected from the mineralised zone which was exposed from historical and current mine workings. Some of the samples were respectively analysed using either XRF or using the laboratory via fire assay with AAS finish.

Some soil samples were also collected on top of the current mine workings, these were collected in 2019, prior to commencement of the ground disturbance or trial mining currently taking place.

***Table 3**: Data on the composition of background values of selected elements, with typical grades for ore for each element (After: Rose et al., 1979; Ridley, 2013). Also, assays of selected elements of a composite sample of Au ore from the study area with the enrichment factor calculated relative to the crustal abundance. Au and Ag were analysed using fire assay preconcentration with ICP-OES finish with the rest of the elements analysed using XRF Quantitative scan. All samples were analysed by Mintek laboratory in South Africa (see Appendix 4a for full list of assays).*

Element	Crustal Abundance (ppm)	Grade in typical Ore	Enrichment Factor (crust to ore) _ Clarke values	Composite Ore samples from study area - XRF Q_Scan	Enrichments factor on ore samples in study area (Crust to ore)
Al	82300	30%	4	7.70%	1
Fe	56300	60%	12	13.08%	2
Mn	950	5%	50	0.75%	8
Ni	75	1%	100	990ppm	13
Zn	70	10%	1000	840ppm	12
Ti	5700	5%	10	1.37%	2
Cu	55	1%	200	1.30%	236
Co	25	0.20%	80	1.22%	488
Ag	0.07	100ppm	1000	5ppm	71
Au	0.004	5ppm	1200	274ppm	68500
Pb	13	10%	10000	ND	-
U	3	0.10%	300	ND	-
Mo	2	0.30%	2000	0.12%	600
W	2	0.30%	2000	471.78	236
Sn	2	1%	5000	ND	-
Cr	100	5%	500	422.78ppm	4

From the analysis of a composite sample of the mineralised ore from the study area, major elements within the mineralised zone were identified via ratios of ore samples against that of the general crustal abundance of selected elements. Major element components related to the mineralisation which can be used as indicator/pathfinder elements based on their mobility include copper, cobalt and molybdenum with minor components being Ag, Zn, Ni and W. Other elements such as Pb, K, Mn, Fe and Cr were also reviewed through graphical plots, so as to have a broader understanding of the soil geochemical baseline of these elements in the different rock formations of the study area.

In geochemical data interpretation, one of the critical factors is developing an effective method to be employed, where multiple populations are put into consideration. A potential orebody or potential mineralisation is one of the hidden factors that may play a role in the development of an over-all geochemical pattern (Rose et al., 1979; Cohen and Bowel, 2014). Various techniques can be employed to establish if the observed geochemical pattern is related to mineralisation which may include techniques such as stochastic modelling and deterministic modelling. Stochastic analysis relies heavily on factor analysis (Reimann et al., 2002) or fractal or associated analysis.

Soil geochemical data for a particular element maybe presented in graphical form as a simple histogram on which the frequency of values is plotted against the element concentration. From the histogram plot, it can be determined whether the element concentration is normally distributed or positively skewed and this gives an overview of how the values are distributed as well as where the statistical parametres such as mean, mode, median and standard deviation occur relative to the distribution curve. A normal distribution curve will have a bell-shaped symmetry with the mean, mode and median located or almost located in the centre of the distribution curve whereas positively or right skewed distribution (mode > median > mean) will have most of the values concentrated on the left tail of the curve and the right part is characterised by fewer values resulting in a tail like curve which terminates towards the positive end. Positively skewed data sets are normalised by log-normalising which will result in having bell-shaped normal distribution from which background values can be ascertained and what is normal or abnormal can be discriminated from this curve.

In most cases, the rule of thumb is to use the mean plus two standard deviations (Mean+2SD) to establish a threshold to distinguish background from anomalies. More recently, a statistical approach of using percentiles is employed in distinguishing background values from anomalous values. iOGas software is preferred for this task, however due the non-availability of this software, the statistical review was done using excel and the spatial plots were done using ArcGIS 10.4.

For a histogram to be used in establishing the distribution of assay data, a minimum of eighty samples is required. For anything less than that, an alternative approach such as the mean plus 2SD is employed or a box and whisker plot is used.

4.1.4 DISTRIBUTION FOR COPPER

Based on the assays from the gold mineralised zones, copper is a major component of the gold enriched zone and therefore will be used as the main pathfinder element within the study area (see Table 5 above). This is also supported by the fact that Cu is more geochemically mobile than Au and therefore any anomalies can easily be picked from the near surface soils as compared to Au. Use of gold as the indicator element was not possible as the laboratory assays indicated that gold could not be detected from the assayed samples (which required assaying using an instrument with lower detection limit). Good pathfinder elements exhibit more favourable and desirable geochemical behaviour than target ore metal (Rose et al., 1979; Cohen and Bowel, 2014).

4.1.4.1 STATISTICAL DISTRIBUTION of COPPER ASSAYS

Using XRF assays for the study area, 1611 samples from a total population 1650 were used to establish the statistical distribution for copper in the study area. The minimum Cu value recorded was 3.94 ppm with the maximum being 968.9 ppm, however in the statistical analysis the 968.9 ppm was not included and was considered as an outlier sample simply

because it would have distorted the spread of the data thereby affecting all the statistical parameters. It was only included in the spatial analysis of the copper soil assays. The maximum was considered as 383.62 ppm as this was not an outlier value and would not affect the spread of the data. The mean, median, mode, standard deviation and coefficient of variation were 45.28, 35.53, 20.81, 1133.39 and 0.74 (74%) (Table 4). The variance of 1133.39 implies that the Cu XRF assays are widely spread and have a high variability as shown by the distribution curve (Figure 35), this was also the case for the standard deviation which was 33.67 ppm implying that most values were further away from the mean. Summary statistics for all the reviewed elements are given in Table 4.

***Table 4**: Average soil geochemical assays for the elements Cu, Co, Mo and Zn*

	Cu		Co		Mo		Zn	
	Normal	Lognormal	Normal	Lognormal	Normal	Lognormal	Normal	Lognormal
Min	3.94	1.37	1.10	0.10	2.02	0.70	6.26	1.83
Max	383.62	5.95	193.00	7.04	14.82	2.70	339.83	5.83
Range	379.68	4.58	191.90	6.95	12.80	1.99	333.57	3.99
Count	1611.00	1611.00	728.00	728.00	1017.00	1017.00	1127.00	1127.00
# of classes (k) = 1+3.3log10(N)	12	12	10	10	11	11	11	11
Class width c=R/K	33	33.00	18	0.67	1	0.18	28	0.33
Variance	1133.39	0.37	655.76	0.86	3.74	0.14	985.65	0.38
Std.Dev	33.67	0.61	25.61	0.93	1.94	0.37	31.40	0.61
Mean	45.28	3.62	27.20	2.92	5.06	1.55	52.07	3.79
Median	35.53	3.57	18.20	2.90	4.67	1.54	47.72	3.87
Mode	20.81	3.04	1.10	0.10	3.57	1.27	40.98	3.71
CoV	0.74	0.17	0.94	0.32	0.38	0.24	0.60	0.16

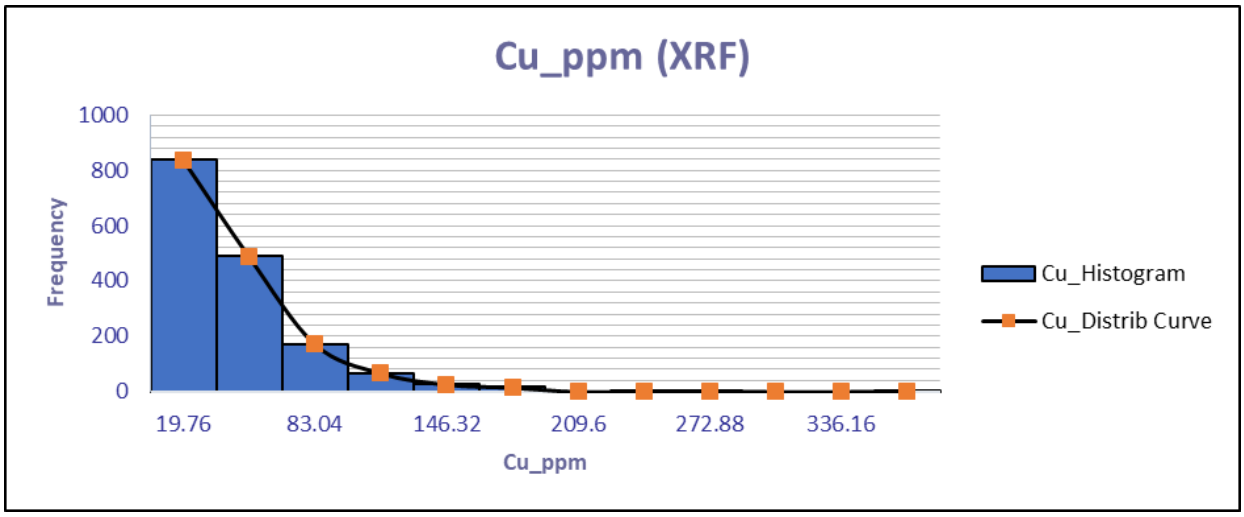

***Figure 35.** Histogram distibution of XRF soil assays for copper*

Based on the histogram plot and the summary statistics for the copper, it was observed that the assay data is positively skewed. To achieve a normal distribution for statistical calculations the data was log-normalised and then plotted on a histogram and it is from the

histogram where the background assays and the anomalous assays will be determined (Figure 36).

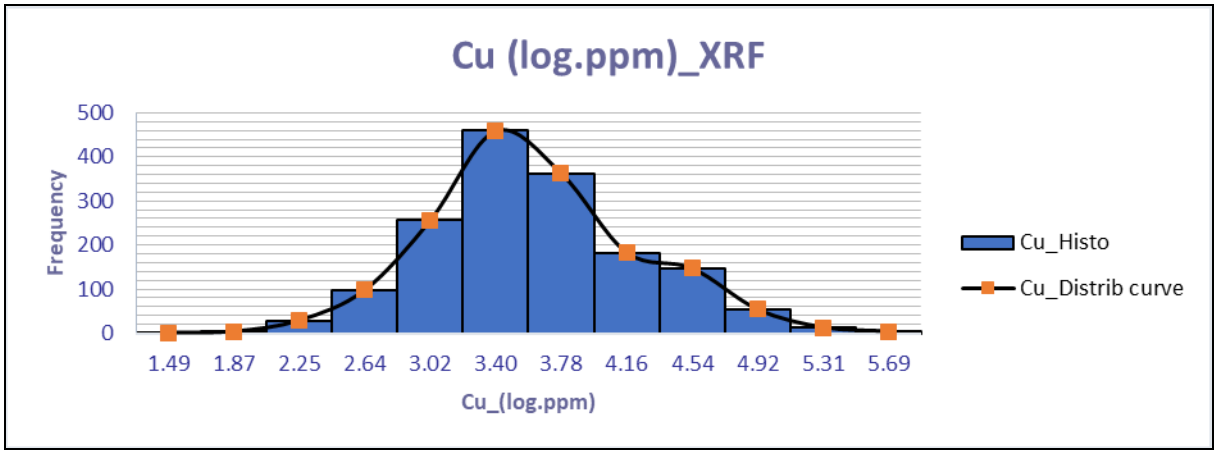

***Figure 36**. Log-normalised histogram distribution of XRF soil assays for copper from the study area*

After log-normalising the Cu assays, a normal distribution curve was obtained with the mean, mode and median centred close to the middle of the distribution curve. It was also established that the log of assay values of between 1.49 and 4.67 log ppm could be considered as normal background values; which implies that copper values below the 108 ppm (95th percentile) will be treated as normal for the study area whereas values above this threshold are considered as anomalous for the study area.

4.1.4.2 SPATIAL DISTRIBUTION of COPPER ASSAYS

Based on the soil geochemistry overlay on the geological map, the soil geochemical assays with values between 60 ppm and 108 ppm have a strong spatial relationship with the Nguba shale and diamictite units which underlie the centre of the study area and strike NE – SW (Fig. 37). The observed soil geochemical trend also coincides with the magnetic high feature of the first vertical derivative (1VD) which also has a NE – SW structural trend (Fig. 38).

The 1VD magnetic high observed in the area which has a structural trend of NE - SW is possibly related to the major shearing event which brought about magmatism which resulted in mafic alteration within the diamictite unit.

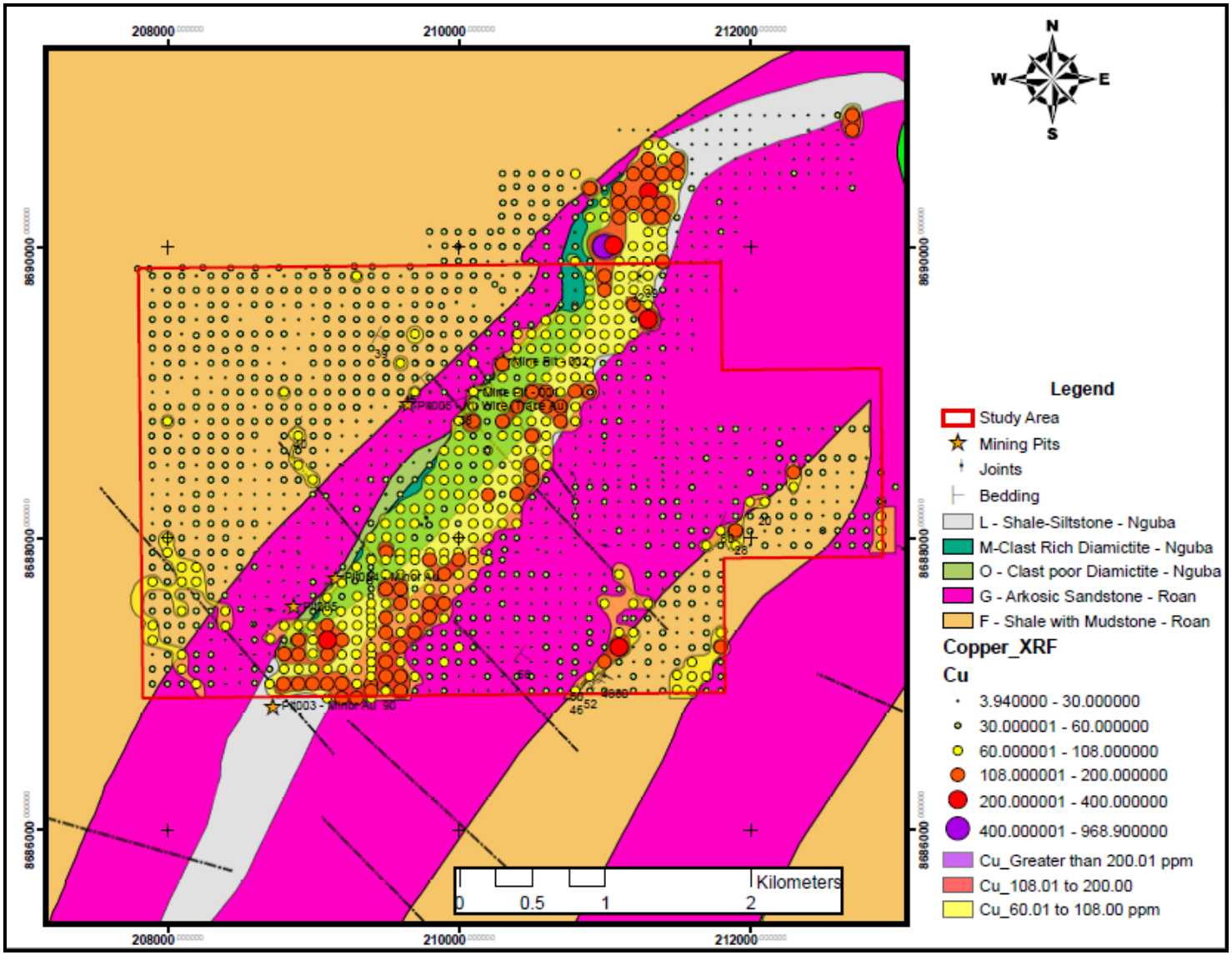

***Figure 37**: Map of soil geochemistry over geology for the XRF copper assays*

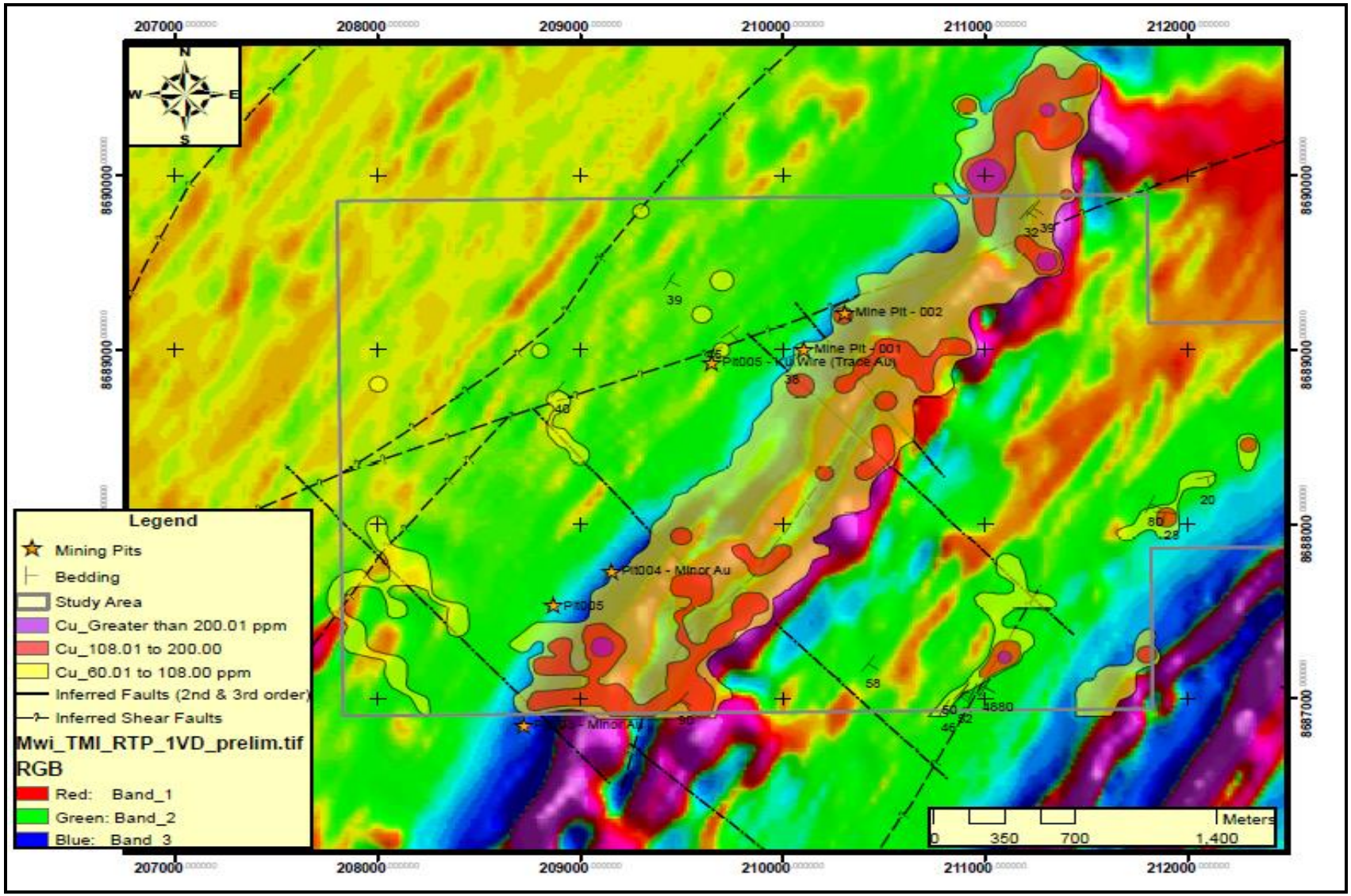

***Figure 38**: Soil geochemical map for Cu over aerial magnetics. Aerial magnetic image is the filtered image of 1st verticle deravitive (1VD).*

4.1.4.3 LOCATION OF COPPER SOIL GEOCHEMICAL ANOMALIES

Most copper anomalies in the study area are observed to be related to the NE-SW trending magnetic high, with this zone underlain by Nguba shale and diamictites (Fig. 39).

Based on the spatial distribution of the soil geochemical assays for copper (marked in Fig. 39), the following anomalies which may require follow-up have been listed in order of importance:

- Copper anomaly 1 which is located at UTM Arc 1950 Zone 35 south 210299mE/8689193mN is located where current gold mining is taking place. Soil sample K01275 was collected in this area prior to commencement of the current mining works. Observed element composition using XRF assays was Cu 166 ppm, Zn 92.71 ppm, Mn 1047 ppm, Ni 51.8, Pb 23.96 and Mo 3.89 ppm with the cobalt analysed by wet chemistry via the lab giving 68.1 ppm. Element composition of the soil sample collected in this zone can be used as a guide to search for other mineralised parts of the study area;
- Copper anomaly 2 located at UTM Arc 1950 Zone 35 south 210984mE/8690005mN, area was observed and identified to have a copper clearing with very poor plant growth and presence of the copper flower plant, this area may portray genuine anomalies;
- Discrete copper anomalies 3 located at UTM Arc 1950 Zone 35 south 208799mE/8687202mN, 209102mE/8687298mN and 209488mE/8687901mN were observed to sit on a magnetic low zone which has been interpreted to be part of a shear zone;
- Anomaly located at UTM Arc 1950 Zone 35 south 211308mE/8689510mN, was to be located on top of magnetic high when overlain on 1VD aerial magnetic map. Follow-up may be required via trenching and pitting to establish if the anomaly emanates from depth;
- Anomalies 4 and 5 located around UTM Arc 1950 Zone 35 south 210618mE/8688933mN, 210482mE/8688398mN and 209593mE/8687636mN were observed to sit in magnetic high zones. Also, from the soil geochemistry over geology and magnetics, these are interpreted to sit on a possible triple point where some NE – SW trending shear structure is intersected by NW – SE trending second order fault structure. Anomalies in this area may be related to possible mineralisation and therefore require follow-up; and
- Anomaly 6 is located around UTM Arc 1950 Zone 35 211117mE/8687244mN, 211910mE/8688027mN, 212318mE/8688445mN and 211805mE/8687255mN were observed to sit on the Roan shale/mudstone – arkose contact. Follow-up work in this area is recommended.

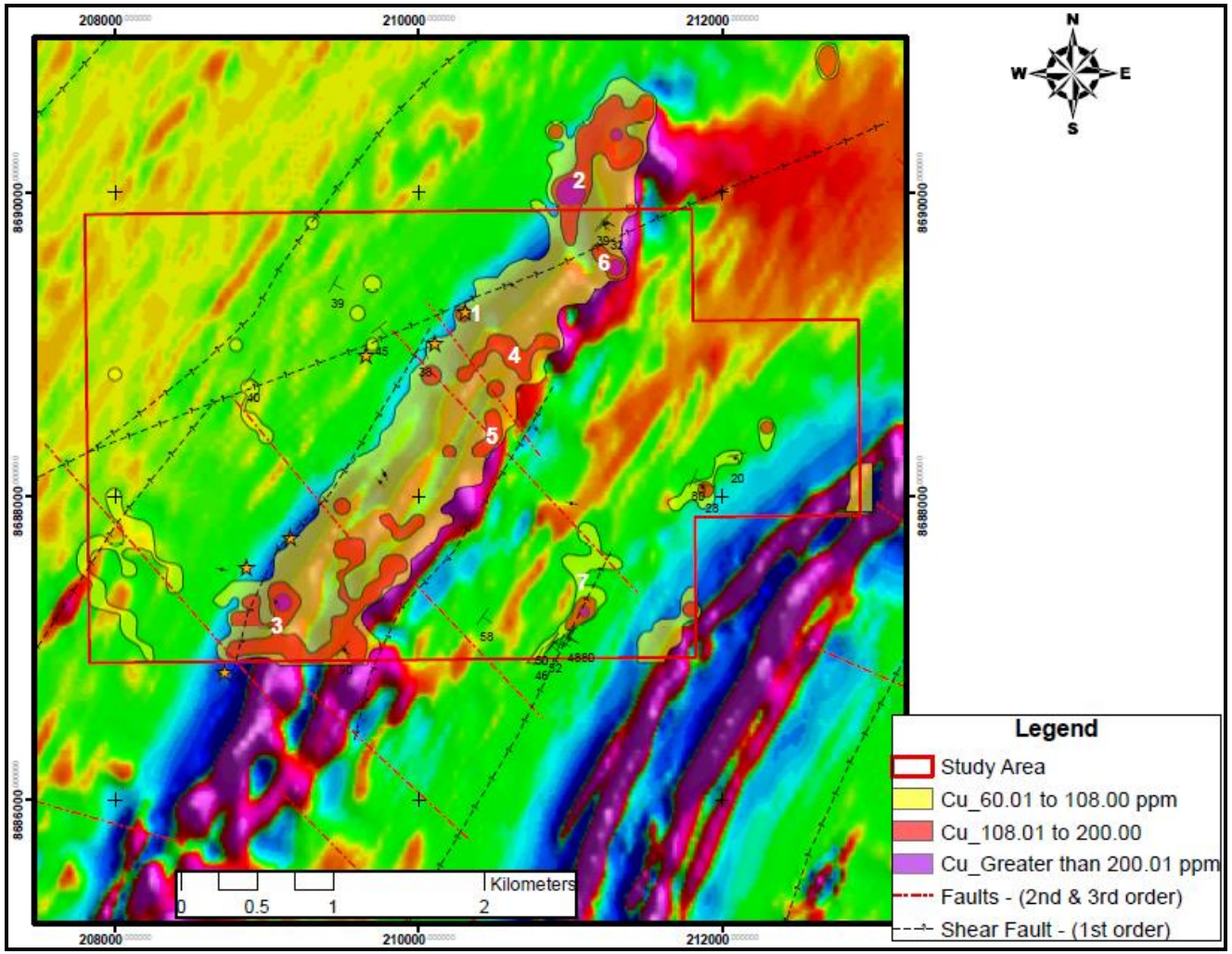

Figure 39: *Soil geochemical anomalies for copper over 1VD aeromagnetic image.*

4.1.5 DISTRIBUTION of COBALT

Cobalt is one of the significant elements of the gold-enriched zone. It has been considered as one of the main pathfinder elements within the study area. Cobalt is more geochemically mobile than gold and has a migration coefficient (K) of between 0.1 and 1, whereas gold has a migration coefficient of less than 0.1. In the surficial environment, elements with a coefficient of migration (K) greater than 10 are considered to be highly mobile, K = 1–10 are considered moderately mobile, K = 0.1–1 are slightly mobile, and K = 0.1 are considered immobile (Rose et al., 1979). Based on their migration coefficient and general geochemical behaviour in the surficial environment, cobalt anomalies can easily be picked up from the near-surface soils as compared to gold.

4.1.5.1 STATISTICAL DISTRIBUTION of COBALT from laboratory assays

Of the 856 reported assays, 729 were used to establish the statistical distribution for cobalt, particularly covering the central parts of the study area where the NE–SW magnetic high signature occurs.

For the statistical and spatial analysis of cobalt assays, laboratory assays were preferred over hand-held XRF assays in that a portable XRF analyser does not give reliable assays for cobalt (see section 4.4.2 for correlational plot). In the presence of iron and/or nickel during cobalt analysis, inter-element spectral interferences may occur from either the iron or nickel or from both. Identification of cobalt in the presence of nickel becomes difficult during analysis when using an XRF analyser, particularly if it occurs in low levels (Olympus Ltd, 2019; Laperche and Lemiére, 2020).

The minimum cobalt value recorded was 1.1 ppm, with the maximum being 1146 ppm. In the statistical analysis, the 1146 ppm was not included and was considered an outlier sample simply because it would have distorted the spread of the data, thereby affecting all the statistical parameters. It was only included in the spatial analysis of the cobalt soil geochemical assays. The maximum considered value for the statistical analysis was 193 ppm, as this was not an outlier value and would not affect the spread of the data. The mean, median, mode, standard deviation, and coefficient of variation were 27.20 ppm, 18.20 ppm, 1.1 ppm, 25.61, and 0.94 (94%). The variance of 655.75 implies that the cobalt XRF assays are widely spread and have high variability, as evidenced by the distribution curve (Fig. 40). This was also the case for the standard deviation, which was 25.61 ppm, implying that most values were further away from the mean.

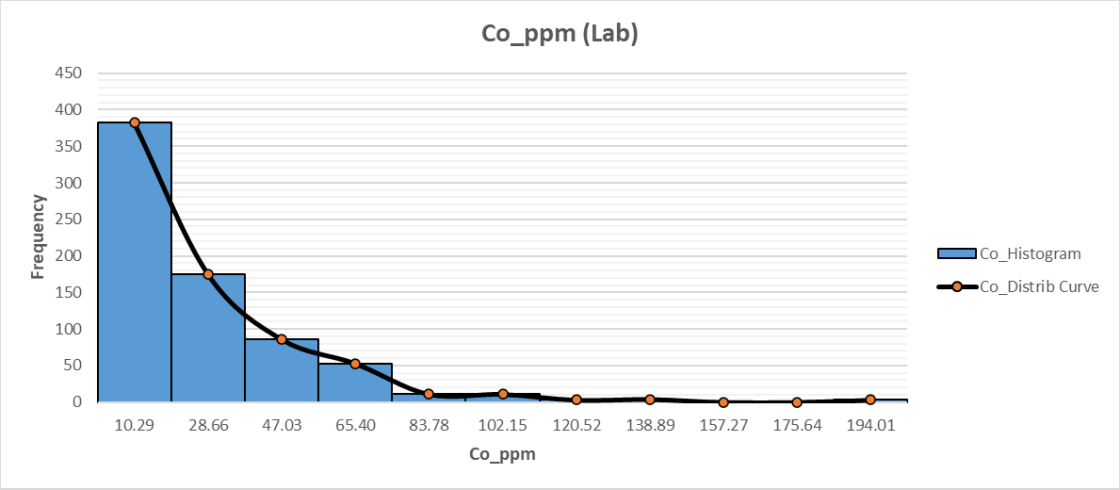

Figure 40: *Histogram distribution of laboratory soil assays for cobalt from the study area*

A log-normalised dataset was obtained in order to derive statistical parameters (Fig 41), which could be used ascertain the background values form the anomalies.

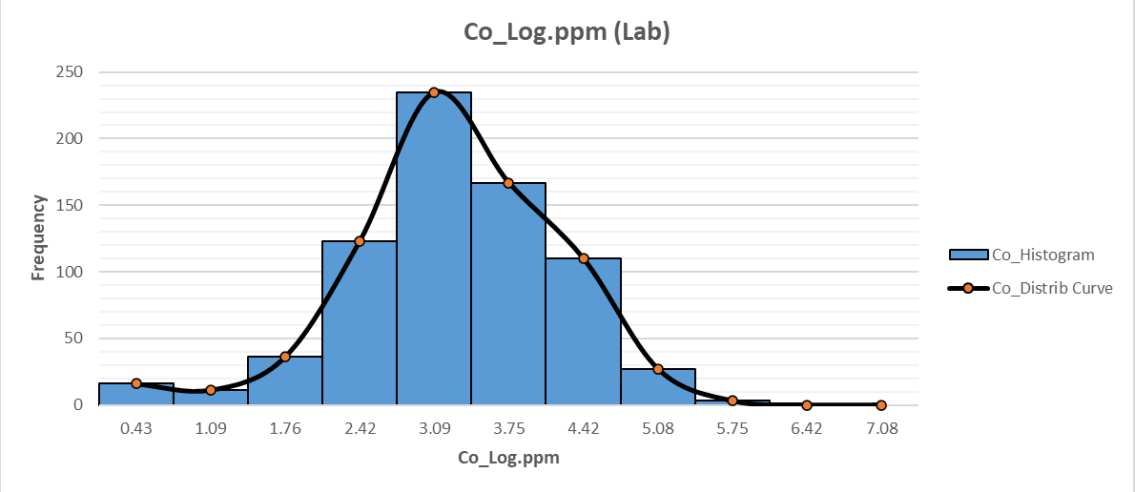

Figure 41*: Log-normalised histogram distribution of laboratory soil assays for cobalt from the study area*

After log-normalising the cobalt assays, a normal distribution bell-shaped curve was obtained (Fig. 41) with the mean, mode and median mostly centred close to the middle of the distribution curve. It was also established that the log of assay values of between 0.1 and 4.45 log.ppm could be considered as normal background values as these values fall within the normal part of the distribution curve. This implies that cobalt values below the 83.6 ppm (96^{th} percentile) will be treated as normal background values for the study area whereas values above this threshold will be considered as anomalous.

4.1.5.2 Spatial distribution of cobalt

After undertaking overlays of soil geochemistry for cobalt over the geological map, higher cobalt assay had a spatial relationship with the Nguba shale and diamictite unit (part of the Grand Conglomerat marker bed), which underlies the centre of the study area and strikes NE–SW, though most of the anomalies were isolated and did not show spatial continuity (Figs. 42 and 43). Spatial continuity trends of anomalies within an area are good indicators of possible orebody-elated mineralisation.

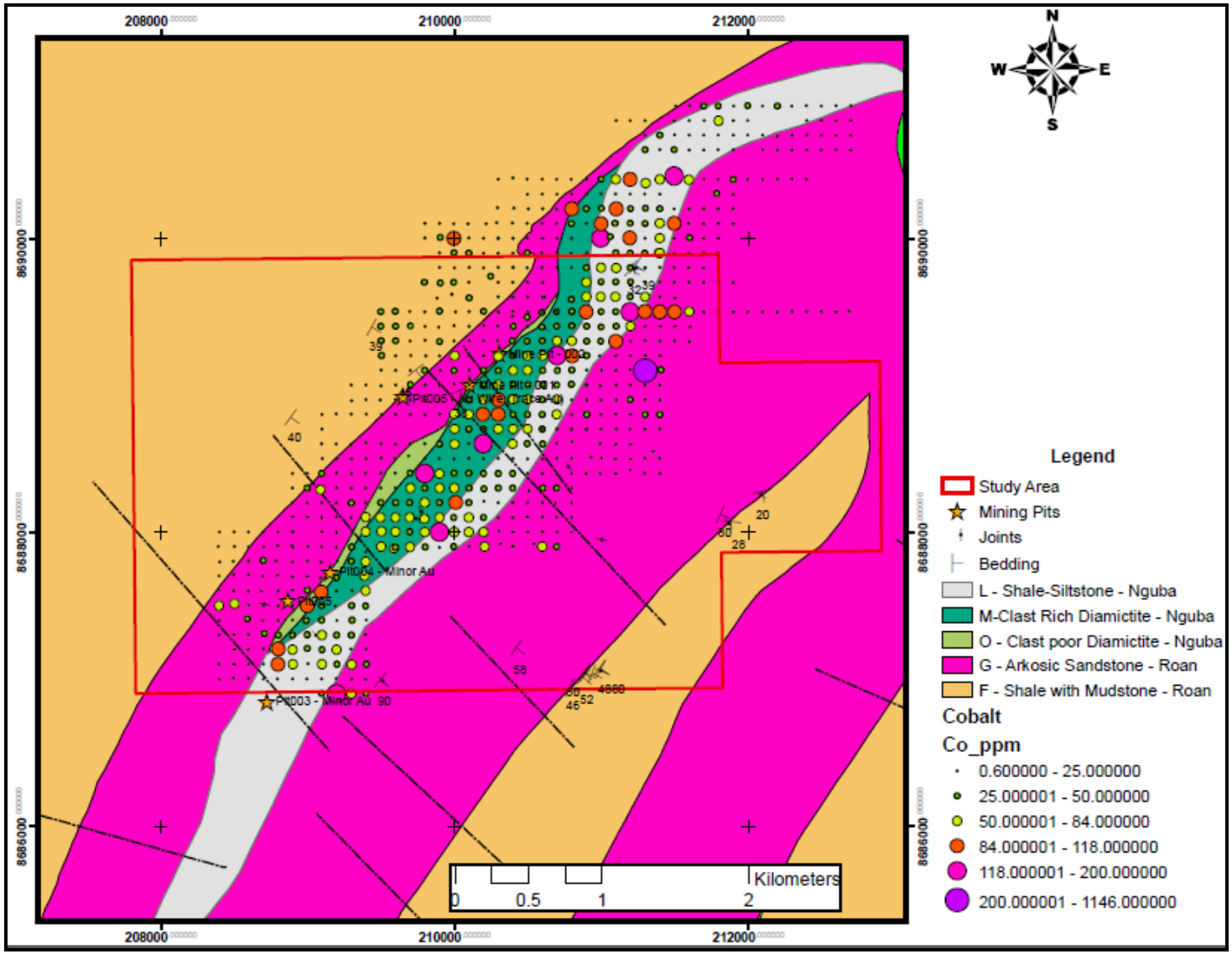

Figure 42: *Map of soil geochemistry for laboratory cobalt assays over geology*

4.1.5.3 LOCATION OF COBALT ANOMALIES

An overlay of cobalt soil geochemical assays over copper soil geochemical anomalies over aerial magnetics shows that a number of cobalt anomalies coincided with some of the copper anomalies (Fig.43). The following were the observed anomalies which may require follow-up;

- Cobalt anomalies 1 located around UTM Arc 1950 Zone 35 south 210984mE/8690005mN, coincide with the observed copper anomalies (tagged as 2 in Fig. 32) and were observed to have a copper clearing with some copper flowers in that area as recorded during the sampling, therefore this area may portray genuine anomalies;
- Cobalt anomalies 2 located at UTM Arc 1950 Zone 35 south 211308mE/8689510mN showed spatial continuity. These also coincide with the copper anomalies (tagged as 6 in Fig. 32) observed within this zone; and
- Discrete anomalies located at UTM Arc 1950 Zone 35 south 208799mE/8687202mN, 209102mE/8687298mN and 209488mE/8687901mN were observed to sit on a magnetic low zone which has been interpreted to be part of the shear zone;

Other observed cobalt anomalies are related to the disintegration of the strongly altered diamictite and Nguba shale units which underlie some parts of the licence area.

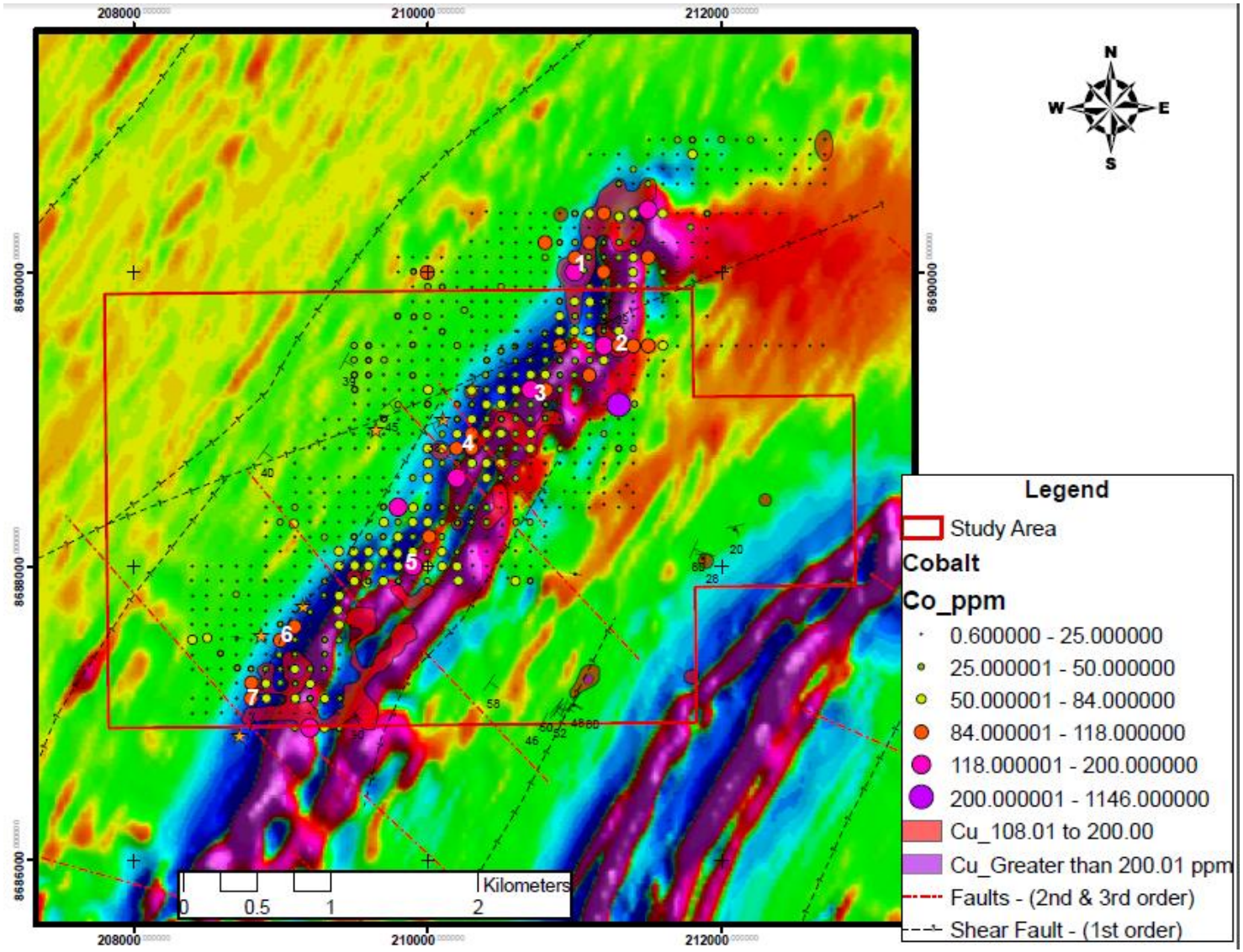

Figure 43: *Maps of Soil geochem for cobalt over aerial magnetics. Aerial magnetic image is the filtered image of 1st verticle derivative (1VD).*

4.1.6 DISTRIBUTION of MOLYBEDNUM

Molybdenum is also one of the significant elements of the gold enriched zones, it has therefore been considered as one of the main pathfinder elements within the study area. In the surficial environment molybdenum is more geochemically mobile than gold and has a migration coefficient of greater than 10 (K>10) whereas gold has a migration coefficient of less than 0.1 (K<0.1) (Rose et al., 1979).

4.1.6.1 STATISTICAL DISTRIBUTION of MOLYBDENUM - pXRF ASSAYS

Out of the total sample population of 1502 samples, 1017 samples were used for the statistical analysis of the portable XRF assays for molybdenum. The minimum molybdenum value recorded was 2.02 ppm with the maximum being 14.82 ppm. The mean, median, mode, standard deviation and coefficient of variation were 5.06 ppm, 4.67 ppm, 1.1 ppm, 3.57 ppm and 0.38 (38%) respectively. From the coefficients of variation and the variance, it can be observed there is moderate variability in the larger population of the data, this is also evidenced by the histogram distribution curve (Fig. 44).

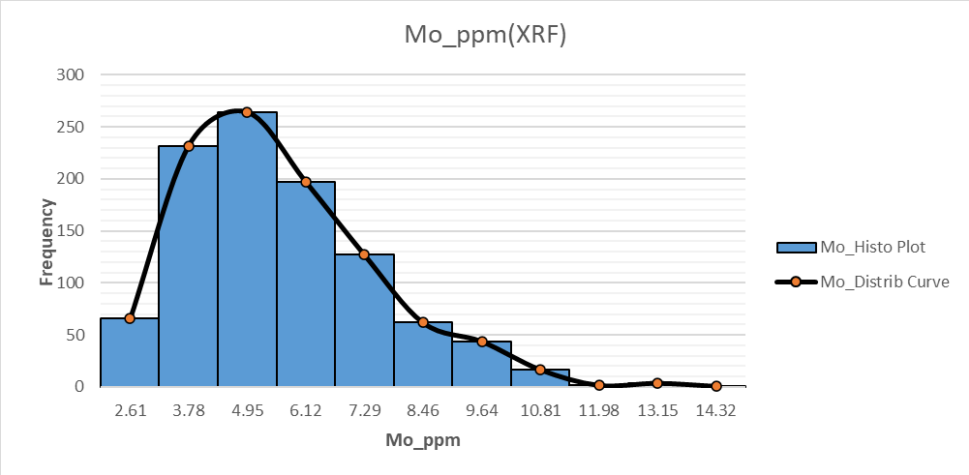

***Figure 44**: Histogram distribution curve for molybdenum*

The histogram plot showed a positively skewed to a near normal distribution of the XRF molybdenum assays. From the histogram distribution curve, it was established that the assays for the molybdenum ranging between 2.0 and 9.0 ppm were to be considered as normal background values as these values fall within the normal zone of the distribution curve which can be considered as normal for the study area. Molybdenum assays above 9.0 ppm were treated as anomalous.

4.1.6.2 SPATIAL DISTRIBUTION of MOLYBDENUM ASSAYS

From the spatial overlay of geochemistry over geology, molybdenum assays were observed to be relatively less in the arkose units when compared to either the diamictite or the shale

(Fig. 45). Anomalous molybdenum assays were observed to be spatially relatable to the shale – arkose contact as well as the inferred shear faults and second order inferred fault at location 209701mE/8687634mN (also see Fig. 45).

Since molybdenum as an element is highly mobile in the surficial environment, its usability as a pathfinder in this case is highly questionable as it has the ability to migrate significantly. Spatial correlation with the copper anomalies showed that it had no direct correlation in other parts of the study area with an exception of location 209734mE/8687608mN where it showed anomalous molybdenum occurrences on the margins of the copper soil anomalies (Fig. 46).

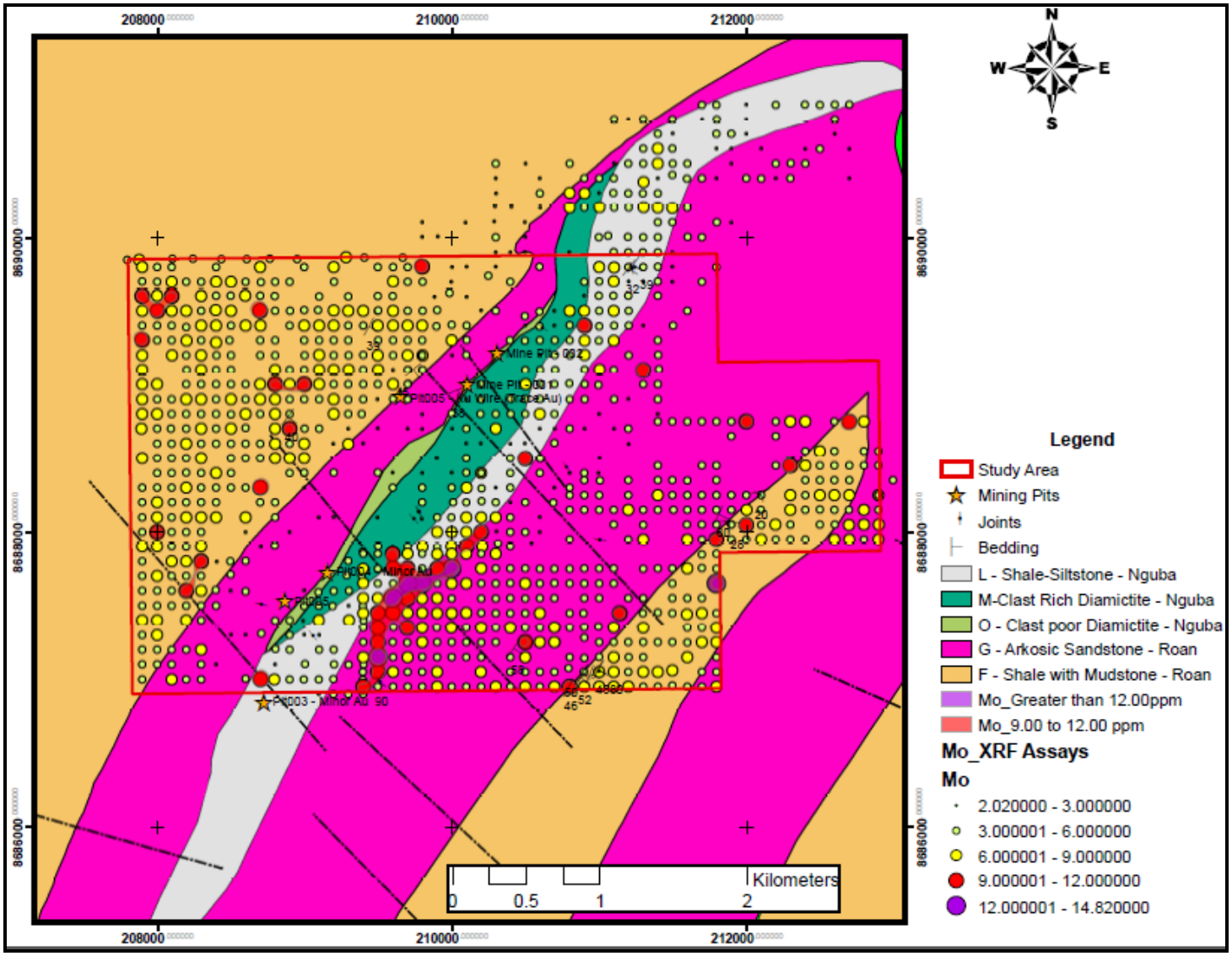

Figure 45: *Map of soil geochemistry for molybdenum assays over geology.*

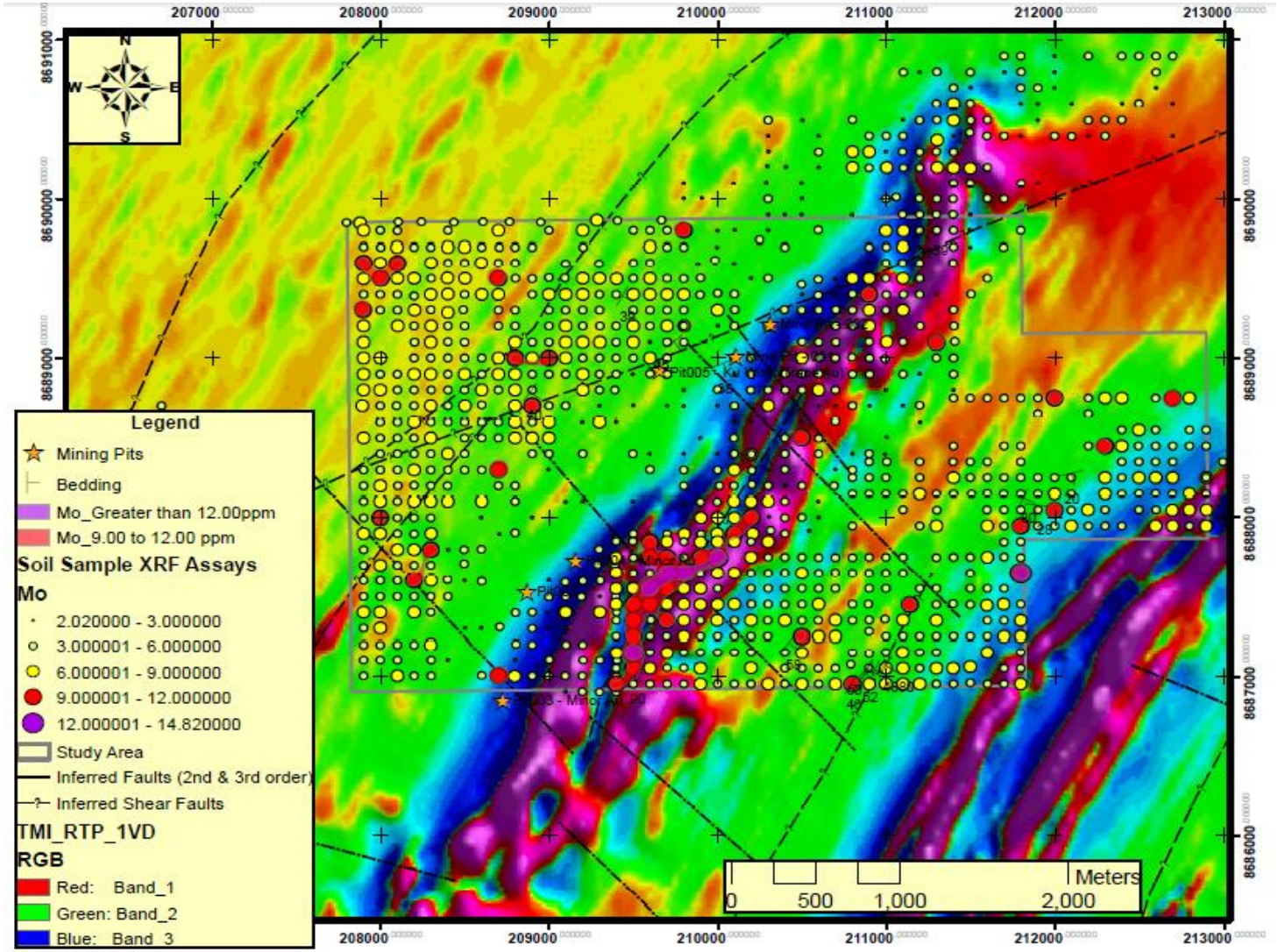

Figure 46: *Maps of Soil geochemistry for molybdenum over soil geochemistry for copper over aerial magnetics. Aerial magnetic image is the filtered image of 1st vertical derivative (1VD).*

4.1.7 DISTRIBUTION of ZINC

Zinc is one of the elements that was considered as one of the main pathfinder elements within the study area, mainly due to its mobility and the possibility of being related to ore mineralisation. In the surficial environment zinc is more geochemically mobile than gold and has a migration coefficient of between 1 and 10 (K = 1 - 10).

4.1.7.1 STATISTICAL DISTRIBUTION of ZINC - pXRF ASSAYS

Out of the total sample population of 1502 samples analysed, 1127 samples were used for the statistical analysis for zinc. The minimum assay for zinc recorded was 6.26 ppm and the maximum of 673.5 ppm. However, in the statistical analysis the 673.5 ppm was not included as it was considered as an outlier sample simply because it would have distorted the spread of the assay data thereby affecting all the statistical parameters. The mean, median, mode, standard deviation and variance were 52.04 ppm, 47.72 ppm, 40.98 ppm, 31.39 ppm and 985.65 respectively. From the variance, it can be observed there is moderate variability in the larger population of the data, this is also evidenced by the histogram distribution curve. The histogram was observed to be very slightly positively skewed (Fig. 47). To normalise the distribution, all the zinc assays were log-normalised so that a normal bell-shaped distribution curve is obtained (Fig. 48) and normal assays and anomalies are identified from the log-normalised data.

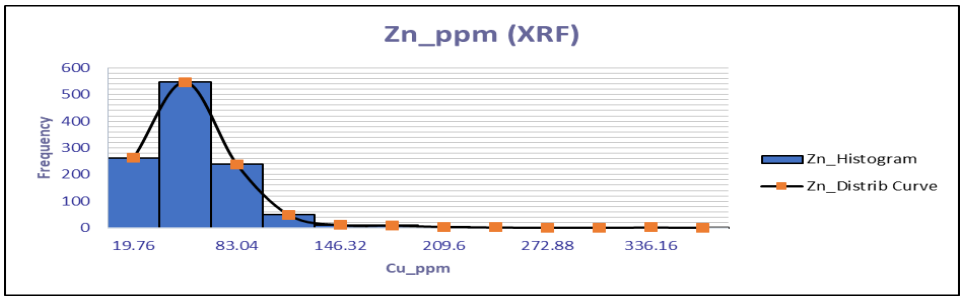

Figure 47: *Histogram distribution of XRF soil assays for zinc from the study area*

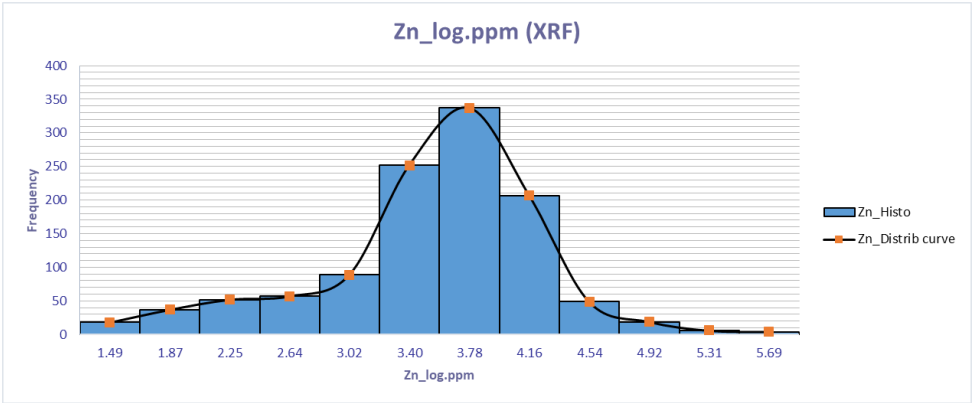

Figure 48*: Log-normalised histogram distribution of XRF soil assays for zinc from the study area*

After log-normalising the XRF zinc assays, it was established that the log of assay values of between 1.83 and 4.60 log.ppm could be considered as normal background values as these values fall within the normal part of the distribution curve. This implies that zinc values below the 100 ppm (96th percentile) will be treated as normal background values for the study area whereas values above this threshold will be considered as anomalous.

4.1.7.2 SPATIAL DISTRIBUTION of ZINC ASSAYS

From the spatial overlay of geochemistry over geology, the zinc assay was observed to be relatively poor in the arkose units when compared to the diamictite (Fig. 49). Anomalous zinc assays were observed to be spatially relatable to the diamictite – Nguba shale contact and these may require follow-up through pitting to check if the observed anomalies originate from depth. Some discrete high zinc values were also observed in the Roan shale, however they did not show any spatial continuity (see Fig 49).

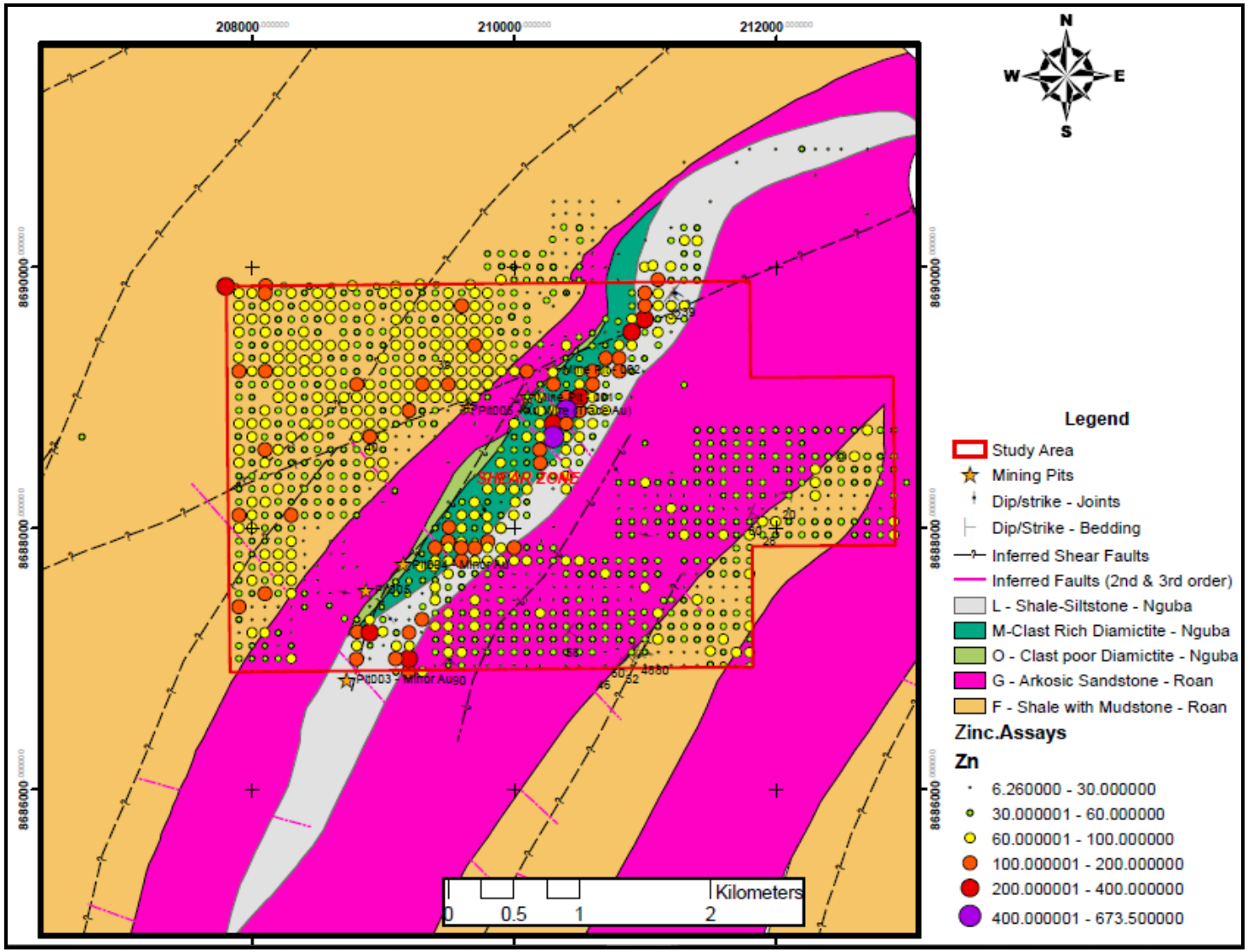

***Figure 49**: Spatial distribution of the zinc assays overlain on the geology.*

4.2 GRAPHICAL CORRELATION OF ELEMENTS TO ROCK UNITS

Apart from the statistical and spatial analysis of the assays, graphical presentation of the average assays for each element in specific rock units was also undertaken (Fig. 50). The elements were subdivided into three categories based on the average assays. Major elements included iron, titanium, potassium and calcium. Intermediate were classified as those with mean assays of between 100 and 500 ppm. Trace elements included copper, molybdenum, niobium, lead, tungsten, zinc, nickel, strontium, uranium, rubidium, thorium and arsenic.

Overall, the observed geochemical signature for the area showed an abundance of iron in the soils overlying the Grand Conglomerat diamictite unit and Nguba shale unit relative to the Roan shale and the arkosic sandstone. Other elements including titanium and potassium showed elevated assays in the soils overlying the Nguba units relative to the Roan member arkosic sandstone and Roan shale (Fig. 50).

For manganese, chromium, zircon and vanadium, the Nguba member units had relatively elevated assays in the residual soils on the Nguba shale and diamictite, with the exception of chromium which showed relative higher assays in the Roan shale (Fig. 43). Average assays in the Nguba units and the Roan shale were observed to be higher relative to the Roan member arkosic sandstone (Fig. 51).

For the trace elements, the Nguba member units were observed to have relatively higher assays for almost all the trace elements with the exception of tungsten which was observed to be relatively higher in the Roan shale (Fig. 52). The Roan member shale unit was also observed to have relatively higher assay averages in most elements the arkosic sandstone with the exception of niobium and rubidium.

The observed trend of element distribution in the soils overlying the major rock units in the study area shows that soils from the Nguba shale and Grand Conglomerat diamictite had elevated average assays for most of the elements. This can partly be attributed to the nature of the Nguba units which have the ability to act as reducing facies as well as their heterogenous nature which may influence their overall geochemical behavior. The diagenetic and post diagenetic composition of the rock units and eventual formation of residual soils has greatly played a major role in the overall soil geochemical signature observed in the study area.

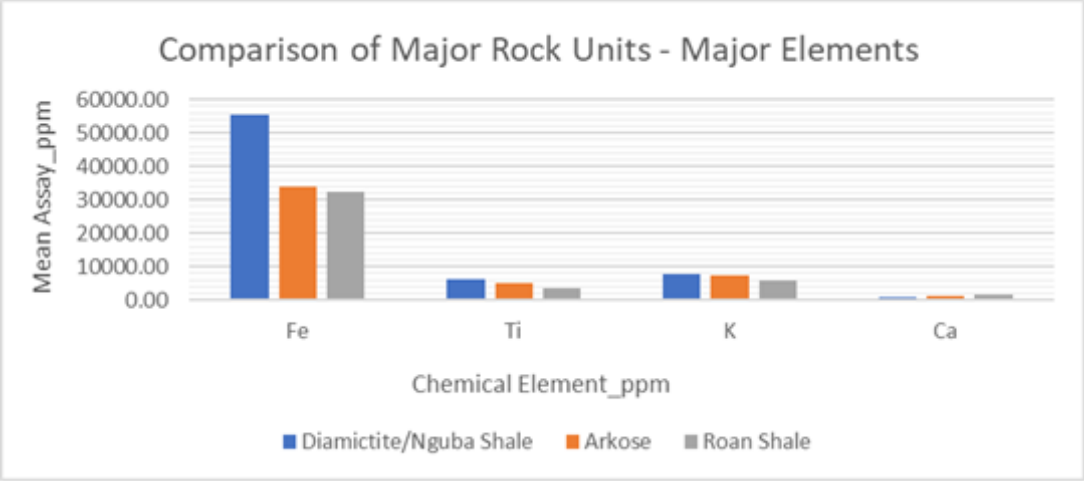

***Figure 50**. Average soil assays for Fe, Ti, K and Ca in each rock formation*

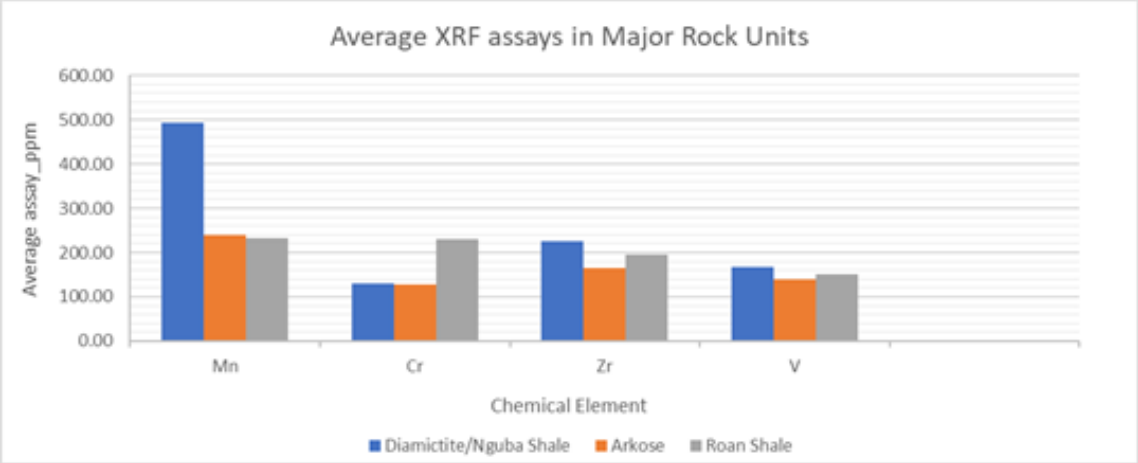

***Figure 51**. Average soil assays for Mn, Cr, Zr and V overlaying each rock formation.*

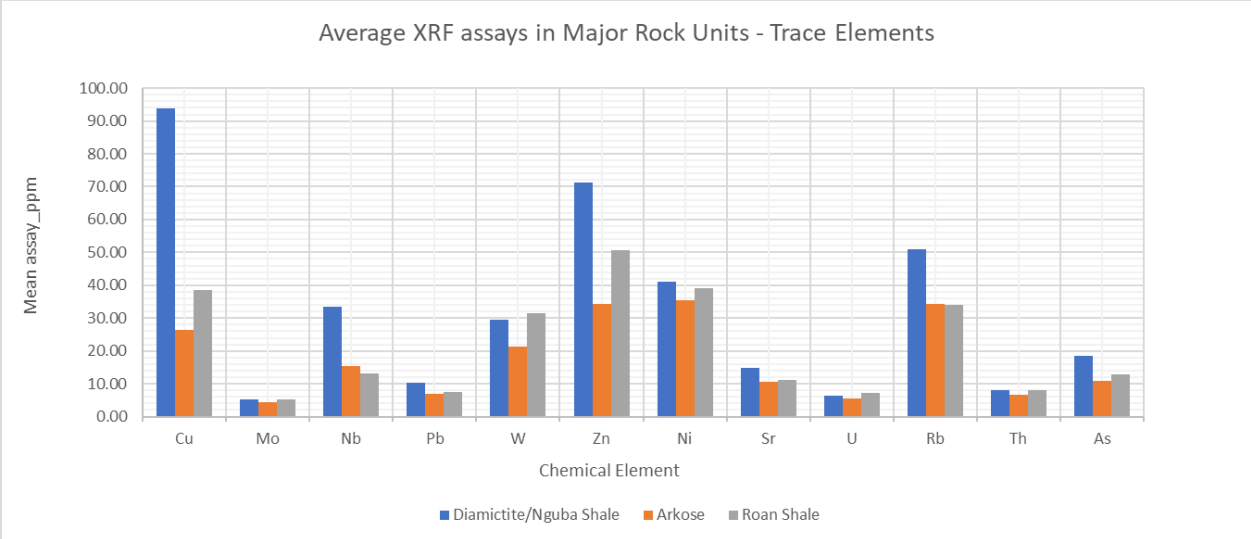

***Figure 52**: Average soil assays, trace elements overlaying each rock formation in the study area.*

4.3 CORRELATION of SELECTED ELEMENTS

Comparison of values of two data sets is essential in establishing how the values of two elements correlate, this also assists in checking the precision of assays if two different techniques are employed in the analysis method. Comparison of values for two data sets can be done either by regression plot, correlation matrix or line and scatter plot. Regression and correlation matrix offer the best correlation method for geochemical data.

4.3.1 COMPARISON of COPPER ASSAYS – pXRF VS LAB

A total of 856 samples were submitted to the laboratory for wet chemistry analysis. These samples were mostly those which were observed to have elevated assays for copper and cobalt. As a result, in order to check the precision of the reported assays from the pXRF assays, a comparison was performed to see how these two sets of assays correlate (Fig. 53). From the 856 samples, a few random samples were selected for correlation purposes.

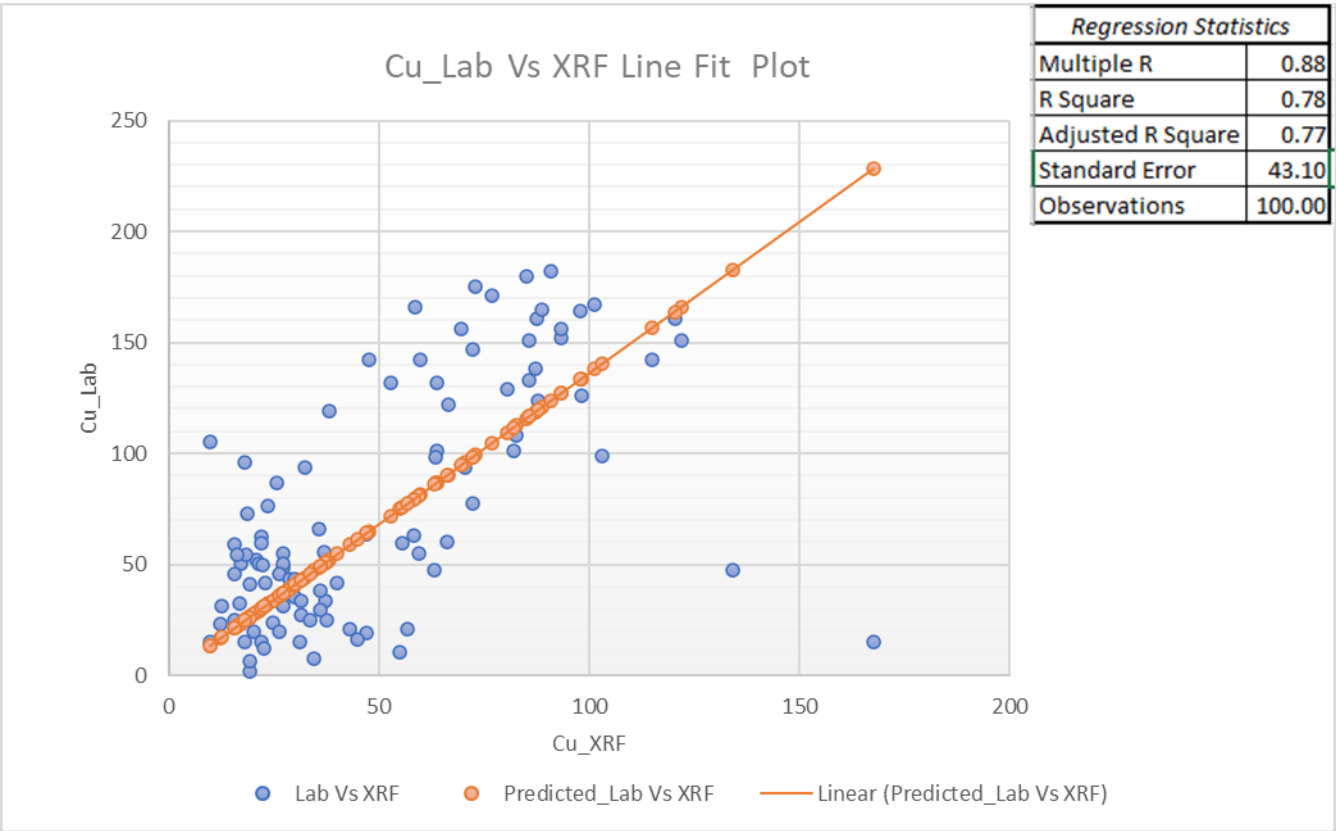

Regression Statistics	
Multiple R	0.88
R Square	0.78
Adjusted R Square	0.77
Standard Error	43.10
Observations	100.00

***Figure 53**: Regression plot comparing lab copper assay data vs XRF copper assay values*

The graphical trend shows that that copper lab assays and pXRF assays correlate, though most of the assays from the pXRF were below those of the laboratory assays. This discrepancy can be attributed to the sample preparation aspect for the lab-based samples,

which undergo crushing, pulverising, and acid soluble leach prior to analysis, which will entail almost full liberation of the elements contained in the sample. pXRF analysed samples are not subjected to this kind of destructive preparation technique. Also, based on the regression plot, it was observed that the copper lab assays versus pXRF assays had a relatively strong correlation of 0.78. The closer R^2 is to 1 the more the assays strongly correlate. The correlational range lies between +1 and -1, with +1.0 representing the best and -1.0 denoting the worst.

4.3.2 COMPARISON of COBALT ASSAYS – pXRF VS LAB

Also, for the cobalt analysis a total of 856 samples were submitted to the laboratory for wet chemistry analysis, these samples were mostly those which were observed to have elevated assays for copper and cobalt. Therefore, with the aim of checking the precision of the reported cobalt assays from the portable XRF assays, comparison was undertaken to check on how these two (02) sets of assays correlate (Fig. 54). From the 856 samples, a few samples were selected for correlation purposes.

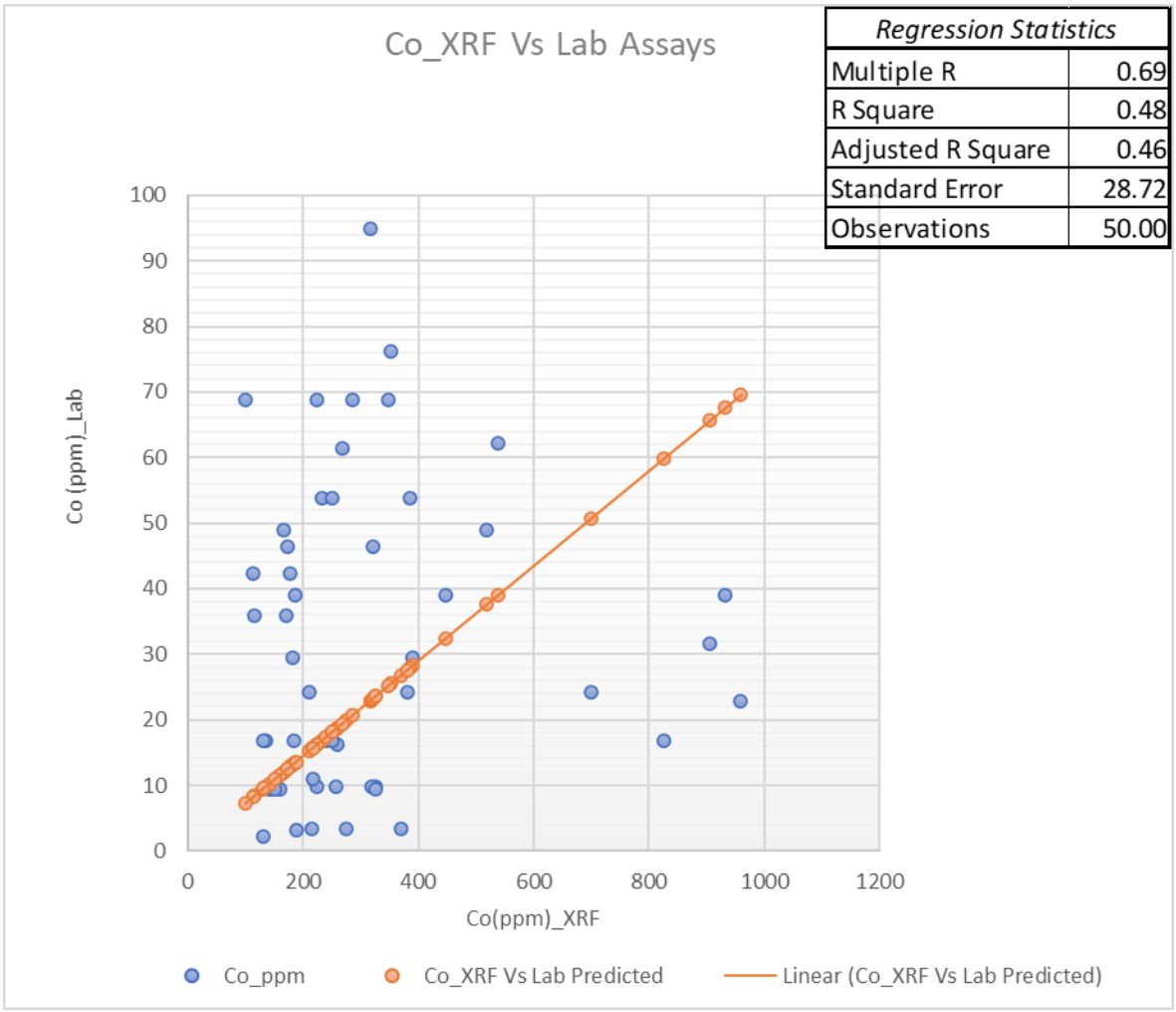

***Figure 54**: Comparison of cobalt assay data analysed by pXRF vs Lab*

Based on the graphical comparisons it was observed that the cobalt laboratory assays versus the pXRF had a weak correlation and most of the cobalt pXRF assays showed higher assays than the laboratory assays. As earlier highlighted in section 4.1.5.1, the observed discrepancy between the lab assays and the pXRF assays can be attributed to the fact that a pXRF analyser does not give reliable assays for cobalt.

4.3.3 CORRELATION of ELEMENTS - XRF ASSAYS

A correlation matrix was generated with aim of establishing how most of the detected elements in the pXRF assays linearly relate. In the event that values relate positively, the variables will increase or decrease correspondingly thereby obtaining a positive or negative correlation outcome. Correlation values range between +1 and -1, with +1 being a perfect and -1 being a converse outcome. This approach gives an insight into which elements strongly or poorly correlate with regards to the reported assays from the study area.

Thorium vs bismuth showed the strongest correlation of 0.9220, though the pXRF assays for bismuth cannot be considered as reliable, as the best analytical method is through atom absorption spectroscopy (AAS). Other elements that showed relatively strong correlation include tungsten vs chromium (0.7093), molybdenum vs tungsten (0.6971), titanium vs vanadium (0.6718) and rubidium vs potassium (0.6145).

***Table 5**: Correlation Matrix of pXRF assays from the study area*

	Cu	*Mo*	*Nb*	*Pb*	*W*	*Zn*	*Ni*	*Co*	*Fe*	*Mn*	*Cr*	*Ti*	*Zr*	*Sr*	*U*	*Rb*	*Th*	*As*	*V*	*Ca*	*K*	*S*	*Bi*
Cu	1	0.1097	0.4758	0.4474	0.1656	0.2811	0.2334	0.3687	0.4465	0.3334	-0.0444	0.1467	0.3225	0.2028	0.0844	0.2886	0.2295	0.5844	0.1517	-0.0170	0.0809	0.0752	0.1301
Mo	0.1097	1	0.0020	0.1297	0.6971	0.1428	0.2471	0.4693	0.1927	0.0544	0.4715	-0.2619	0.1863	0.0270	0.2560	-0.3002	0.0942	0.0754	0.1593	0.1980	-0.4048	0.0245	0.1772
Nb	0.4758	0.0020	1	0.2230	-0.0523	0.3010	0.1936	0.3411	0.6110	0.2817	-0.3115	0.4940	0.5182	0.3182	-0.0259	0.4426	0.2256	0.3435	0.2181	-0.1176	0.1866	0.0245	0.1082
Pb	0.4474	0.1297	0.2230	1	0.178289	0.2355	0.1575	0.2429	0.3151	0.3335	-0.0023	0.0894	0.1948	0.1111	0.1043	0.1248	0.1835	0.4234	0.1089	-0.0243	0.0359	0.0500	0.1412
W	0.1656	**0.6971**	-0.0523	0.1783	1	0.0595	0.2764	0.6309	0.2782	0.1065	0.7093	-0.3619	0.1868	0.1202	0.3991	-0.3479	0.1450	0.1841	0.2997	0.4025	-0.4704	0.1204	0.1448
Zn	0.2811	0.1428	0.3010	0.2355	0.0595	1	0.262161	0.2048	0.3507	0.2910	0.0015	0.0515	0.1883	0.0964	0.2150	0.1242	0.2204	0.2635	0.0563	-0.2554	0.0398	0.1722	0.3904
Ni	0.2334	0.2471	0.1936	0.1575	0.2764	0.2622	1	0.3185	0.3997	0.3103	0.0852	0.0223	0.2040	0.2232	0.3355	0.2589	0.2482	0.1666	0.0693	0.0528	-0.0260	-0.2573	0.1997
Co	0.3687	0.4693	0.3411	0.2429	**0.6309**	0.2048	0.3185	1	0.7356	0.2480	0.2389	0.0947	0.2837	0.1693	0.2027	-0.0158	0.0747	0.4138	0.3154	0.1725	-0.1176	0.0821	0.0191
Fe	0.4465	0.1927	**0.6110**	0.3151	0.2782	0.3507	0.3997	**0.7356**	1	0.3307	-0.0439	0.3038	0.3800	0.1982	0.0823	0.2199	0.0671	0.4890	0.3595	0.0377	0.0437	0.0609	0.0315
Mn	0.3334	0.0544	0.2817	0.3335	0.1065	0.2910	0.3103	0.2480	0.3307	1	-0.1479	0.1665	0.1340	0.3368	0.0602	0.2858	0.1183	0.2589	0.0713	-0.0644	0.2074	0.0533	0.1294
Cr	-0.0444	0.4715	-0.3115	-0.0023	**0.7093**	0.0015	0.0852	0.2389	-0.0439	-0.1479	1	-0.2440	0.1631	-0.0310	0.2758	-0.6060	0.0169	-0.1191	0.4655	0.4328	-0.4089	0.0650	-0.0361
Ti	0.1467	-0.2619	0.4940	0.0894	-0.3619	0.0515	0.0223	0.0947	0.3038	0.1665	-0.2440	1	0.1547	0.0543	-0.2160	0.2506	-0.0227	0.1025	0.6718	-0.1535	0.6485	-0.1130	-0.1906
Zr	0.3225	0.1863	0.5182	0.1948	0.1868	0.1883	0.2040	0.2837	0.3800	0.1340	0.1631	0.15468	1	0.2021	0.2886	0.1973	0.3840	0.1524	0.2976	-0.0220	-0.0017	0.0545	0.2256
Sr	0.2028	0.0270	0.3182	0.1111	0.1202	0.0964	0.2232	0.1693	0.1982	0.3368	-0.0310	0.05426	0.2021	1	0.2369	0.3409	0.2107	0.1643	0.0160	0.0332	0.2460	0.0275	0.1861
U	0.0844	0.2560	-0.0259	0.1043	0.3991	0.2150	0.3355	0.2027	0.0823	0.0602	0.2758	-0.21598	0.2886	0.2369	1	0.1477	0.5222	0.1349	0.0101	0.0341	-0.0440	0.1409	0.4919
Rb	0.2886	-0.3002	0.4426	0.1248	-0.3479	0.1242	0.2589	-0.0158	0.2199	0.2858	-0.6060	0.25058	0.1973	0.3409	0.1477	1	0.3805	0.3794	-0.1721	-0.3225	0.6145	0.0796	0.2873
Th	0.2295	0.0942	0.2256	0.1835	0.1450	0.2204	0.2482	0.0747	0.0671	0.1183	0.0169	-0.02267	0.3840	0.2107	**0.5222**	0.3805	1	0.2473	-0.0046	-0.0979	0.1219	0.2370	0.9220
As	**0.5844**	0.0754	0.3435	0.4234	0.1841	0.2635	0.1666	0.4138	0.4890	0.2589	-0.1191	0.10254	0.1524	0.1643	0.1349	0.3794	0.2473	1	0.0898	-0.0185	0.1358	0.0408	0.1093
V	0.1517	0.1593	0.2181	0.1089	0.2997	0.0563	0.0693	0.3154	0.3595	0.0713	0.4655	**0.67180**	0.2976	0.0160	0.0101	-0.1721	-0.0046	0.0898	1	0.1690	0.2707	-0.0539	-0.0750
Ca	-0.0170	0.1980	-0.1176	-0.0243	0.4025	-0.2554	0.0528	0.1725	0.0377	-0.0644	0.4328	-0.15349	-0.0220	0.0332	0.0341	-0.3225	-0.0979	-0.0185	0.1690	1	-0.3314	0.0412	-0.1229
K	0.0809	-0.4048	0.1866	0.0359	-0.4704	0.0398	-0.0260	-0.1176	0.0437	0.2074	-0.4089	0.64850	-0.0017	0.2460	-0.0440	**0.6145**	0.1219	0.1358	0.2707	-0.3314	1	-0.029	0.1017
S	0.0752	0.0245	0.0245	0.0500	0.1204	0.1722	-0.2573	0.0821	0.0609	0.0533	0.0650	-0.11305	0.0545	0.0275	0.1409	0.0796	0.2370	0.0408	-0.0539	0.0412	-0.0286	1	0.1996
Bi	0.1301	0.1772	0.1082	0.1412	0.1448	0.3904	0.1997	0.0191	0.0315	0.1294	-0.0361	-0.19061	0.2256	0.1861	0.4919	0.2873	**0.9220**	0.1093	-0.0750	-0.1229	0.1017	0.1996	1

CHAPTER 5

NOVEL GEOLOGICAL MODEL for GOLD MINERALISATION IN MWINILUNGA AREA

5.1 INTRODUCTION

Based on the observations from the soil geochemical studies, petrographic studies, and structural geology, a new modelled exploration approach around the Mwinilunga area and beyond has been suggested.

5.2 GEOLOGICAL UNITS, STRUCTURES AND MINERALISATION

The stratigraphic position of the units that have shown to have a strong relation to gold mineralisation in the Mwinilunga area include the Roan member arkosic sandstone which is oxidised facies, the Nguba member diamictite (or Grand Conglomerate) and the Nguba shale which acts as the reducing facies. The presence of oxidising units or their equivalent in this environment played an important role in the focusing and transportation of gold bearing fluids which are derived from the basement or lower stratigraphic levels of the Katanga sequence. The fluid migration is mainly vectored via structures onto the reducing facies which are the diamictite unit and the Nguba shale, with the clast poor variety of the diamictite as the preferred host units for the mineralisation.

The presence of the mafic igneous outcrops 15 km northeast of the study area is suspected to be the engine for the fluid migration with the diamictite and Nguba shales located in the study area acting as the appropriate trap sites for the gold and sulphide mineralisation. The presence of an engine to drive the mineralised fluids is also important for fluid migration.

Exploration implications are that not all units from the study area and beyond are capable of hosting mineralisation. This is based on the observed trend both from the petrographic studies and the soil geochemistry. The target rock formation for gold mineralisation in the study area and its surroundings should include the Grand Conglomerat Formation which comprises the diamictite and Nguba shale units as these units have shown the ability to act as reducing facies, as evidenced by the presence sulphide minerals in both units (samples, L0427, A3109 for diamictite unit and sample L05959 for Nguba shale unit). Also based on the petrographic studies (and soil geochemistry), Roan member units of shale and arkosic sandstone did not exhibit much potential to host gold and/copper mineralisation, though vein hosted gold mineralisation was intersected in the arkosic sandstone in one of the diamond drill holes. The arkosic sandstone may have also played a critical role in the location of the observed mineralisation in the study area in that, due to its porosity, it was easily able to allow fluid flow within it and the brittle fractures that developed during later stages of D2 deformation. The entire study area and the surrounding areas have been affected by post-diagenesis deformation events which were accompanied by fluid flow, resulting in alteration of some of the units in the area.

Mineralisation is more pronounced in alteration haloes in the clast-poor diamictite which surrounds the quartz veins around the diamictite – arkosic sandstone contact zone, with most of the copper and gold related mineralisation in the vein itself observed to be along fractures on microscopic scale. Folding with a northwest – southeast axial trace form saddle reefs where richer pockets of gold mineralisation have been observed. The presence of this physiochemical redox boundary of arkosic sandstone – diamictite – quartz vein is one of the critical controlling factors to the presence of gold mineralisation in this area. An observed magnetic high response of the diamictite unit from the processed aeromagnetic images proves that magnetics can reliably be used not only for lithological mapping but for picking out crosscutting structures within units with a high magnetic response.

Major structural controls to the mineralisation are the observed ductile shear faulting and folding which have a northeast – southwest structural trend and represent the ductile phase of the second deformation (D2). Northwest – southeast trending faults, joints and veins represent the brittle phase of the second deformation (D2). The entire D2 deformation event is suspected to have been accompanied by albitisation which has resulted in almost all the units in the study having vein and replacement albite. From TIMA studies, albite has been observed to be rimed by potassic minerals like biotite whereas orthoclase was observed to be rimed by albite (Appendix 4). Overall, respectively identifying district-scale, deposit-scale and micro-scale structures such as shear faults, folds, normal faults, and saddle reefs are critical in understanding the mineralisation controls for this area.

CHAPTER 6

DISCUSSION AND CONCLUSION

6.1 PETROGRAPHY, STRUCTURAL GEOLOGY AND SOIL GEOCHEMISTRY

Gold mineralisation in the Nguba group of the Katanga Supergroup is not common, therefore in the quest to obtain the best exploration model, petrographic, structural geology and soil geochemical studies were conducted over the study area.

The study area lies in the Lufilian Arc Fold and Thrust Belt and is mainly underlain by the Roan member shale, the Roan member arkosic sandstone and the Nguba member diamictite and banded shale which are part of Grand Conglomerat marker unit. Among the units that were analysed under polished thin section include arkosic sandstone and its subunits of conglomerate and ferruginous mudstone (or referred to as shale when banded), diamictite which comprised clast-rich and clast poor variety, the Nguba member shale and the mineralised quartz veins.

The arkosic sandstone is composed of quartz, albite, biotite, orthoclase, calcite with, minor specular hematite related to quartz veins and accessory mineral ilmenite, apatite and rutile. Based on the composition ratios of quartz (43%), feldspar(47%), and lithics(10%), the unit qualified it to be classified as an arkosic sandstone, though some of the observed minerals like albite, biotite, and muscovite relate to post-diagenetic alteration, particularly the strong albitisation which is the vein and replacement alteration that accompanied the northeast – southwest ductile shearing and the northwest -southeast trending faulting and recumbent folding.

The conglomerate and ferruginous subunits show evidence of the coarsening upward of the units in the sediment deposition cycle of the arkosic sandstone unit, with the conglomerate and coarse grained arkosic sandstone mostly observed in the top zones of the unit. Finer grained arkosic sandstone and ferruginous mudstone (or shale) are mostly observed in the lower zones, with the ferruginous mudstone signifying a sediment deposition phase in an oxic lagoon set-up. The conglomerate unit mainly comprises quartz, albite, biotite, orthoclase and chlorite and accessory minerals apatite, ilmenite and rutile. The albite, biotite, and quartz veins respectively represent post-diagenetic sodic and potassic and alteration phases, with the overall mineral composition of the conglomerate being very similar to the main arkosic sandstone unit. The ferruginous mudstone is mainly rich in iron and clay minerals.

The diamictite was classified as clast-poor and clast-rich based on the observed appearance in the hand-size sample. The mineralogy and alteration phases for both varieties of diamictite was quite similar comprising quartz, albite, biotite, orthoclase and muscovite. The potassic alteration represented by the presence of biotite and muscovite in the units and the strong albitisation is represented by albite which is vein and replacement related.

The Nguba shale comprised major quartz, albite, biotite, orthoclase and others with veinlet-related sulphides including pyrite, pyrrhotite, sphalerite and trace chalcopyrite. Accessory minerals include ilmenite, rutile and trace hematite and magnetite. Hydrothermal alteration minerals in this unit includes vein-related and replacement albite, potassic phases of biotite and muscovite and the late-stage silicification represented by some of the observed quartz veins in the unit.

On a district scale, the study area and its surroundings are extensively folded and faulted, and the area has undergone episodic deformation resulting in the development of various structures. Among the notable structures within the study area which can be related to the regional structural set-up of the LAFTB include folding, shear faulting, normal faulting, and the development of joints.

The structural aspect plays a critical role with regards to the location of mineralisation. Observed structural features which were critical in the deposition of auriferous/mineralised fluids include folding with a NNE – SSW oriented axial trace, NE – SW oriented shear faults and shear zones, NW – SE faults and veins which are the structures related to the mineralisation, and the NW – SE oriented folding where saddle-reef mineralisation has been observed. The physiochemical redox boundary between the Nguba member diamictite (reducing facies) and pre-Nguba arkosic sandstone (oxidised facies) played a critical role in the location of the mineralisation in the area.

On a regional scale, observed geology and structures in the study area can be attributed to the following events; early sediment deposition in the Katanga resulting from the episodic rifting events that took place on the southern margin or edge of the Congo Craton during the Neoproterozoic era. This was followed by the Roan and Mwashya Groups sediment deposition which was accompanied by local volcanism, then the deposition of Nguba and Kundelungu sediments. These activities were then followed by the passive margin convergence of the Congo craton to the north and the Kalahari craton to the south between ca. 570 – 530 Ma, resulting in the collision that brought about the Pan-African orogenic belts of the Lufilian Arc, Zambezi Belt and Damara belt. Ultimately the collision of stable cratonic masses was part of the amalgamation of the supercontinent Gondwana (Johnson et al., 2006; De Waele, et al., 2007;).
In the study area and beyond the following activities are diagnostic in the rock record;

1) Deposition of Roan sediments between 880 and 765 Ma on older basement units. Basement units are older than 900Ma. One of the regional reference points is the Nchanga granite where Roan sediments unconformably overlay the granite. Granite has been dated to be 880Ma (Porada and Berhurst, 2000);
2) Magmatism around 765 Ma which created a large volcanic edifice (Lwawu volcanics) that has affected Katanga units west of the study area, this magmatism signifies a rifting event in the area (Armstrong, 2000; Liyungu et al., 2000; De Waele et al., 2007);
3) Erosion or hiatus in sediment deposition within the Mwinilunga area (study area) which is part of the larger Kundelungu basin. This resulted in absence of Upper Roan

and Mwashya units. The absence of these units can partly be attributed to the deposition set-up of the Kundelungu and Nguba sediments which were not in existence during the deposition of Roan sediments in the rift basin lagoonal environment. Kundelungu and Nguba sediment deposition only commenced in an extensional basin that developed in the later-stages of Roan rifting, during Mwashya sediment deposition (Porada and Berhorst, 2000). The extensional rifting event is evidenced by the mafic igneous rocks that overlie the Mwashya units within the Katanga strata and these have been dated to be 765 Ma. Erosion or hiatus of Mwashya and Upper Roan sediments prior to the deposition of Kundelungu and Nguba sediments cannot be ruled out; and

4) Beginning of the deposition of the Nguba sediments marked by the diamictite or Grand Conglomerat (Sturtian glaciation) coupled with continued magmatism which resulted in the mafic alteration observed in the diamictite unit. Mafic igneous bodies lie within the Nguba Group, between Grand Conglomerat and Pétit Conglomerate and have been dated to be 735 Ma (Armstrong, 2000; De Waele et al., 2008).

Using a statistical approach and spatial assessment, elements copper, cobalt, molybdenum and zinc were assessed, with a view of establishing if any or all of these elements can be used as pathfinder elements in locating gold mineralised zones in the study area and beyond. Their usage as pathfinders was based on their mobility in the surficial environment relative to the gold which is generally immobile and may not give a dispersion halo in the soils, that signifies mineralisation or ore. Copper showed strong spatial relationships to the Nguba diamictite and shale units with some of the identified anomalies coinciding with the northwest trending structure inferred from the surface geology and aeromagnetic images. Cobalt did not show any spatial continuity but some discrete anomalies with no specific trend were observed within the Nguba member units. Molybdenum equally did not show any spatial trend which would assist in anomaly identification in relation to gold-copper mineralisation for the study area; this may be attributed to its high mobility in the surficial environment. Zinc showed a spatial trend particularly on the contact between the diamictite and Nguba shale which may require follow-up.

Use of statistics greatly assisted in identifying what is normal and anomalous for each element for this area, which gave ideal grouped data through frequency distribution tables before spatially plotting the data for each element.

Correlation of other elements to the lithologies was also done, it was observed that most elements had a higher signature in the diamictite and Nguba shale as compared to the Roan member shale and arkosic sandstone.

6.2 CONCLUSION

Presence of gold mineralisation the in the study area and particularly in the Nguba member units of the Katanga Supergroup gives a target zone for gold/-copper exploration in the Mwinilunga area and within Copperbelt stratigraphy in general. Mineralisation in the area is mostly structurally controlled as evidenced by the observed ductile shear faulting, folding and normal faulting structures present in the study area and beyond. These structures coupled with the observed geology layout of a redox boundary between Roan member arkosic sandstone and Nguba member units played a critical role in location of the observed gold mineralisation in the area as well as the observed copper anomalies in the soils.

Traditionally soil geochemical sampling has been an ideal tool for copper exploration in Zambia, though in this case the primary commodity being sought was gold and therefore its geochemical response was unknown, particularly the use of pathfinder elements like copper, zinc, molybdenum and cobalt in this case which were suspected to be related to gold mineralisation in the study area. The soil geochemical sampling proved to be an ideal approach in early-stage mineral exploration for this area. Only copper showed that it may reliably be used as pathfinder in the exploration for gold mineralisation and/or deposits particularly in this area and beyond. Relatively mobile elements like cobalt and molybdenum did not show clear cut spatial continuity within the soils which is one of the key indications for mineralisation. From the soil geochemical studies, Nguba member units are expected to give elevated geochemical response for elements like iron, manganese, zircon, vanadium, rubidium, zinc, nickel, and potassium relative to the other units that underlie the study area like the Roan member arkosic sandstone and the Roan member shale. This observed soil geochemical responses can also assist in marking out local lithological boundaries.

Recommended future works include;

1) Trenching or alternatively exploration pot holes to test if the observed soil geochemical anomalies for copper (and/ zinc) root up to depth. Trenches are to be oriented NE – SW so that the cut across NW-SE oriented structures such as veins, joints and faults which are related to the gold mineralisation.
2) Further soil geochemical studies to establish the distribution of gold in the residual soil within all the units in the study area. This will ensure overall soil geochemical signature for gold is understood for the area. Available pulp/coarse laboratory rejects will need be analysed using a mass sensitive laboratory analytical technique like ICP MS (i.e., capable of detecting gold in part per billion or ppb).
3) Detailed mineralogical analysis using QEMSCAN so that the grain relationship and micro structures are respectively fully understood. This may also include comparison studies to establish the effect of lithostatic pressure on the consistency and continuity of gold mineralisation, with emphasis on mineral alteration/transition due to lithostatic pressure. Gold mineralisation in the study area was observed to be near-surface and hosted in relatively younger units and affected by later-stage orogenic events, with the mineralisation appearing to be more localised and occurring in pockets.

4) Further stratigraphic and stratigraphy correlation studies. The Grand Conglomerat formation was observed to be thicker in Mwinilunga area relative to the traditional ZCB, where it is either absent or relatively thinner. Also, the absence of Mwashya and Upper Roan units within the study area also brings in further gaps in the sediment deposition events in the basin that hosts the study area, these may require detailed basin analysis.

The study area is located in an interesting area with an upside potential of not only hosting economic quantities of gold mineralisation but also the possibility of hosting world-class copper deposits similar to that of either the Kamoa in DRC or Kansanshi in Zambia.

REFERENCES

1) Annels, A.E. and Simmonds, J.R., 1984. Cobalt in the Zambian Copperbelt. Precambrian Research., 25: 75--98.

2) Armstrong, R.A., Robb, L.J., Master, S., Kruger, F.J. and Mumba, P.A.C.C.,2000, New U-Pb age constraints on the Katangan sequence, Central African Copperbelt: Journal of African Earth Sciences, v. 28, p. 6−7.

3) Broughton, D. W. and Rogers, T., 2010. Discovery of the Kamoa Copper Deposit, Central African Copperbelt, D.R.C. Society of Economic Geologists (SEG). Special Publication 15, 287 - 297.

4) Broughton, D.W., Hitzman, M.W., and Stephens, A.J., 2002, Exploration history and geology of the Kansanshi Cu-(Au) deposit, Zambia: Society of Economic Geologists Special Publication 9, 141−153.

5) Bull, S., Selley, D., Broughton, D., Hitzman, M., Cailteux, J., Large, R., McGoldrick, P., 2011. Sequence and carbon isotopic stratigraphy of the Neoproterozoic Roan Group strata of the Zambian Copperbelt. Precambrian Research 190, 70–89.

6) Cahen, L., Snelling, N.J., Delhal, J., Vail, J.R., Bonhomme, M., Ledent, D., 1984. The Geochronology and Evolution of Africa. Oxford University Press, Oxford, p. 512.

7) Cailteux, J.L.H., Kampunzu, A.B., Lerouge, C., Kaputo, A.K., and Milesi, J.P., 2005, Genesis of sediment-hosted stratiform copper-cobalt deposits, Central African Copperbelt: Journal of African Earth Sciences, v. 42, p. 134-158.

8) Cailteux, j. L. M., Kampunzu, A.B. and Batumike, M.J., 2007. Lithostratigraphy, basin development, base metal deposits, and regional correlations of the Neoproterozoic Nguba and Kundelungu rock successions, central African Copperbelt. International Association for Gondwana Research, Vol. 11. P 432 – 447.

9) Carranza, E.J.M., 2009. Exploratory analysis of geochemical Anomalies. Handbook of Exploration and Environmental Geochemistry, 11. 51-84.

10) Coats, J.S., Mosley, P.N., Mankelow, J. M., Mwale, M., Chikambwe, E. M., Muibeya, B., Ndhlovu, K. C. and F Nzabara, F. 2001. The Geology and Mineral Resources of Zambia. Geological Survey Department of Zambia. Memoir No. 6.

11) Cohen, D. R. and Bowel, B.J., 2014. Exploration Geochemistry. Treatise on Geochemistry, second edition. 623 – 648.

12) Corriveau, L. and Spry, P.G., 2014. Metamorphosed Hydrothermal Ore Deposits. Treatise on Geochemistry, second edition. 175 – 192.

13) Cosi, M., De Bonis, A., Gosso, G., Hunziker, J., Martinotti, G., Moratto, S., Robert, J.P. and Ruhlman, F., 1992. Late Proterozoic thrust tectonics, high pressure metamorphism and uranium mineralization in the Domes Area, Lufilian Arc, northwestern Zambia. Precambrian Research., 58, 215-240.

14) Crocket, J.H., 1992. Gold Metallogeny and Exploration; Distribution of gold in the Earth's crust. 1–36.

15) Daly, M.C., Chakraborty, S.K., Kasolo, P., Musiwa, M., Mumba, P., Naidu, B., Namateba, C., Ng'ambi, O. and Coward, M., 1984, The Lufilian arc and Irumide belt of Zambia: results of a traverse across their intersection. Journal of African Earth Sciences., 4, 311-318.

16) Daly, M.C. and Unrug, R., 1982. The Muva Supergroup in Northern Zambia: a craton to mobile belt sedimentary sequence. Trans. Geol. Soc. South Africa, 85,

17) De Waele, B., Johnson, S. P. and Pisarevsky, S. A., 2008. Palaeoproterozoic to Neoproterozoic growth and evolution of the eastern Congo Craton: Its role in the Rodinia puzzle. Precambrian Research. 160, 127 -141.

18) First Quantum Minerals (FQM), March 2019. Annual Information Form for the period ending 31st December 2018. P13 – 25. Site: https://www.sedar.com/FindCompanyDocuments.do

19) First Quantum Minerals (FQM), March 2020. Annual Information Form for the period ending 31st December 2019. P13 – 25 https://www.sedar.com/FindCompanyDocuments.do

20) Fleischer, V.D., Garlick, W.G. and Haldane, R., 1976. Geology of the Zambian Copper Belt. 223-352, In: K.R.Wolf (Ed.), Handbook of Strata-bound and Stratiform Ore Deposits, Vol. 6., Elsevier, Amsterdam.

21) Francois, A., 1974. Stratigraphy, tectonics and mines in the Shaba Arc (Re´p.du Zai¨re). In: Bartholome´, P. (Ed.), Stratiform sites and provinces. Centenary of the Geological Society of Belgium, Liege, pp. 79–101.

22) Francois, A., Wendorff, M., Tack, L. (Eds.), 1995. Problems relating to the Katangans of Shaba. In: Late Proterozoic Belts in Central Africa. Muse´e Royal of Central Africa, Tervuren, Belgium. Annals of Geological Sciences 101, 1–20.

23) Freeman, P.V., July – December,1988. Description of Mineral Deposits on the Copperbelt (And Kabwe and Nampundwe). Compilation Report. ZCCM Technical Services.

24) Groves, D., Goldfarb, R. J., Robert, F., and Hart, C.J.R., 2003. Gold Deposits in Metamorphic Belts: Overview of Current Understanding, Outstanding Problems, Future Research, and Exploration Significance. Economic Geology. 98, 1-29.

25) Halley, W. S., Wood W., Stoltze A., Godfroid J., Goswell H. and Jack D., 2016. Using Multielement Geochemistry to Map Multiple Components of a Mineral System: Case Study from a Sediment Hosted Cu-Ni Camp, NW Province, Zambia. Society of Economic Geologists (18 – 20. 104.

26) Hitzman, M.W., Kirkham, R.V., Broughton, D.W., Thorson, J.P., and Selley, D., 2005. The sediment-hosted stratiform copper ore system: Society for Economic Geologists, 100th Anniversary Volume, p. 609-642.

27) Hitzman, M. W., Selley D., and Bull, S., 2009. Formation of Sedimentary Rock Hosted Stratiform Copper Deposits through Earth History. Society for Economic Geologists 18 – 20.105.

28) Hitzman, M.W., Broughton, D., Selley, D., Woodhead, J., Wood, D., and Bull, S., 2012, The Central African Copperbelt: Diverse stratigraphic, structural, and temporal settings in the world's largest sedimentary copper district: Society of Economic Geologists, Special Publication 16, p. 487-514.

29) Guernsey, T.D., 1941. Reconciliation of Mineral Deposits covering Loangwa, Rhodesia and Rhokana Concession Areas. Mineral occurrence compilation report. P 1 – 180.

30) Johnson, S.P., De Waele, B., Tembo, F., Evans, D., Iizuka, T., Tani, K., 2007a. Geochronology of the Zambezi Supracrustal sequence, southern Zambia: a record of Neoproterozoic divergent processes along the southern margin of the Congo Craton. Journal of Geology 115, 355–374.

31) Kampunzu, A.B., and Cailteux, J., 1999. Tectonic evolution of the Lufilian arc (Central African Copperbelt) during Neoproterozoic Pan African orogenesis: Gondwana Research, 2, 401−421.

32) Key, R. M., De Waele, B. and Liyungu, A. K., 2004. A Multi-element baseline geochemical database from the western extension of the Central Africa Copperbelt in northwestern Zambia. Applied Earth Science B1-B22. 113.

33) Key, R.M., Liyungu, A.K., Njamu, F.M., Somwe, V., Banda, J., Mosley, P.N., Armstrong, R.A., 2001. The western arm of the Lufilian Arc in NW Zambia and its potential for copper mineralisation. Journal of African Earth Sciences 33, 503–528.

34) Key, R. M. and Banda, J., 2000. 'Report on the geology of the Kalene Hill area'. Geological Survey Department of Zambia. Report No. 107, 1–48.

35) Key, R. M., Banda, J., Liyungu, A. K., Dokowe, A., and Mosley, P. N., 2001. 'The geology and stream sediment geochemistry of the Mwinilunga Sheet'. Geological Survey Department of Zambia. Memoir No. 5, 1–175.

36) Laperche, V. and Lemiére, B., 2020. Possible Pitfalls in the Analysis of Minerals and Loose Material by Portable XRF, and How to Overcome Them. Minerals

37) Liyungu, K., 2017. The Assessment of Copper, Cobalt and Gold Mineralisation in the Mwinilunga Area. Unpublished report.

38) Liyungu, A. K., Mosley, P. N., Njamu, F.M and Banda, J., 2000. Geology of Mwinilunga area, Explanation of Quarter Degree Sheet 1124SW. Geological Survey of Zambia, Report No. 110.

39) Master, S., Rainaud, C., Armstrong, R.A., Phillips, D., and Robb, L.J., 2005. Provenance ages of the Neoproterozoic Katanga Supergroup (central African Copperbelt), with implications for basin evolution: Journal of African Earth Sciences, v. 42, p. 41–60.

40) Muchez, P. H., and Corbella M., 2012. Factors controlling the precipitation of copper and cobalt minerals in sediment-hosted ore deposits: Advances and restrictions. Journal of Geochemical Exploration. 118. 38 – 46

41) Mulela, D. and Seifert, A. V., 1998. 'The geology of the Mwombezhi Dome area and Jiwundu Swamp area; explanation of degree sheet 1225, NE quarter and 1125, SE quarter'. Mapping Report No. 83. Geological Survey of Zambia. 1–26.

42) Porada, H. and Berhorst, V., 1998, Thrust tectonics in the Domes region and Copperbelt of Zambia: Outline and Outlook: Freiberger Forschungshefte, Hans-Jürgen Behr-Festschrift, v.475, p. 145-162.

43) Porada, H. and Berhorst, V., 2000. Towards a new understanding of the Neoproterozoic-Early Palaeozoic Lufilian and northern Zambezi Belts in Zambia and the Democratic Republic of Congo. Journal of African Earth Sciences. 30. 727 -771.

44) Reimann, C., Filzmoser, P. and, Garrett, R.G., 2002. Factor analysis applied to regional geochemical data: problems and possibilities. Journal of Applied Geochemistry, volume 17, P185 – 206.

45) Reeve, W. H., 1963. The Geology and Mineral Resource of Northern Rhodesia. Bulletin of the Geological Survey of Northern Rhodesia. 1.

46) Rose, H. W., Hawkes, E. H., and Webb, J. S.,1979. Geochemistry in Mineral Exploration. 2nd Edition. Text Book.

47) Saunders, J. A., Hofstra, A.H., Goldfarb, R.J. and Reed, M. H., 2014. Geochemistry of Hydrothermal Gold Deposits.

48) Schmandt, D., Broughton, D., Hitzman, M.W., Plink-Bjorklund, P., Edwards, D., and Humphrey, J. 2013. The Kamao Copper Deposit, Democratic Republic of Congo: Stratigraphy, Diagenetic and Hydrothermal Alteration and Mineralisation. Society of Economic Geologists (SEG). Journal. 108, 287 - 297.

49) Selley, D., Broughton, D., Scott, R., Hitzman, M., Bull, S.W., Large, R.R., McGoldrick, P.J., Croaker, M., Pollington, N., and Barra, F., 2005. A new look at the geology of the Zambian Copperbelt: Economic Geology 100th Anniversary Volume, p. 965-1000.

50) SRK Consulting, 2008. Technical Report on the Mineral Resources for the Konkola North Copper Project, Chililabombwe, Zambia. SRK Project No. 384408. Technical Report.

51) Steven, N.M., 1995. Quarterly report for April-June 1995 on Luamata Prospecting Licence No. 1035: Termination Report (Unpublished), Anglo American Corporation Central Africa Limited, Lusaka.

52) Thieme, F. and Johnson, R. L, 1981. '1:1 000 000 National Geological Map of Zambia'. Geological Survey Department of Zambia.

53) Torremans, K., Gauquie, J., a, Boyce, A.J., Barrie, C.D, Dewaele, S., Sikazwe, O., and Muchez, Ph., 2013. Remobilisation features and structural control on ore grade distribution at the Konkola stratiform Cu–Co ore deposit, Zambia. Journal of African Earth Sciences, 79, 10 – 23.

54) Unrug, R., 1983. 'The Lufilian Arc: a microplate in the Pan-African Collision Zone of the Congo and the Kalahari cratons. Precambrian Research, 21, 181–196.

55) Unrug, R., 1988. 'Mineralization and source of metals in the Lufilian Fold Belt, Shaba (Zaire), Zambia and Angola', Economic Geology. V.83. 1247–1258.

56) VINMIC REPORT, 2020. Ground Magnetics Geophysics Report for ZCCM-IH Block 24988-HQ-SEL and 24999-HQ-SEL. Unpublished Geophysics Exploration Report. P1-18.

57) Watts, Griffis and McQuat, 1991. Assessment of Mineral Exploration in Zambia. Minex Ltd, Zambia, Lusaka. 345 -374.

58) Wendorff, M. and Key, R.M., 2009, The relevance of the sedimentary history of the Grand Conglomérat Formation (Central Africa) to the interpretation of climate change during a major Cryogenian glacial event: Precambrian Research, v. 172, p. 127-142.

59) Woodhead, J. 2013. The Neoproterozoic Roan Group in the Zambian Copperbelt: Sequence Stratigraphy, Alteration and Mineralisation. PhD Thesis. Colorado School of Mines.

60) Young, K. E., Evans, C.A, Hodges, K. V., Bleacher, J. E., and Graff, T. G., 2016. A review of the handheld X-ray fluorescence spectrometre as a tool for field geologic investigations on Earth and in planetary surface exploration. Applied Geochemistry. 72, 77 – 87.

APPENDIX 1a: TESCAN INTERGRATED MINERAL ANALYSIS (TIMA) REPORT

SAMPLE L04032, Arkosic Sandstone unit - Mineral Phases	%	SAMPLE A3109, Clast rich Diamictite unit - Mineral Phases	%	SAMPLE L05791, Conglomerate unit - Mineral Phases	%
Quartz	43.48	Quartz	35.62	Quartz (SiO_2)	42.43
Albite	22.67	Albite	30.12	Albite	27.83
Biotite low Mg	17.13	Biotite	20.67	Biotite	16.13
Orthoclase	6.87	Chlorite_HighFe	3.09	Orthoclase	7.26
Calcite	3.42	Orthoclase	2.87	Chlorite_HighFe	1.47
Hematite/Magnetite	1.24	Muscovite	1.67	Calcite	0.54
Muscovite	1.1	Calcite	1.49	Biotite Albite Quartz mixture	2.09
Hematitte/Magnetite Ti Si	0.73	Hematite/Magnetite	0.6	Hematite/Magnetite Al Si	0.62
Dolomite/Ankerite mixture	0.54	Alumosilicates - mixture	0.41	Muscovite	0.3
Ilmenite Fe	0.2	Pyrite	0.25	Alumosilicates - mixture	0.16
Biotite Albite mixture	1.35	Biotite Albite Quartz mixture	1.66	Ilmenite Fe	0.13
Apatite	0.16	Apatite	0.2	Apatite	0.04
Ilmenite	0.14	Rutile	0.09	Rutile	0.03
Chlorite_HighFe	0.11	Ilmenite	0.09	Dolomite	0.02
Rutile	0.09	Hematite/Magnetite/Pm	0.08	Ilmenite	0.02
Alumosilicates - mixture	0.07	Dolomite	0.06	Biotite Ca	0.01
Other sillicates		Other sillicates	0.06	Biotite_HighTi	0.01
[Unclassified]	0.7	Chalcopyrite	0.02	[Unclassified]	0.86
The rest		Pyrrhotite	0.02	**The rest**	**0.04**
Total	**100**	Biotite Ca	0.02	**Total**	**100**
		Zircon	0.02		
		Ilmenite Fe	0.01		
		Chlorite_Low_mg	0.01		

		[Unclassified]	0.6		
		The rest	**0.04**		
		Total	**100**		
Sample L0427, Diamictite (sheared) with Calcite veins	**%**	**Sample LPV01A, Mineralised Quartz vein - Mineral phases**	**%**	**SAMPLE M1, Diamictite unit - Mineral Phases**	**%**
Calcite	32.8	Quartz	74.6	Albite-biotite	34.79
Biotite low Mg	25.81	FeO-Si Cu P mixture	14.46	Quartz	28.41
Quartz	13.62	FeO Si Cu	1.82	Biotite-Albite	21.66
Albite	11.53	Chalcopyrite	1.61	Muscovite	3.22
Dolomite Ankerite mixture	5.8	Pseudomalachite	0.87	Biotite Albite Quartz mixture	6.43
Chlorite_HighFe	2.67	Malachite	0.95	Orthoclase	2.54
Pyrite	0.69	Chalcocite	0.62	Hematite/Magnetite	0.47
Biotite Ca	0.54	Albite	0.43	Barite	0.21
Alumosilicates - mixture	0.49	Biotite	0.42	Other sillicates	0.2
Orthoclase	0.41	Chlorite_HighFe	0.42	Chlorite_HighFe	0.18
Muscovite	0.34	Ferripyrophyllite	0.31	Quartz(Impure)_001	0.17
Biotite Albite Quartz Calcite mixture	3.08	Alumosilicates - mixture	0.6	Apatite	0.13
Apatite	0.12	Bornite	0.22	Alumosilicates - mixture	0.1
Chalcopyrite	0.09	Libethenite	0.21	Rutile	0.08
Rutile	0.07	Delafossite mixture	0.2	Ilmenite	0.07
Allanite	0.05	Chrysocolla	0.25	Chlorite_Low_mg	0.04
Pyrrhotite	0.03	Oxide Fe P Cu Al	0.09	Ilmenite Fe	0.03
Ilmenite	0.02	Romanechite Co Cu Fe	0.32	Hematitte/Magnetite/Pm	0.02
Titanite_High Mg_Al	0.02	[Unclassified]	1	Titanite	0.02
Gypsum	0.02	**The rest**	**0.6**	Titanite_High Mg_Al	0.02
Chalcocite	0.02	**Total**	**100**	Zircon	0.01
Chlorite_Low_mg	0.01			[Unclassified]	1.14

[Unclassified]	1.7
The rest	**0.06**
Total	**100**

The rest	**0.06**
Total	**100**

SAMPLE L05959, Nguba shale unit - Mineral Phases	%	Sample L04696, Clast poor diamictite - Mineral phases	%
Quartz	22.27	Quartz	27.32
Albite	20.18	Albite	20.2
Biotite	10.74	Biotite	10.61
Orthoclase	6.03	Calcite	7.24
Pyrite	5.76	Chlorite_HighFe	6.92
Hematite/Magnetite_High_Al	4.06	Alumosilicates - mixture	6.66
Chlorite_HighFe	4.01	Biotite-Albite-Quartz-Calcite mixture	14
Biotite Albite Quartz mixture	9.13	AlbiteQuartz Apatite mixture	1.5
Calcite	2.93	Apatite	0.95
Pyrrhotite	2.81	Pyrrhotite	0.81
Muscovite	1.87	Orthoclase	0.81
Apatite	1.12	Muscovite	0.24
Sphalerite	1.02	Biotite Ca	0.16
Alumosilicates - mixture	0.71	Ilmenite	0.09
Ilmenite	0.26	Dolomite	0.07
Dolomite	0.13	Biotite_HighTi	0.06
Other sillicates	0.12	Titanite_High Mg_Al	0.06
Rutile	0.08	Hematite/Magnetite_High_Al	0.05
Hematite/Magnetite	0.07	Zircon	0.02
Chalcopyrite	0.04	Other sillicates	0.02
Chlorite_Low_mg	0.01	Chalcopyrite	0.03

[Unclassified]	6.59	Rutile	0.01
The rest		[Unclassified]	2.59
Total	**100**	**The rest**	**0.06**
		Total	**100**

APPENDIX 1b: MINERAL DEPICTION FROM TIMA ANALYSIS, L04032 = arkosic sandstone, A3019 = Clast-rich diamictite, M1 = Clast poor diamictite and L05791 = Conglomerate.

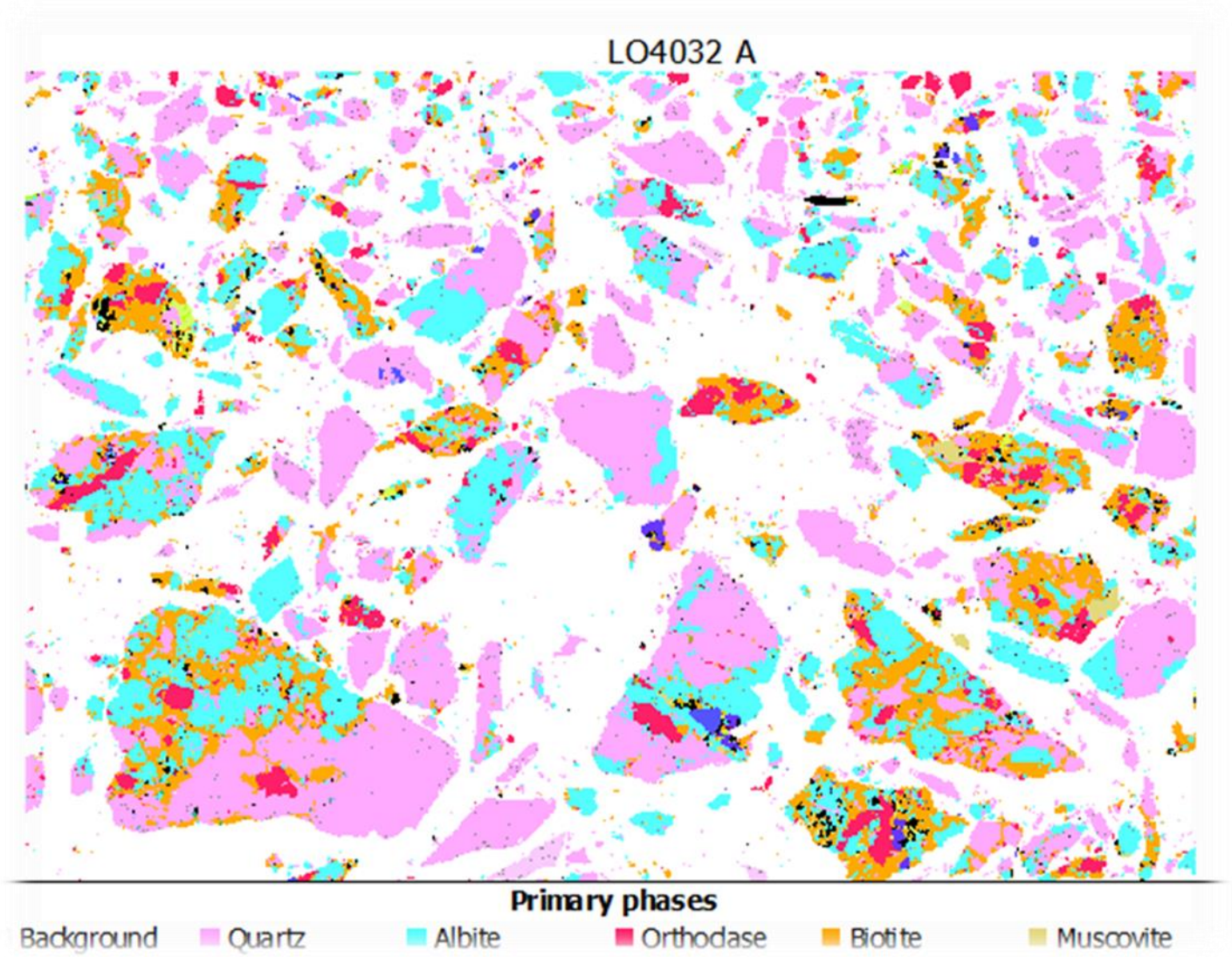
LO4032 A
Primary phases
Background
Quartz
Albite
Orthoclase
Biotite
Muscovite

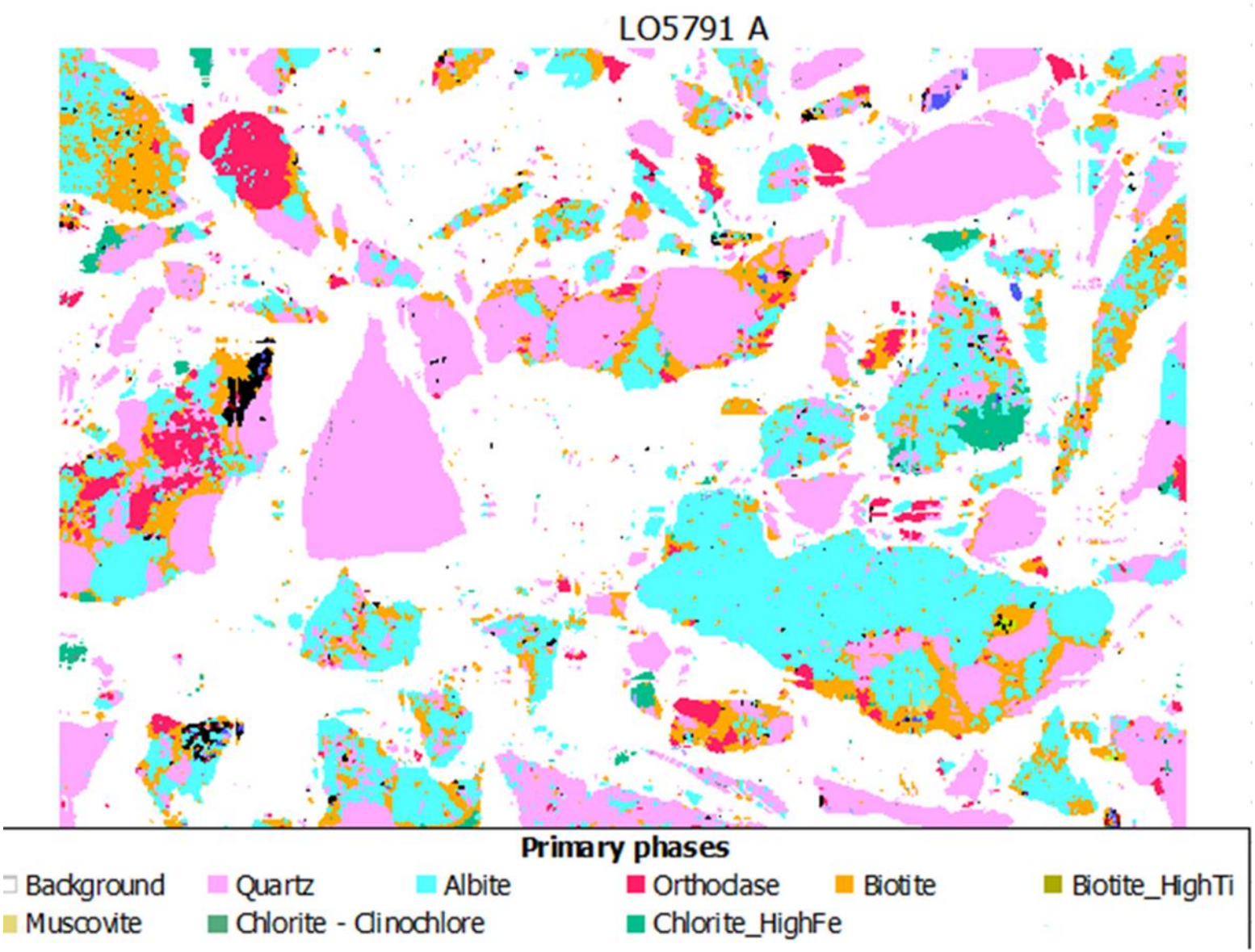
LO5791 A
Primary phases
Background
Quartz
Albite
Orthoclase
Biotite
Biotite_HighTi
Muscovite
Chlorite - Clinochlore
Chlorite_HighFe

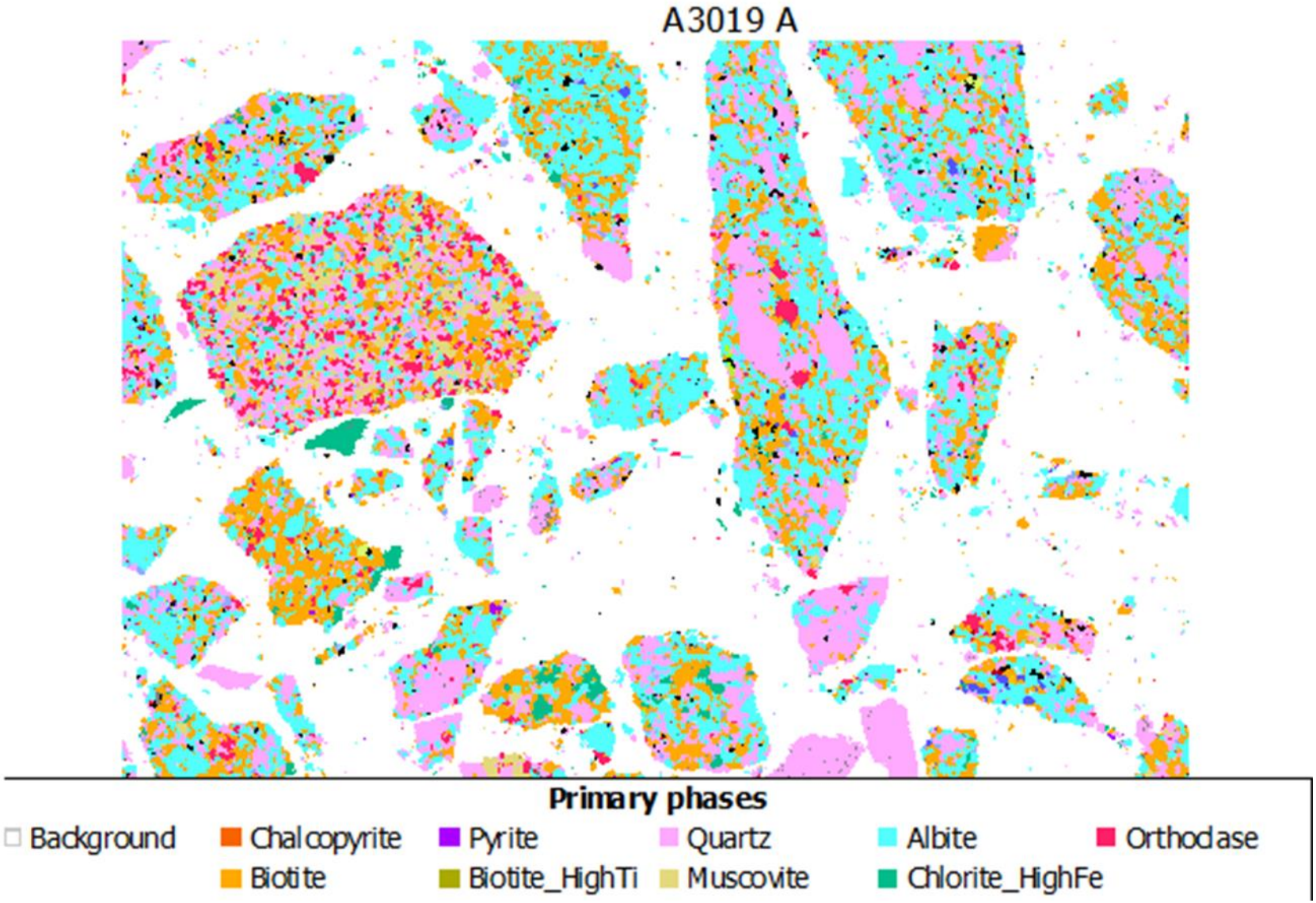
A3019 A
Primary phases
Background
Chalcopyrite
Pyrite
Quartz
Albite
Orthoclase
Biotite
Biotite_HighTi
Muscovite
Chlorite_HighFe

APPENEDIX 2: PETROGRAPHY SAMPLES - DESCRIPTIONS

S/N	FIELD ID	FROM (m)	TO (m)	ANALYSIS	FIELD NAME	DESCRIPTION
1	L0427	65.25	65.3	PTS	Diamictite	Sheared diamictite with calcite veinlet, sheared with minor mineral banding. Clay, qtz, cal, with fine pyrite disseminations. Collected from drill core, from hole ID KSLDD0023
2	L04032	68.23	68.33	PTS	Arkosic sandstone	Arkose with quartz-calcite-specularite vein. Antitaxial type of veins. Minor specularite along bedding relics. Sample collected from drill core with hole ID KSLDD0023
3	L04039	73.5	73.6	PTS	Arkosic sandstone	Arkose with quartz-calcite vein (~20mm thick). Antitaxial vein type with perpendicular veinlets, brown to red FeOx alteration. Fine grained massive to weekly laminated, qtz, cal, kfs mineralogy with minor calcite and kaolinite. Collected from drill core with hole ID KSLDD0023
4	L04043	76.4	76.5	PTS	Arkosic sandstone	Arkose with quartz-calcite vein. Fine grained massive to weekly laminated, qtz, cal, kfs mineralogy with fine specularite enriched zones along healed microfractures. Collected from drill core with hole ID KSLDD0023
5	L03073	189.2	189.3	PTS	Arkosic sandstone	Ferrugenious-shale in arkosic sandstone with quartz-calcite veinlets. (Act-tremolite alteration on veinlet edges).
6	A3109	24.6	24.6	PTS	Diamictite	Clast-rich diamictite strongly altered, with rounded granitic xenoclast. Qtz-cal veinlet cutting through the unit (~5mm). With breccia texture, qtz+clay+granite clasts in clayey groundmass. Diss pyrite along qtz-cal veinlet

9	LPV001A	210323	8689193	PTS	Quartz vein	Quartz-calcite vein with minor malachite, chalcopyrite and pyrite collected on near shale-arkose contact. Brecciated with secondary pyrite and FeOx weathering. Collected from Pit-2 mining face
10	LPV001B	210323	8689193	PTS	Quartz vein	Quartz-calcite vein with minor malachite, chalcopyrite and pyrite collected on near shale-arkose contact. Brecciated with secondary pyrite and FeOx weathering. Collected from Pit-2 mining face
11	M1	209061	8687283	PTS	Diamictite	Diamictite, breccia texture, gravel size clasts in basic extrusive igneous altered ground mass. Collected from surface outcrop around aero-mag high area

APPENDIX 3: SURFACE GEOLOGY STRUCTURAL READINGS – BEDDING AND JOINT

No.	Eastings	Northings	Elevation	Lithology	Strike	Dip	dip direction	Polarity	Azimuth_Dip	Type
1	209522	8686974	1432	Roan shale	33	90	SE	-1	123	Bedding
2	209522	8686974	1432	Roan shale	39	90	SE	-1	129	Bedding
3	208912	8688760	1364	Roan shale	34	40	SE	-1	124	Bedding
4	208912	8688760	1364	Roan shale	36	40	SE	-1	126	Bedding
5	208912	8688760	1364	Roan shale	186	29	SE	-1	96	Bedding
6	209757	8689078	1378	Roan shale	52	45	SE	-1	142	Bedding
7	209466	8689376	1379	Roan shale	29	39	SE	-1	119	Bedding
8	212101	8688239	1427	Arkose	64	19	SE	-1	154	Bedding
9	212101	8688239	1481	Arkose	88	22	SE	-1	178	Bedding
10	212101	8688239	1481	Arkose	76	20	SE	-1	166	Bedding
11	211259	8689793	1443	Nguba	22	32	SE	-1	112	Bedding

				shale						
12	211259	8689793	1443	Nguba shale	22	36	SE	-1	112	Bedding
13	211259	8689793	1443	Nguba shale	35	39	SE	-1	125	Bedding
14	210045	8688934	1410	Nguba shale	68	38	SE	-1	158	Bedding
15	210045	8688934	1410	Nguba shale	74	26	SE	-1	164	Bedding
16	211227	8689771	1434	Nguba shale	38	28	SE	-1	128	Bedding
17	211227	8689771	1434	Nguba shale	38	32	SE	-1	128	Bedding
18	211881	8688037	1407	Arkose	71	21	SE	-1	161	Bedding
19	211881	8688037	1407	Arkose	96	28	SE	-1	186	Bedding
20	211881	8688037	1407	Arkose	90	20	SE	-1	180	Bedding
21	211881	8688037	1407	Arkose	84	30	SE	-1	174	Bedding
23	211016	8687049	1391	Roan shale	38	80	SE	-1	128	Bedding
24	210819	8686929	1387	Roan shale	24	44	SE	-1	114	Bedding
25	210819	8686929	1387	Roan shale	28	46	SE	-1	118	Bedding
26	210819	8686929	1387	Roan shale	30	45	SE	-1	120	Bedding
27	210905	8687021	1378	Roan shale	23	47	SE	-1	113	Bedding
28	210905	8687021	1378	Roan shale	30	50	SE	-1	120	Bedding
29	210905	8687021	1378	Roan shale	40	47	SE	-1	130	Bedding
30	210919	8687024	1380	Roan shale	21	50	SE	-1	111	Bedding
31	210919	8687024	1380	Roan shale	28	50	SE	-1	118	Bedding
32	210967	8687023	1387	Roan shale	22	50	SE	-1	112	Bedding
33	211024	8687046	1392	Roan shale	28	48	SE	-1	118	Bedding
34	210902	8686985	1372	Arkose	42	52	SE	-1	132	Bedding
35	210902	8686985	1372	Arkose	36	40	SE	-1	126	Bedding

36	211842	8688106	1412	Arkose	24	80	SE	-1	114	Bedding
37	210447	8687186	1377	Arkose	35	58	SE	-1	125	Bedding
38	211183	8687227	1391	Roan shale	55	42	SE	-1	145	Bedding

No.	Eastings	Northings	Elevation	Lithology	Strike	Azimuth_Dip	Dip	Polarity	Dip Direction	Type
1	209522	8686974	1432	Arkose	136	226	90	-1		Joint
2	209522	8686974	1432	Arkose	321	051	90	-1		Joint
3	209522	8686974	1432	Arkose	121	211	90	-1		Joint
4	209068	8687284	1408	Arkose	142	232	90	-1		Joint
5	209068	8687284	1408	Arkose	140	230	90	-1		Joint
6	209068	8687284	1408	Arkose	120	210	90	-1		Joint
7	209068	8687284	1408	Arkose	142	232	90	-1		Joint
8	209068	8687284	1408	Nguba Shale	38	128	85	-1	SE	Joint
9	209068	8687284	1408	Nguba Shale	26	116	88	-1	SE	Joint
10	208725	8687509	1418	Arkose	104	194	78	-1	SE	Joint
11	209783	8688122	1419		159	249	88	-1	SE	Joint
12	209783	8688122	1419		136	226	90	-1		Joint
13	209783	8688122	1419		146	236	81	-1	SE	Joint
14	209783	8688122	1419		108	198	80	-1	SE	Joint
15	209783	8688122	1419		52	142	90	-1		Joint
16	209757	8688078		Roan shale	138	228	90	-1		Joint
17	212101	8688239	1481	Arkose	122	212	90	-1		Joint
18	212101	8688239	1481	Arkose	40	130	87	-1	SE	Joint
19	212101	8688239	1481	Arkose	124	214	90	-1		Joint
20	212101	8688239	1481	Arkose	38	128	90	-1		Joint
21	212101	8688239	1481	Arkose	46	136	83	-1	SE	Joint

22	212101	8688239	1481	Arkose	19	109	90	-1		Joint
23	210787	8688429	1437	Nguba Shale	144	234	90	-1		Joint
24	210787	8688429	1437	Nguba Shale	140	230	90	-1		Joint
25	210787	8688429	1437	Nguba Shale	44	134	86	-1	SE	Joint
26	210787	8688429	1437	Nguba Shale	58	148	90	-1		Joint
27	211259	8689793	1443	Nguba Shale	108	198	89	-1	SE	Joint
28	211227	8689771	1434	Nguba Shale	166	256	80	-1	SE	Joint
29	211227	8689771	1434	Nguba Shale	168	258	90	-1		Joint
30	211227	8689771	1434	Nguba Shale	148	238	90	-1		Joint
31	211227	8689771	1434	Nguba Shale	152	242	80	-1	SE	Joint
32	210630	8689380	1414	Nguba Shale	228	318	74	-1	SE	Joint
33	210630	8689380	1414	Nguba Shale	224	314	90	-1		Joint
34	210630	8689380	1414	Nguba Shale	226	316	76	-1	SE	Joint
35	210630	8689380	1414	Nguba Shale	126	216	75	-1	SE	Joint
36	211881	8688037	1407	Arkose	139	229	90	-1		Joint
37	211881	8688037	1407	Arkose	132	222	89	-1	SE	Joint
38	211881	8688037	1407	Arkose	132	222	90	-1		Joint
39	211881	8688037	1407	Arkose	146	236	90	-1		Joint
40	211881	8688037	1407	Arkose	40	130	90	-1		Joint

41	211881	8688037	1407	Arkose	38	128	90	-1		Joint
42	211881	8688037	1407	Arkose	122	212	90	-1		Joint
43	211881	8688037	1407	Arkose	115	205	90	-1		Joint
44	211881	8688037	1407	Arkose	134	224	90	-1		Joint
46	211024	8687946	1392	Roan shale	102	192	90	-1		Joint
49	211016	8687044	1391	Roan shale	114	204	90	-1		Joint

APPENDIX 4a: ASSAYS FROM MINTEK LAB REPORT (HG = High grade, MG = Medium Grade and LG = Low Grade Ore)

Element	Unit	HG Composite	LG Composite	MG Composite	Main Composite
Al	%	6.42	6.87	7.02	6.57
Ca	%	0.4	0.2	0.1	0.3
Co	%	1.17	<0.05	<0.05	0.57
Cr	%	<0.05	<0.05	<0.05	<0.05
Cu	%	0.9	<0.05	0.29	0.47
Fe	%	5.93	5.06	3.67	5.57
Mg	%	2.1	1.7	1.81	1.88
Mn	%	0.44	0.22	<0.05	0.33
Ni	%	<0.05	<0.05	<0.05	<0.05
Pb	%	<0.05	<0.05	<0.05	<0.05
Si	%	28	31.1	30.8	19.7
Ti	%	0.64	0.6	0.74	0.62
V	%	<0.05	<0.05	<0.05	<0.05
Zn	%	0.05	<0.05	<0.05	<0.05
Au	g/t	1150	0.39	0.45	274
Ag	g/t	10.4	<5.00	8.32	<5.00

APPENDIX 4b: SAMPLE OF ASSAYS FROM MOPANI COPPER MINE LABORATORY

MOPANI

MOPANI COPPER MINES plc

NKANA ANALYTICAL SERVICES

FM-AS-007

SPECIAL SAMPLES REPORT

Client's Name: Misenge Environmental and Technical Services Limited
Material Type: Ore (Core, Rock chips)
Sample state: Samples delivered by client
Date Received: 30.09.21
Date Reported: 05.10.21

SAMPLE DATE	SAMPLE ID	%Al	%Ca	ppm Co	ppm Cu	%Fe	%Mg	ppm Mn	ppm Pb	ppm Zn	ppm Ni	ppm Cd	%Na	%K	ppm Cr	ppm As	ppm Ba	ppm V	ppm Sn	ppm Bi	g/t Au
16.09.20	M1	7.28	0.17	3	64	5.29	1.80	275	48	44	45	<0.5	1.96	3.10	83	<0.2	3010	149	5	<10	
16.09.20	LP002	7.83	0.13	9	25	6.62	2.26	360	45	59	62	<0.5	2.43	2.95	99	<0.2	236	189	5	<10	
16.09.20	LPV001	0.27	0.08	114	16900	4.37	0.11	270	101	71	10	<0.5	0.11	0.06	15	<0.2	100	103	11	<10	0.2
16.09.20	LPV003	0.07	0.05	<2	79	0.20	0.02	61	51	7	5	<0.5	0.10	0.04	11	<0.2	38	3	<1	<10	0.2
16.09.20	LO2570	7.82	0.26	24	17	5.85	3.15	122	51	37	91	<0.5	1.16	5.13	137	<0.2	535	135	2	<10	
16.09.20	LO2913	6.87	0.67	30	155	3.88	3.03	1100	56	148	96	<0.5	2.99	3.16	77	<0.2	417	238	<1	<10	0.6
18.08.21	LO3116SBX	6.63	0.24	10	5	4.21	2.08	95	42	38	70	<0.5	1.35	3.88	85	<0.2	478	200	<1	<10	
16.09.20	LO3116SSH	7.18	0.15	36	590	6.16	2.89	1230	46	39	52	<0.5	1.65	2.72	100	<0.2	287	198	3	<10	0.1
18.08.21	LO3146	5.55	0.13	3	14	2.62	1.33	101	35	18	24	<0.5	2.08	2.56	32	<0.2	355	85	<1	<10	
16.09.20	LO3213	5.81	0.15	<2	6	2.52	1.33	75	35	6	42	<0.5	1.48	3.66	33	<0.2	687	75	<1	<10	
16.09.20	LO4006	6.92	0.2	7	40	3.79	1.78	195	40	32	39	<0.5	1.81	3.38	68	<0.2	462	142	<1	<10	0.2
16.09.20	LO5530	7.66	0.37	37	162	3.80	3.48	270	44	36	97	<0.5	3.17	3.37	104	<0.2	196	191	<1	<10	0.2
18.08.21	LO5539	4.72	0.13	<2	185	0.46	0.16	503	24	16	7	<0.5	3.44	0.53	19	<0.2	113	28	<1	<10	0.5
18.08.21	LO5543	5.15	0.16	<2	30	0.75	0.40	121	31	9	16	<0.5	3.04	1.86	27	<0.2	382	52	2	<10	
18.08.21	LO5570	6.2	0.2	<2	10	2.71	1.27	80	40	14	42	<0.5	2.69	2.61	33	<0.2	577	93	<1	<10	
18.08.21	LO5575	0.34	10.72	<2	10	1.73	5.04	3660	<1	2	6	<0.5	0.21	0.19	17	<0.2	85	3	<1	<10	
ANALYTICAL METHOD		ICP-OES	ICP-OES	ICP-OES	ICP-OES	ICP-OES	ICP-OES	ICP-OES	ICP-OES	ICP-OES	ICP-OES	ICP-OES	ICP-OES	ICP-OES	ICP-OES	ICP-OES	ICP-OES	ICP-OES	ICP-OES	ICP-OES	FIRE ASSAY-AAS FINISH

COMPILED BY: _____
SENIOR SECTIONAL CHEMIST

SCRUTINISED BY: _____
SUPERINTENDENT - ANALYTICAL SERVICES

APPENDIX 4c: SAMPLE OF LABORATORY ASSAYS – FROM SGS SA

SGS South Africa (Pty) (Ltd)
Reg No. 1949/032643/07
Off The R559
Zuurbekom, Randfontein
1760
Phone: +27 11 100 2170
Email: South.Africa@sgs.com
Internet: www.sgs.com

Lab Ref RD21-11989
Client Ref **Batch-KSLDD-061**
Project DEFAULT
Reported 28/04/21
Status Final
Page Page 2 of 6

TEST REPORT

	WtRec	-75µm	Au*
Scheme	**WGH79**	**SCR32**	**FAA303**
Units	**g**	**%**	**g/t**
Reporting Limit	**0.00**	**0.01**	**0.01**
Test Completed	**2021-04-06**	**2021-04-08**	**2021-04-28**
A0871	145.80	93.0	<0.01
A0872	142.60	-	<0.01
A0873	130.40	-	<0.01
A0874	132.40	-	<0.01
A0875	139.20	-	<0.01
A0876	125.40	-	<0.01
A0877	123.30	-	0.03
A0878	119.30	-	<0.01
A0879	135.20	-	<0.01
A0880	142.70	-	<0.01
A0881	103.00	-	11.0
A0882	142.40	-	<0.01
A0883	133.70	-	0.34
A0884	141.50	-	0.25
A0885	124.00	-	<0.01
A0886	123.50	-	<0.01
A0887	122.30	-	<0.01
A0888	135.90	-	0.01
A0889	126.50	-	0.01
A0890	141.70	85.0	<0.01
A0891	138.30	-	<0.01
A0892	148.50	-	<0.01
A0893	122.10	-	<0.01
A0894	156.40	-	<0.01
A0895	135.30	-	<0.01
A0896	129.80	-	<0.01
A0897	126.00	-	<0.01
A0898	121.20	-	<0.01
A0899	126.00	-	<0.01
A0900	130.20	-	0.01
A0901	103.90	-	0.58
A0902	123.70	-	<0.01
A0903	151.60	-	<0.01
A0904	136.60	-	<0.01
A0905	134.00	-	<0.01
A0906	127.90	-	<0.01

- not analysed / -- element not determined / I.S. insufficient sample / L.N.R. listed not received / U.T.D. Unable To Determine

CONTAM - contaminated / D.I.P. - destroyed in prep / L.I.P. - lost in process / N.D. - not detected / NVL - not validated

APPENDIX 5a and 5b: Simplified 3D Geological Model for the study area (SSH-MWA = Roan Shale, SAK= Arkosic Sandstone, SBX= Diamictite, SSH-NGU= Nguba Shale.

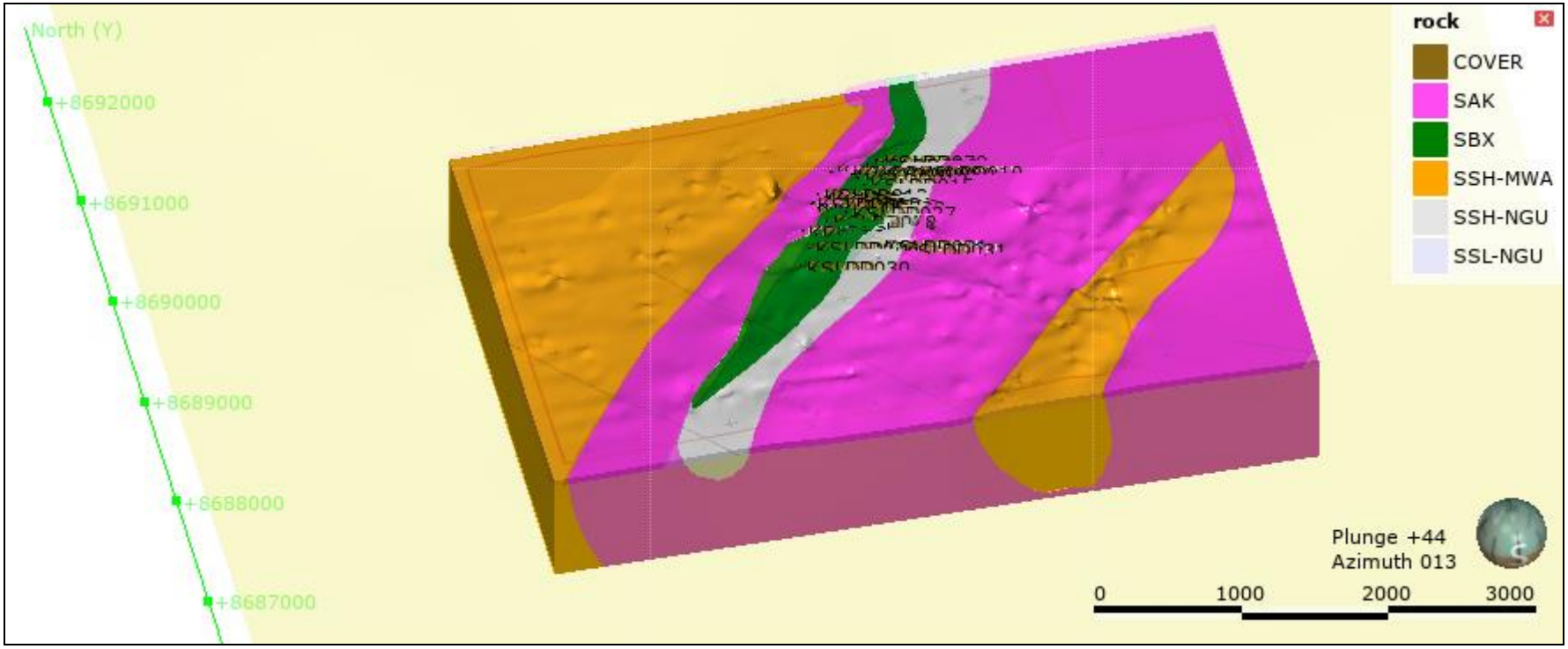

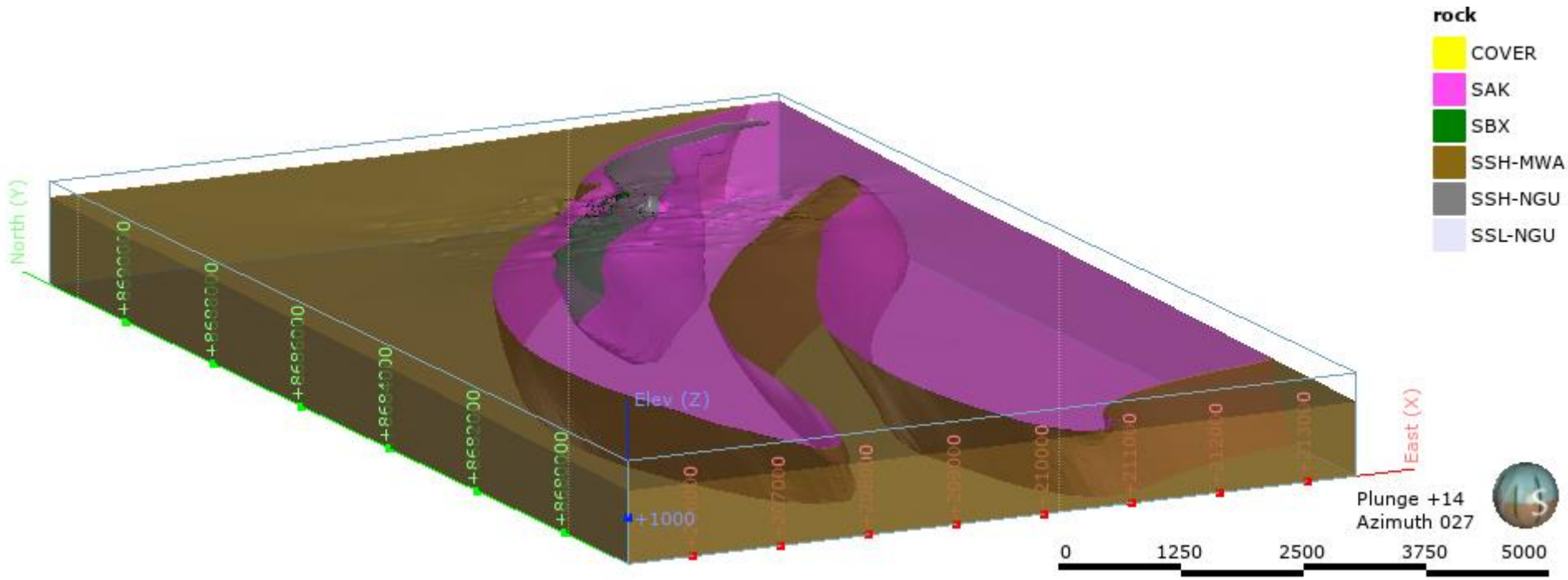
rock
COVER
SAK
SBX
SSH-MWA
SSH-NGU
SSL-NGU
North (Y)
Elev (Z)
East (X)
+1000
Plunge +14
Azimuth 027
0
1250
2500
3750
5000